1. Report No. FHWA/TX-13/5-6037-01-1	2. Government Accession No.	3. Recipient's Catalog No.	
4. Title and Subtitle IMPLEMENTATION OF CURING, TEXTURING, SUBBASE, AND COMPACTION MEASUREMENT ALTERNATIVES FOR CONTINUOUSLY REINFORCED CONCRETE PAVEMENT		5. Report Date February 2013 Rwdnkujgf<"Crtkn'4236	
		6. Performing Organization Code	
7. Author(s) Dan Zollinger, Moon, Won, Tyler Ley, Kyle Riding, Andrew Wimsatt, Wujun Zhou, Seongwoo Ryu, , and Pangil Choi		8. Performing Organization Report No. Report 5-6037-01-1	
9. Performing Organization Name and Address Texas A&M Transportation Institute College Station, Texas 77843-3135		10. Work Unit No. (TRAIS)	
		11. Contract or Grant No. Project 5-6037-01	
12. Sponsoring Agency Name and Address Texas Department of Transportation Research and Technology Implementation Office 125 E. 11th Street Austin, Texas 78701-2483		13. Type of Report and Period Covered Technical Report: June 2010–August 2012	
		14. Sponsoring Agency Code	
15. Supplementary Notes Project performed in cooperation with the Texas Department of Transportation and the Federal Highway Administration. Project Title: Implementation of Alternatives to Asphalt Concrete Subbases for Concrete Pavement URL: http://tti.tamu.edu/documents/5-6037-01-1.pdf			

16. Abstract

This report evaluates four different subbase types, two different concrete mix designs (a standard Texas Department of Transportation gradation and an optimized gradation), three different curing compounds, and four different surface textures that researchers tested on a new section of continuously reinforced concrete pavement. In particular, researchers found:

- The instrumented roller package was effective in locating areas of low stiffness in subgrade soils.
- falling weight deflectometer and dynamic cone penetrometer data can be used to evaluate the stiffness of stabilized subbases before concrete paving commences.
- The proposed curing compound evaluation protocol not only considered the moisture loss throughout the maturing process of concrete, but also introduced the relative humidity, surface abrasion strength, and water content of cured concrete samples to assess the curing compound effectiveness.
- It appears that the use of geotextile between Continuously Reinforced Concrete Pavement (CRCP) and the subbase is questionable and may not provide the desired pavement performance.
- The ConcreteWorks program was effectively calibrated using the data collected from this project.

17. Key Words Concrete, Pavement, CRCP, Curing, Subbase, Aggregate, k-value, Roller, Coarseness, FWD, HWTD, Mix Design,		18. Distribution Statement No restrictions. This document is available to the public through NTIS: National Technical Information Service Alexandria, Virginia http://www.ntis.gov	
19. Security Classif. (of this report) Unclassified	20. Security Classif. (of this page) Unclassified	21. No. of Pages 136	22. Price

Form DOT F 1700.7 (8-72) Reproduction of completed page authorized

IMPLEMENTATION OF CURING, TEXTURING, SUBBASE, AND COMPACTION MEASUREMENT ALTERNATIVES FOR CONTINUOUSLY REINFORCED CONCRETE PAVEMENT

by

Dan Zollinger
Professor
Texas A&M University

Moon Won
Associate Professor
Texas Tech University

Tyler Ley
Associate Professor
Oklahoma State University

Kyle Riding
Assistant Professor
Kansas State University

Andrew Wimsatt
Materials and Pavements Division Head
Texas Transportation Institute

Wujun Zhou
Graduate Student
Texas Tech University

Seongwoo Ryu
Post Doctoral Researcher
Texas Tech University

and

Pangil Choi
Post Doctoral Researcher
Texas Tech University

DISCLAIMER

This research was performed in cooperation with the Texas Department of Transportation (TxDOT) and the Federal Highway Administration (FHWA). The contents of this report reflect the views of the authors, who are responsible for the facts and the accuracy of the data presented herein. The contents do not necessarily reflect the official view or policies of the FHWA or TxDOT. This report does not constitute a standard, specification, or regulation.

This report is not intended for construction, bidding, or permit purposes. The engineer in charge of the project was Andrew J. Wimsatt, Ph.D., P.E., #72270 (Texas).

The United States Government and the State of Texas do not endorse products or manufacturers. Trade or manufacturers' names appear herein solely because they are considered essential to the object of this report.

ACKNOWLEDGMENTS

TABLE OF CONTENTS

Page

LIST OF FIGURES

Page

LIST OF TABLES

CHAPTER 1 INTRODUCTION

In 2010, TxDOT let a contract to construct a continuously reinforced concrete pavement (CRCP) on a new section of FM 1938 in Westlake, Texas. This project, which was completed in late 2012, incorporates various features that researchers tested and evaluated during the course of this study. The project incorporated four different subbase types, two different concrete mix designs (a standard TxDOT gradation and an optimized gradation), three different curing compounds, and four different surface textures. Figure 1 contains an excerpt of the plan sheet and shows the layout of this project with descriptions of the various features. These features will be described in more detail later in this report.

2" ACP TY B — 1" ACP TY D — GEO — STA 175+00 STA 190+00

***9" CRCP	***9" CRCP	***9" CRCP	*** | *** | **** 9" CRCP
8"CEMENT TREATED SUBGRADE	6" CSB	6" CSB	4"ACP TY B
STA. 98+23 TO 115+00	8"CEMENT TREATED SUBGRADE	8"CEMENT TREATED SUBGRADE	* TREATED SUBGRADE
	STA. 115+00 TO 132+00	STA. 132+00 TO 160+00	STA. 160+00 TO 205+00

CONCRETE MEMBRANE CURING COMPOUND
STA 98+23 TO 115+00: TY I LITHIUM-BASED (TXDOT SUPPLIED)
STA 115+00 TO 160+00: TY II LITHIUM-BASED (CONTRACTOR SUPPLIED)
STA 160+00 TO 205+00: TYPE II

* 8" CEMENT OR 8" LIME OR 18" LIME IAW TYPICAL SECTION SHEETS

SURFACE TEXTURING
STA 98+23 TO 115+00: LONGITUDINAL TINING SPACED AT 1"
STA 115+00 TO 132+00: CARPET DRAG, ONLY
STA 132+00 TO 160+00: TRANSVERSE TINING SPACED AT ½"
STA 160+00 TO 205+00: TRANSVERSE TINING SPACED AT 1"

CRCP
** STA 98+23 TO 175+00: OPTIMIZED GRADED COARSE AGGREGATE — 4 SOURCE BLEND
*** STA 175+00 TO 190+00: OPTIMIZED GRADED COARSE AGGREGATE – 3 SOURCE BLEND
****STA 190+00 TO 205+00: STANDARD CONCRETE WITH COARSE AGGREGATE GR-3 OR GR-4 CORRESPONDING TO ASTM C33

NONWOVEN GEOTEXTILE
STA 132+00 TO 160+00: SHALL MEET REQUIREMENTS OF SPECIAL SPECIFICATION 5731

CEMENT STABILIZED BASE
STA 115+00 TO 123+00 & STA 146+00 TO 160+00: 7-DAY COMPRESSIVE STRENGTH SHALL BE 250 PSI
STA 123+00 TO 146+00: 7-DAY COMPRESSIVE STRENGTH SHALL BE 500 PSI

CEMENT TREATED SUBGRADE
STA 98+23 TO 106+00: 7-DAY COMPRESSIVE STRENGTH SHALL BE 400 PSI
STA 106+00 TO 205+00: 7-DAY COMPRESSIVE STRENGTH SHALL BE 200 PSI

EMBANKMENT COMPACTION
STA 98+23 TO 160+00: INTELLIGENT COMPACTION
STA 160+00 TO 205+00: DENSITY CONTROL TY D

: Revised, 7/24/09, RAD

STATE OF TEXAS
RALPH A. BROWNE
69769
REGISTERED PROFESSIONAL ENGINEER

FM 1938
TYPICAL SECTION/ PAVING LAYOUT
Texas Department of Transportation

STP 2009(880)MM	
TEXAS 02	TARRANT
1978 01 048 FM 1938	

Figure 1. Plan Sheet – FM 1938 Layout with Feature Descriptions.

The report contains the following chapters:

- Chapter 1 is the introduction to this report.
- Chapter 2 describes the work done to evaluate subbase support conditions.
- Chapter 3 describes the work done to evaluate erodability of various subbase materials used on this project.

- Chapter 4 describes the work done to evaluate the concrete pavement structural response.
- Chapter 5 describes the work done to evaluate curing effectiveness.
- Chapter 6 contains an analysis of noise and skid resistance data obtained on top of the CRCP for all four surface textures.
- Chapter 7 describes the development and evaluation of the concrete mix design using an optimized aggregate gradation.
- Chapter 8 describes the calibration of the ConcreteWorks computer program using data collected during this study.
- Chapter 9 contains the conclusions and recommendations for this study.

CHAPTER 2 EVALUATE SUBBASE SUPPORT CONDITIONS

Various field tests were conducted to characterize the structural support condition of each subbase type, including:

- Instrumented roller (for subgrade compaction).
- Plate bearing test (PBT).
- Dynamic cone penetrometer (DCP).
- Falling weight deflectometer (FWD) – data collection provided by TxDOT.

Figure 2 shows the four different test sections with different subbase types: (1) 2-inch type B asphalt concrete pavement (ACP), (2) 1-inch type D ACP over 6-inch cement stabilized base (CSB), (3) geotextile over 6-inch CSB, and (4) 4-inch type B ACP.
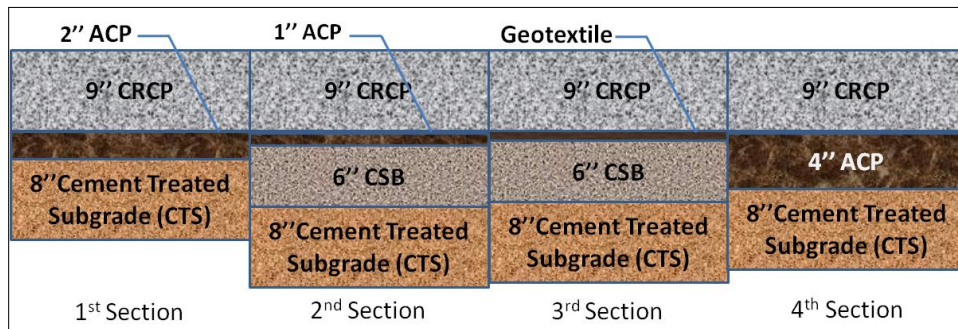
Figure 2. Test Section Layout.

The instrumented roller was used throughout the project. DCP, PBT, and FWD testing were conducted at the same locations on top of different layers, as shown in Figure 3. DCP testing was conducted on top of the stabilized subgrade at two different times: (1) at least three days before the placement of the stabilized base, and (2) at least one week after placement of the stabilized base. PBT testing was conducted on natural and cement treated subgrade (CTS). FWD testing was conducted on all layers. All testing was conducted at the same selected locations.
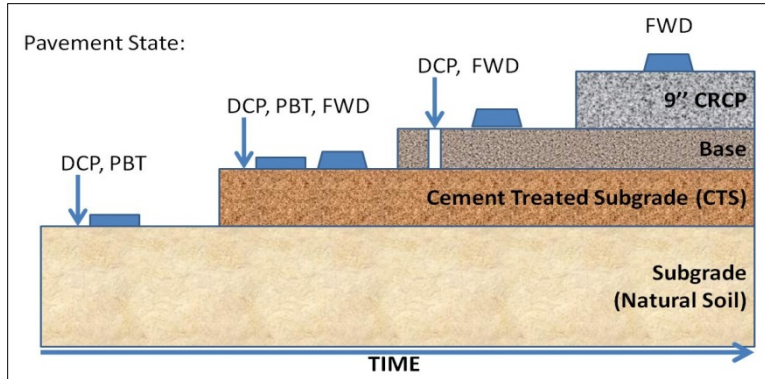
Figure 3. Field Testing.

INSTRUMENTED ROLLER

The Texas A&M Transportation Institute (TTI) developed an instrumented roller package under Project 0-4774, "Pilot Implementation of Instrumented Rollers for Compaction Control." Figure 4 shows the main components of this package, which is intended to be installed on a roller. The package includes a global positioning system (GPS) for distance measurement, a computer with display, and an accelerometer mounted on the roller. Results from Project 0-4774 showed that the roller measurements relate to the stiffness of the pavement foundation layer.

Figure 4. Components of the Instrumented Roller Package.

Figure 5 shows results from an area on the northern end of the project using two different roller vibration settings (high and low). Lower roller drum response readings indicate that the subgrade is weaker in those areas, as indicated by the areas marked B and D in Figure 5. Also, the same pattern is present for both vibration settings.
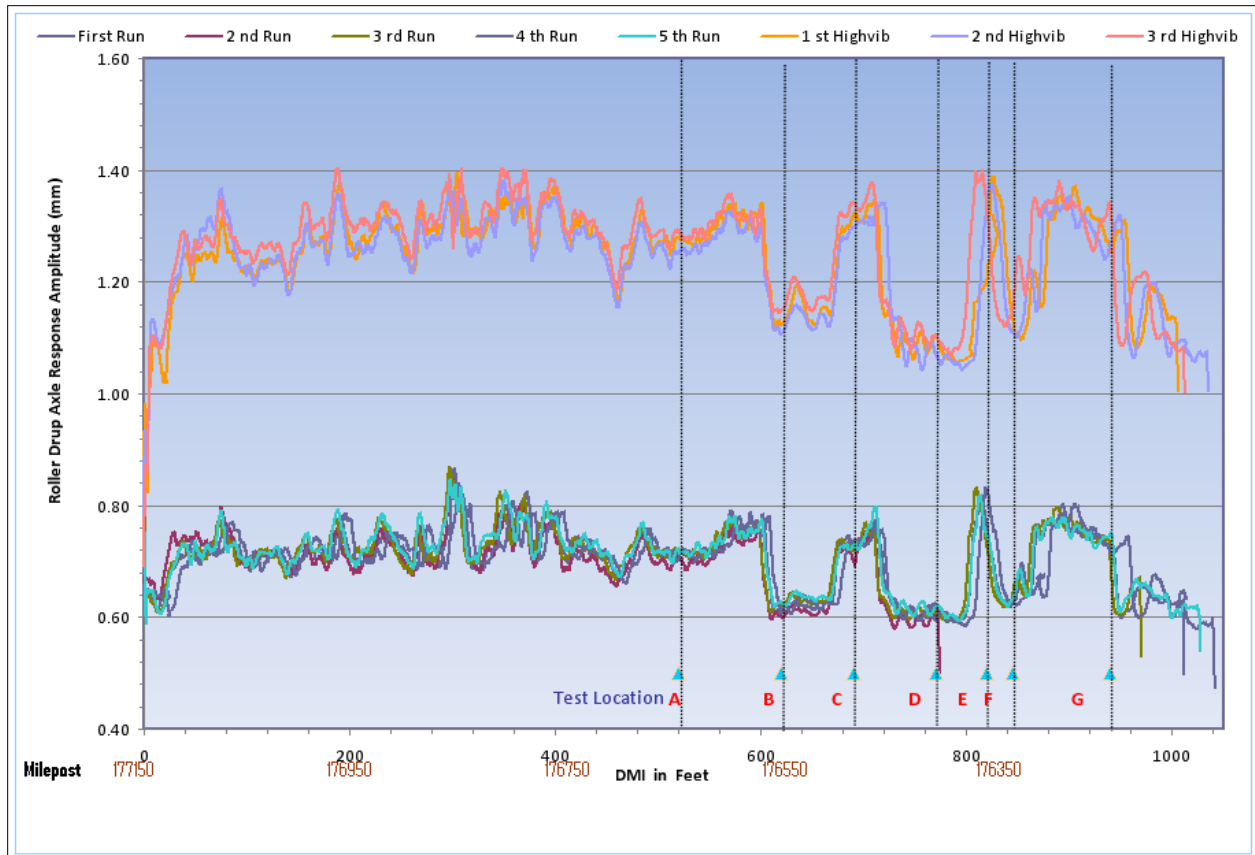
Figure 5. Instrumented Roller Data from FM 1938.

DYNAMIC CONE PENETROMETER TESTING

Dynamic cone penetrometer testing is widely used in pavement and subgrade soil evaluation due to its simplicity and economy (Figure 6). The cone penetration caused by one blow of a 17.6 lb sliding hammer from a height of 22.6 inches is recorded. The cone has an angle of 60 degrees with a diameter of 0.79 inches. The DCP test was conducted in accordance with ASTM D 6951-03.

Over the years, a substantial amount of research work has been conducted to develop empirical relationships between DCP penetration resistance and resilient modulus. Past research studies developed a number of correlations between resilient modulus and DCP. In this study, correlations developed by the Army Corps of Engineers are followed. The following conversion equations are used for evaluating California bearing ratio (CBR) and elastic modulus (E) (*1*).

$$CBR = 292/PR^{1.12} \tag{2.1}$$

$$E = 2550 \times CBR^{0.64} \tag{2.2}$$

Where:
 PR = penetration rate, mm per blow.

Figure 6. DCP Testing.

The roller drum response from the instrumented roller package can be correlated to California bearing ratio values obtained from the DCP. Figure 7 shows a set of data from the instrumented roller package from a section south of the Dove Road intersection. Figure 8 shows the correlation between the CBR and the roller drum response for the areas marked A through E in Figure 7. As Figure 8 shows, the correlation is not very strong, although the overall trend is realistic.
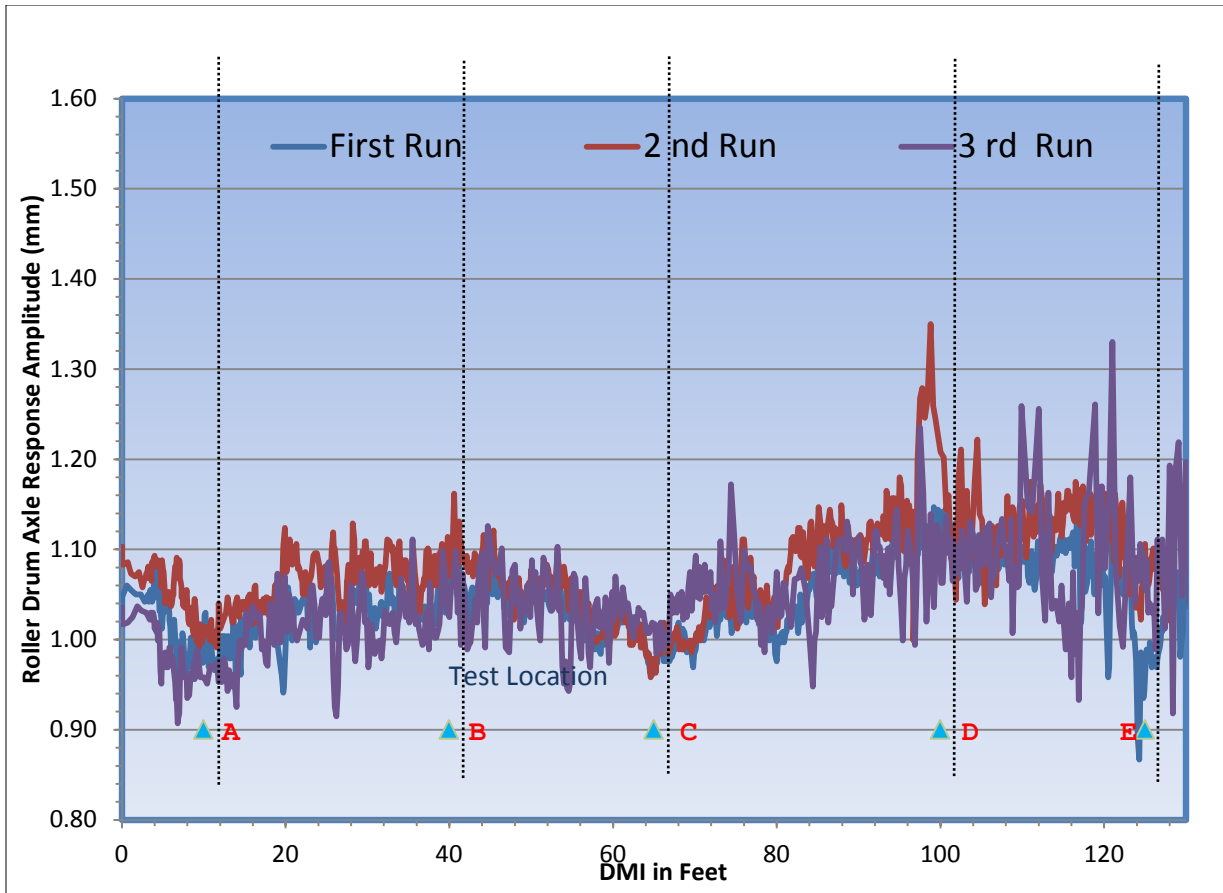
Figure 7. Instrumented Roller Data for the FM 1938 Section South of Dove Road.
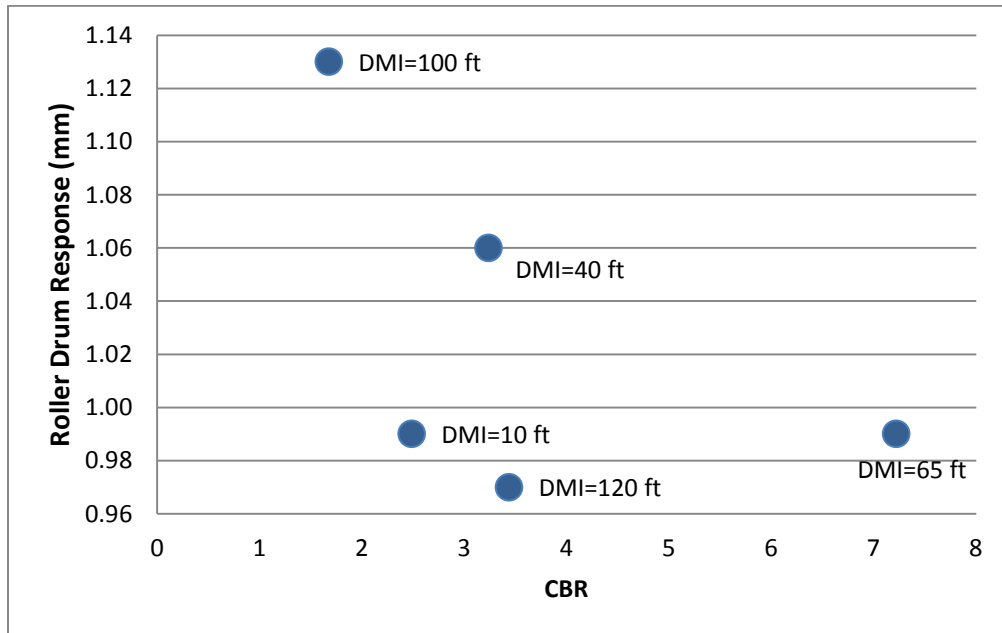
Figure 8. CBR versus Roller Drum Response for the FM 1938 Section South of Dove Road.

Figure 9 shows a set of data from the instrumented roller package on a section of Dove Road. Figure 10 shows the correlation between the CBR and the roller drum response for the areas marked A through D in Figure 9. As Figure 10 shows, there is a strong correlation.
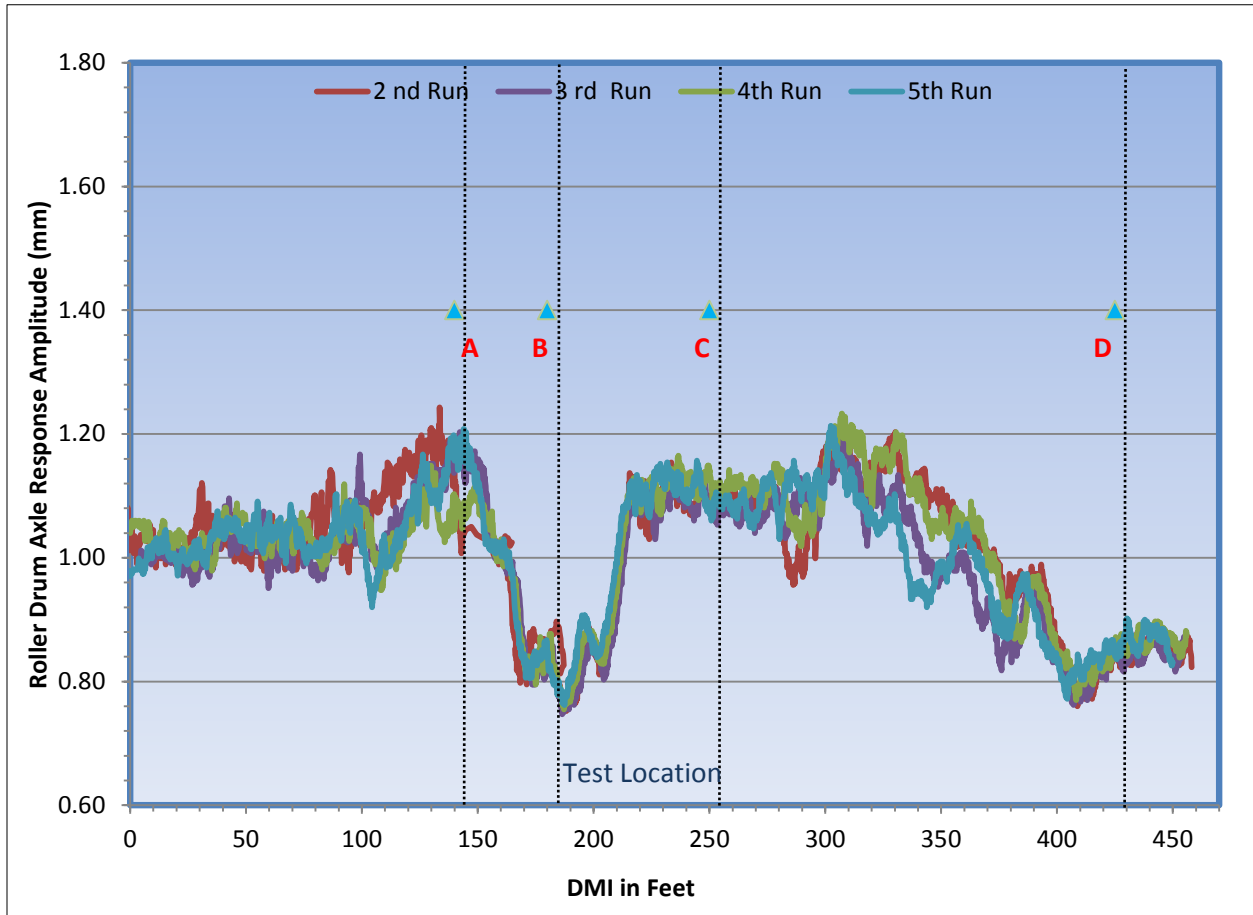
Figure 9. Instrumented Roller Data on Dove Road.
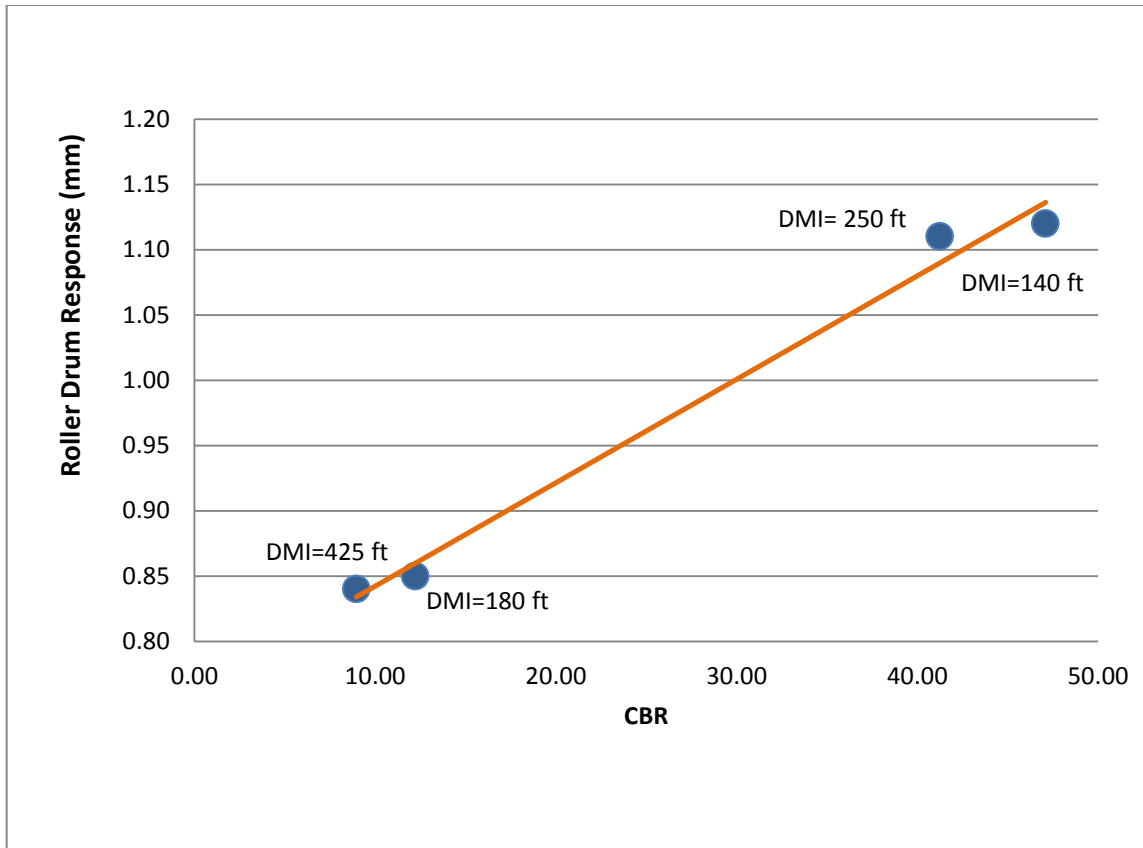
Figure 10. CBR versus Roller Drum Response for Dove Road.

In order to develop more accurate comparisons of the support conditions from DCP and PBT, the DCP test locations are close to each plate bearing test location. When a bound layer is above the nonbound layers, a ⅞-inch hole is drilled through the bound layers before the DCP test, as shown in Figure 11.

Figure 11. DCP Test after Placement of Stabilized Base.

PLATE BEARING TEST

The plate bearing test was used to evaluate the stiffness of subgrade soil in either compacted condition or natural state. In this testing, a steel bearing plate was pressed into the surface by a hydraulic jack. The surface deflection and load level were measured by linear variable differential transformers (LVDTs) and load cell, respectively, and recorded automatically. PBT was conducted in accordance with ASTM D 1196-93 (*2*), as shown in Figure 12.
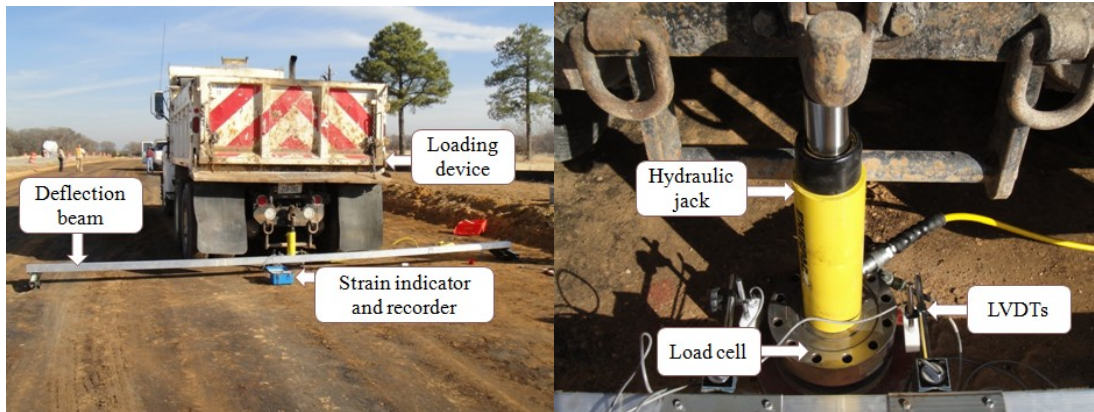
Figure 12. Plate Bearing Test at Field.

The modulus of subgrade reaction (*k*-value) can be determined by the equation below:

$$k = p/S \qquad (2.3)$$

Where:
p = contact pressure.
S = settlement of the loading area.

According to ASTM D 1196-93, the diameters of bearing plates should range from 6 to 30 inches. In this study, a 12-inch diameter bearing plate was used because the PBT with 30-inch bearing plate would require a heavy load truck, which was not available. The *k*-value obtained from the PBT with the 12-inch plate was converted to *k*-value with the 30-inch plate by dividing by two (*3*).

Load was applied at a moderately rapid rate in uniform increments. A sufficient number of load-settlement points (more than six) should be made to develop accurate load-settlement curves by controlling the magnitude of each load increment. Load intensity and corresponding settlement were plotted for modulus of subgrade reaction calculation at the point with a 0.05-inch deflection (*4*).

FWD TESTING

TxDOT's Dynatest 8000 FWD unit, with a 5.9-inch radius loading plate, was used for deflection data collection in this study. Seven geophones were spaced at 0, 12, 24, 36, 48, 60, and 72 inches from the center of the loading plate, as shown in Figure 13. In each testing, four loading drops corresponding to approximately 6,000; 9,000; 12,000; and 16,000 lb of loading were made after two seating drops.

Figure 13. FWD Testing.

For the evaluation of pavement support condition, AREA method A4 suggested by Hall et al. was used (*5,6*). In this method, AREA is defined as follows:

$$\text{AREA} = 6 + 12\left(\frac{d_{12}}{d_0}\right) + 12\left(\frac{d_{24}}{d_0}\right) + 6\left(\frac{d_{36}}{d_0}\right) \tag{2.4}$$

Where:
d_i = deflection in mils at 9,000 lb at distance i inches from the loading plate.

AREA thus determined has a unit of length, which is determined by the shape of the deflection bowl. The shape of the deflection bowl depends on the relative stiffness of the concrete layer and the layers below. Thus, a unique relationship exists between AREA and the radius of relative stiffness l, as shown below, which was suggested by Hall et al. (*6*):

$$\text{Radius of relative stiffness } l = \left(\frac{\ln\left(\frac{36 - \text{AREA}}{1812.279}\right)}{-2.559}\right)^{4.387} \tag{2.5}$$

Once the radius of relative stiffness is determined, k-value is estimated as follows (7):

$$k = \left[\frac{d_0}{D_0}\right]\left[\frac{P}{ll^2}\right] \tag{2.6}$$

Where:

d_0 denotes nondimensional sensor deflections corresponding to the measured deflection D_0:

$$d_0 = \frac{D_0 D}{P ll^2} = \frac{D_0 k ll^2}{P} \tag{2.7}$$

Where:

D is the slab flexural stiffness, given by:

$$D = \frac{Eh^3}{12(1-u^2)} \tag{2.8}$$

Where:

E = concrete modulus of elasticity.

h = Concrete slab thickness.

u = concrete Poisson's ratio.

Back-calculated dynamic k-values need to be reduced by a factor of approximately two for use in pavement design as static elastic k-value (6).

PAVEMENT SUPPORT RESULTS

At each section, 10 test locations were selected for support condition evaluations, except for the second section where only five locations were selected due to the vertical slope of the section. The comparisons of static k-values obtained from PBT and normalized FWD deflection on the top of the CRCP are shown in Figure 14–17. In Figure 14, at locations P5, P6, and P10, k-values on top of 2-inch asphalt stabilized base are smaller than those on cement treated subgrade, which is counter-intuitive. It is postulated that k-values from PBT are sensitive to localized density of asphalt, and the densities in these three locations were low. It is also shown that, in general, that there is no good correlation between k-values and deflections.
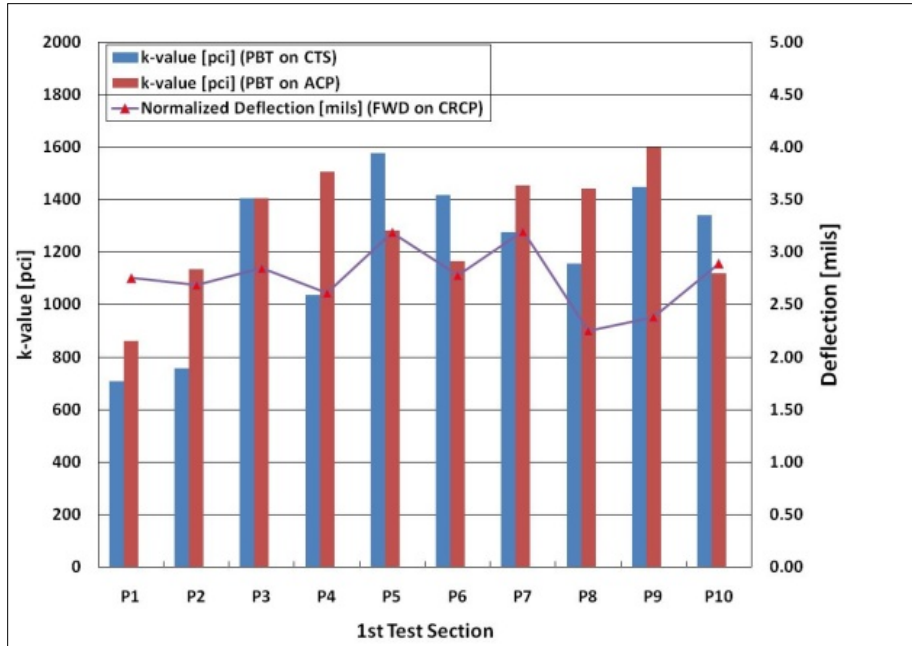
Figure 14. Variations in *k*-Value and Deflection (1st Section).
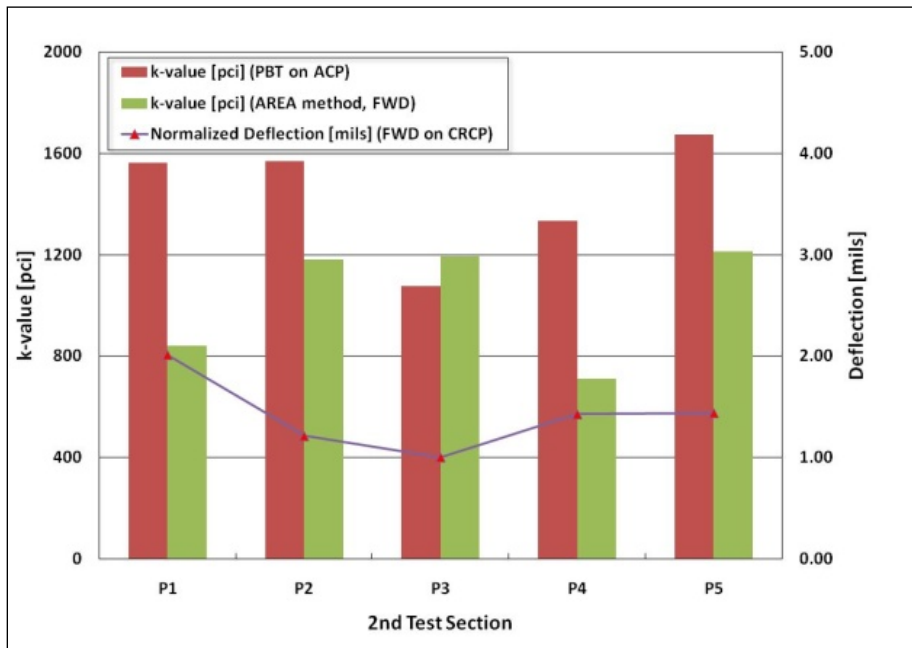
Figure 15. Variations in *k*-Value and Deflection (2nd Section).

Figure 15 shows the comparisons between *k*-values from PBT and the AREA method, as well as deflections in the second section. Except for location P3, *k*-values from the AREA method are much smaller than those from PBT, which indicates that PBT is not an appropriate method to evaluate *k*-values on top of stabilized base. It also shows a decent correlation between

14

k-values from the AREA method and deflections, while a poor correlation was obtained between *k*-values from PBT and deflections.
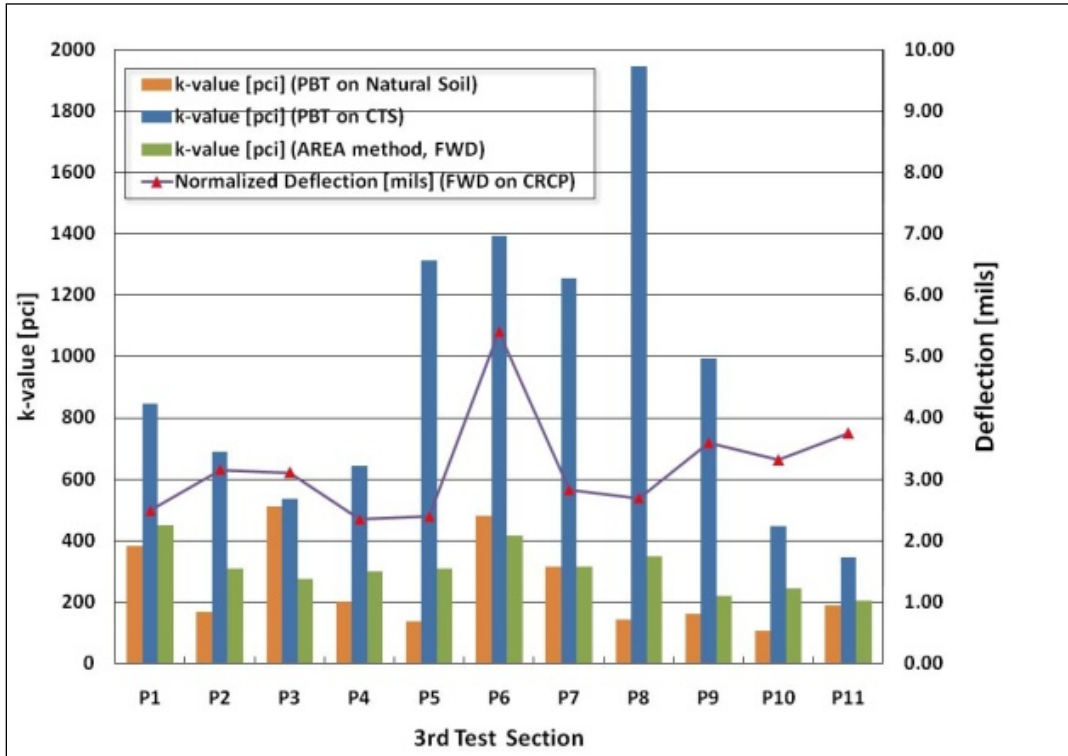
Figure 16. Variations in *k*-Value and Deflection (3rd Section).

Figure 16 illustrates *k*-values and deflections in the third section. It shows that: (1) no good correlation exists between *k*-values on top of natural soil and on top of cement treated subgrade, (2) 4-percent cement treatment of natural subgrade increased *k*-value substantially, (3) *k*-values from the AREA method are much smaller than those on top of cement treated subgrade, and (4) a poor correlation exists between deflections and *k*-values from either method. It should be noted that nonwoven geotextile was used in this section, and the correlation between deflections and *k*-values from the AREA method is not as good.

Figure 17 illustrates *k*-values and deflections in the fourth section. Except for location P8, *k*-values from the AREA method are larger than those from PBT on cement treated subgrade, which differs from the observations in Figure 16. It is believed that the use of nonwoven geotextile in the third section resulted in larger deflections and lower *k*-values from the AREA method.
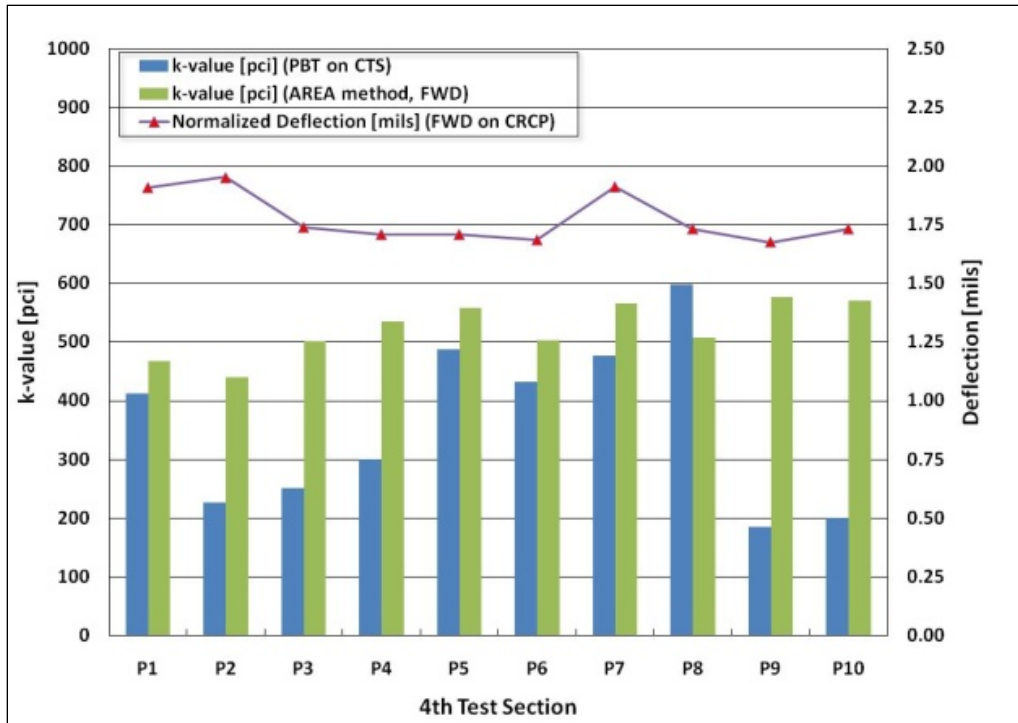
Figure 17. Variations in *k*-Value and Deflection (4th Section).

With the same CRCP thickness, distinctive effects of various base types on deflection on CRCP were identified, as shown in Figure 18. In general, the second section has the smallest deflections on CRCP, where 1-inch ACP + 6-inch CSB was used, and the third section contained the largest deflections on CRCP, where nonwoven fabric replaced 1-inch ACP in the base on top of 6-inch CSB.
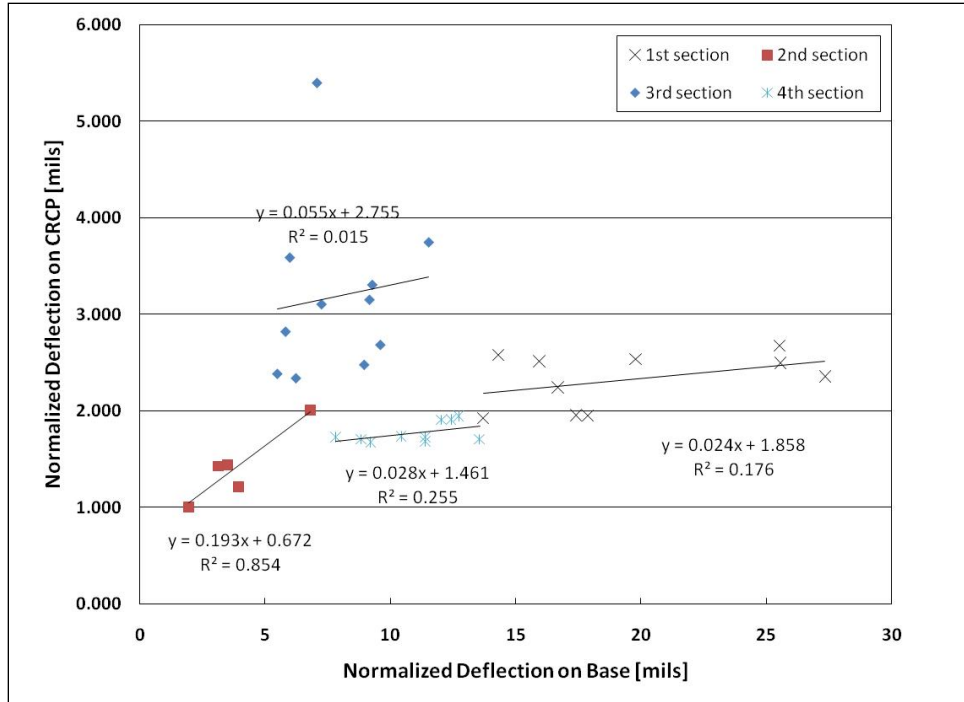
Figure 18. FWD Deflections on Base and CRCP.

The variability of the deflections in the third section is largest. It is believed that the use of nonwoven geotextile is responsible for the increased deflections with a large variability. Since large deflections in CRCP are not desirable for the pavement performance, the value of geotextile as a replacement of 1-inch ACP for base in CRCP is questionable. Deflections in the fourth section where 4-inch ACP was used are low and quite uniform, while those in the first section where 2-inch ACP was used are larger than those in the second and fourth sections. The average reduction in deflections is about 40 percent.

Also, TxDOT personnel collected FWD data at a 0.1-mile spacing along the project on top of the stabilized subgrade and on top of the stabilized subbase. Researchers analyzed the data and identified areas that may indicate poor stabilization or inadequate compaction. Figure 19 shows a graph of the surface curvature index (SCI) versus distance on a section of FM 1938 south of Dove Road. TxDOT personnel obtained these data on top of a 6-inch-thick cement stabilized base layer.

The SCI is the difference between the deflection underneath the FWD load plate and the deflection 12 inches away from the load plate. If the SCI is greater than 20, a possible problem exists. If the SCI is greater than 40, a weak base is present. As Figure 19 shows, there are several areas where the SCI is above 20 and a few areas where the SCI is above 40. The researchers provided this information to TxDOT personnel, who determined that the base needed to be restabilized. This example shows that the FWD could be a useful tool to determine the quality of stabilized subbases after they are constructed and to identify areas that may need to be reworked or restabilized.

17
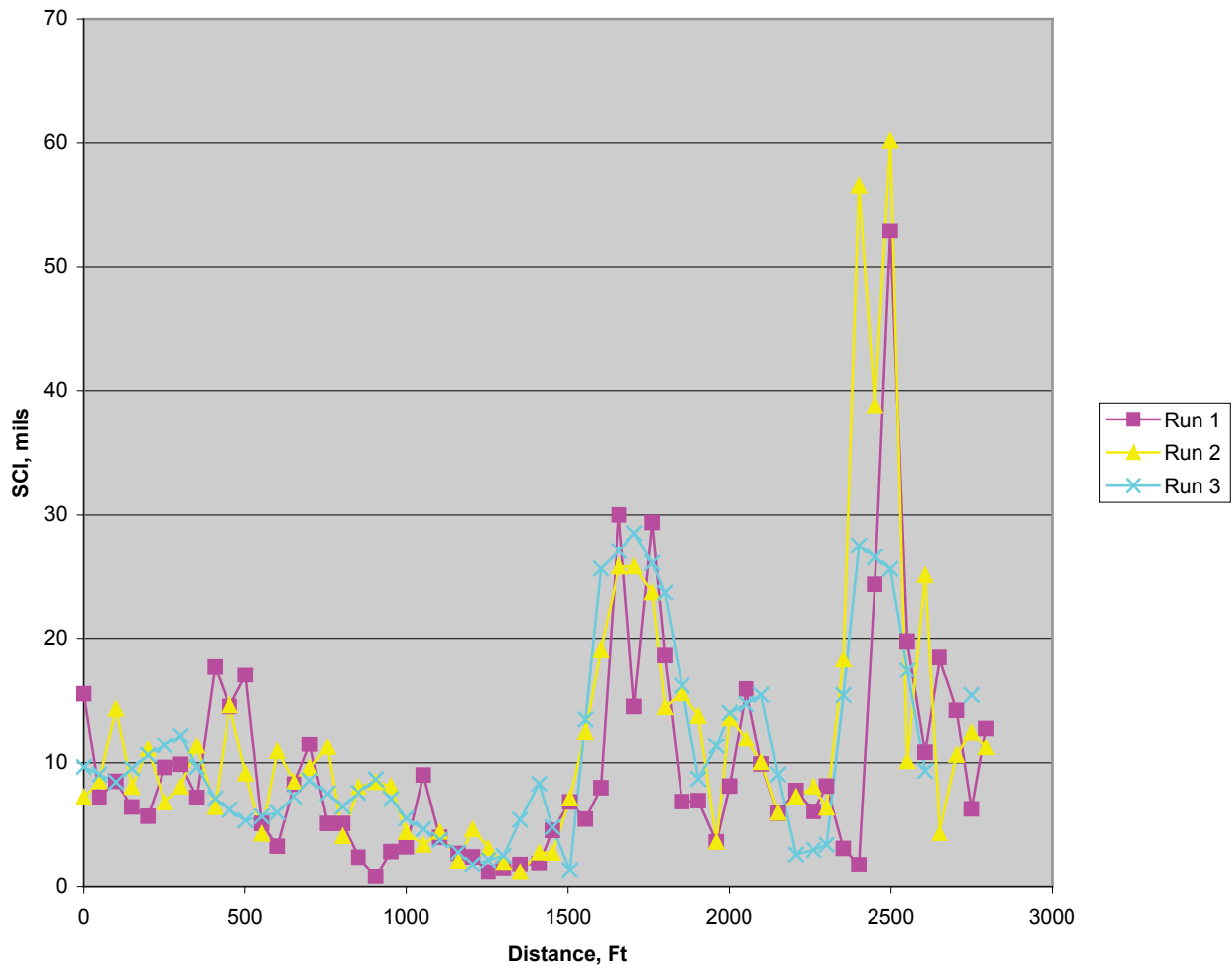
Figure 19. SCI versus Distance: FWD Testing on Top of a Cement Stabilized Base Section

CONCLUSIONS

The findings from this study can be summarized as follows:

1. The instrumented roller package was effective in locating areas of low stiffness in subgrade soils. However, the correlation was rather weak in one area with the California bearing ratio obtained from the DCP. It appears the package can be used for proof rolling, i.e., checking the stiffness of the subgrade before construction operations commence on the upper pavement layers. The researchers recommend further field testing with this equipment in other areas of the state.

2. The falling weight deflectometer and dynamic cone penetrometer data can be used to evaluate the stiffness of stabilized subbases before concrete paving commences. The

18

researchers recommend that the FWD and DCP be considered for use in evaluating such subbases in construction projects.

3. No good correlations were observed between k-values from the PBT on cement treated subgrade and on asphalt stabilized base, which implies that k-values from the PBT are sensitive to the stiffness of the material immediately below the loading plate. In general, the k-value from PBT is sensitive to moisture and the time when the test was performed, especially to chemically stabilized materials. In this study, both moisture content and temperature were not measured and recorded at the time of the tests. Poor correlations observed in this study should be interpreted with caution and further evaluations are needed.

4. In general, k-values on stabilized base from the AREA method are smaller than those obtained by the PBT, which indicates that the PBT is valid only on natural subgrade.

5. When nonwoven fabric is used as base material, the AREA method should not be used to estimate k-values.

6. No good correlations were observed between deflections on the CRCP and k-values from the PBT on natural subgrade or cement treated subgrade. In general, the k-value from PBT is sensitive to moisture and the time when the test was performed, especially to chemically stabilized materials. In this study, both moisture content and temperature were not measured and recorded at the time of the tests. Poor correlations observed in this study should be interpreted with caution. However, it appears that the deflections on the CRCP are more influenced by the thickness and stiffness of the base layer. Decent correlations were observed between deflections on top of the base and on top of the CRCP.

REFERENCES

1. Texas Department of Transportation. Pavement Design Guide Manual, Chapter 4 Section 4 Non-Destructive Evaluation of Pavement Structural Properties. 2011.

2. ASTM Standard D 1196-93, Nonrepetitive Static Plate Load Tests of Soils and Flexible Pavement Components, for Use in Evaluation and Design of Airport and Highway Pavements to Evaluate Modulus of Subgrade Reaction. ASTM International. West Conshohocken, PA. 2004.

3. Teller, L.W., and E.C. Sutherland. The Structural Design of Concrete Pavements, Part 5, An Experimental Study of the Westergaard Analysis of Stress Conditions in Concrete Pavements of Uniform Thickness. Public Roads, Vol. 23, No. 8. 1943.

4. Texas Department of Transportation. Tex-125-E Determining Modulus of Subgrade Reaction (k value). ftp://ftp.dot.state.tx.us/pub/txdot-info/cst/TMS/100-E_series/pdfs/ soi125.pdf. Accessed March 1, 2012.

5. Hall, K.T. Performance, Evaluation, and Rehabilitation of Asphalt-Overlaid Concrete Pavements. Thesis presented to the University of Illinois, Urbana, IL. 1991.

6. Hall, K.T., M.I. Darter, T.E. Hoerner, and L. Khazanovich. LTPP Data Analysis—Phase I: Validation of Guidelines for *k*-Value Selection and Concrete Pavement Performance Prediction. Publication FHWA-RD-96-198. FHWA, U.S. Department of Transportation. 1997.

7. Ioannides et al. Interpretation of Falling Weight Deflectometer Test Results Using Principles of Dimensional Analysis. In Proceedings, Fourth International Conference on Concrete Pavement Design and Rehabilitation, Purdue University, W. Lafayette, IN. 1989. pp. 231–247.

CHAPTER 3 EROSION TESTING FOR SUBBASE MATERIAL SELECTION

INTRODUCTION

This chapter describes the collection of data regarding erodibility testing done in the laboratory using the Hamburg wheel-tracking device (HWTD) on both subgrade and subbase materials. Soil and base samples were obtained from a construction site on FM 1938 in Tarrant County that consisted of different subbase types under a 9-inch-thick CRCP. Figure 20 shows the test site location, and Figure 21 shows the section plan.
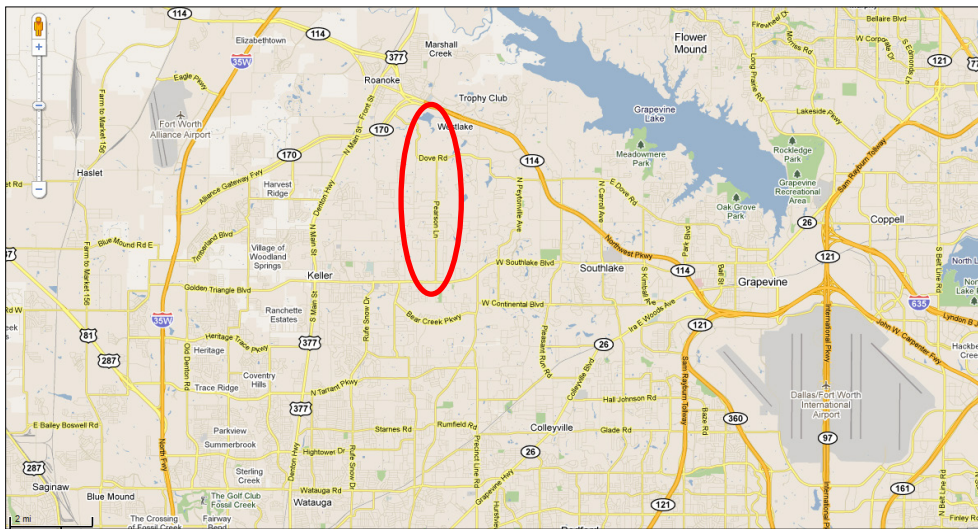
Figure 20. Test Site of FM 1938.

TxDOT subbase design practice calls for either a 6-inch cement stabilized base with a 1-inch asphalt concrete (AC) bond breaker or a 4-inch AC layer over a treated subgrade. A 4-inch AC base typically provides good performance; however, increasing asphalt prices led TxDOT personnel to re-think if using a reduced AC layer thickness is possible to produce lower cost or if alternatives are available for subbase construction. Therefore, four different subbase types (two current base types and two alternative types) were constructed over an 8-inch cement stabilized subgrade as shown in Figure 21:

- Current 4-inch AC base.
- 6-inch CSB with a 1-inch AC bond breaker.
- 6-inch CSB with geotextile.
- 2-inch AC base on 8-inch cement stabilized subgrade.

In addition, two different levels of stabilization were used for the subgrade and subbase layers relative to target 7-day compressive strengths:

- Cement treated subgrade 7-day compressive strengths = 200 and 400 psi.
- Cement treated subbase 7-day compressive strengths = 250 and 600 psi.
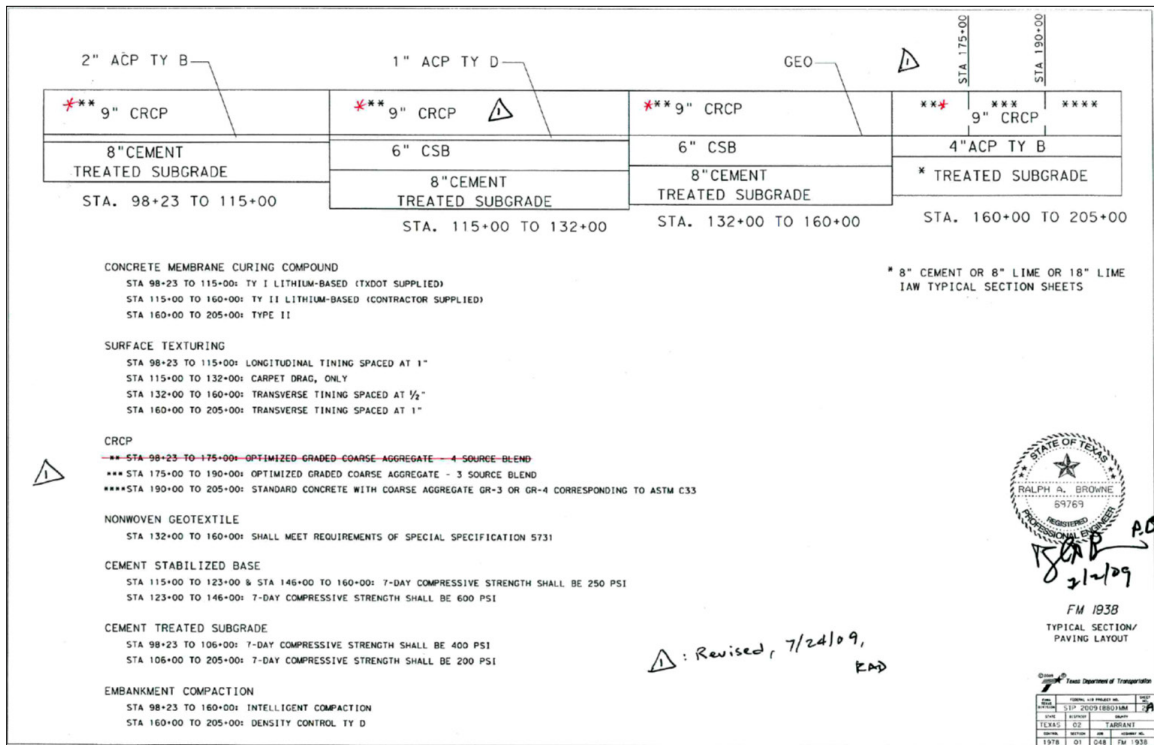
Figure 21. Section Plan of FM 1938.

Figure 22 shows one drilling log of the natural subgrade. As shown in the figure mostly brown and tan moist sandy soil with some yellowish clayey sand seams (SC-SM) were present. Figure 23 shows cores of subgrade layer.

Figure 22. Drilling Log of FM 1938.

Figure 23. Subgrade Core Samples from FM 1938.

Figure 24 shows examples of the dynamic cone penetrometer test results on the subgrade layer. DCP testing indicates the in-situ strength of the subgrade materials. It consists of upper and lower shafts. The upper shaft has a 17.6-lb drop hammer with a 22.6-inch drop height and is attached to the lower shaft through the anvil. The lower shaft contains an anvil and a cone attached at the end of the shaft. The cone is replaceable and has a 60-degree cone angle. Equation 3.1 shows the relationship between the penetration rate and elastic modulus of soils (*1*).

$$E = 2550 \times CBR^{0.64} \tag{3.1}$$

$$CBR = 292/PR^{1.12}$$

Where:
E = elastic modulus (psi).
CBR = California bearing ratio.
PR = penetration rate (mm/blow).

Back-calculated moduli of natural subgrade of section 3 ranged between 5,000 psi and 35,000 psi, while those of section 4 were between 10,000 psi and 30,000 psi.
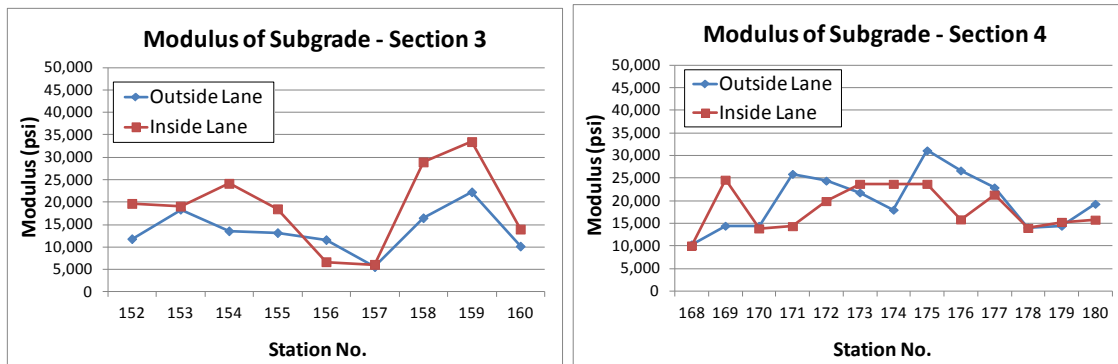
Figure 24. Back-Calculated Modulus of Subgrade.

DCP testing seemed to be an easy and useful way to track the effects of stabilization on subgrade layer. Figure 25 shows how the penetration rate (PR) decreases after stabilization (lower PR means stiffer layers). For instance, stations 157 and 168 show very high PRs in natural subgrade materials (which mean low moduli) but after stabilization those stations show similarly low PR when compared with other areas, as shown in Figure 25. Stabilized subgrade shows more constant performance over all stations with increased stiffness.
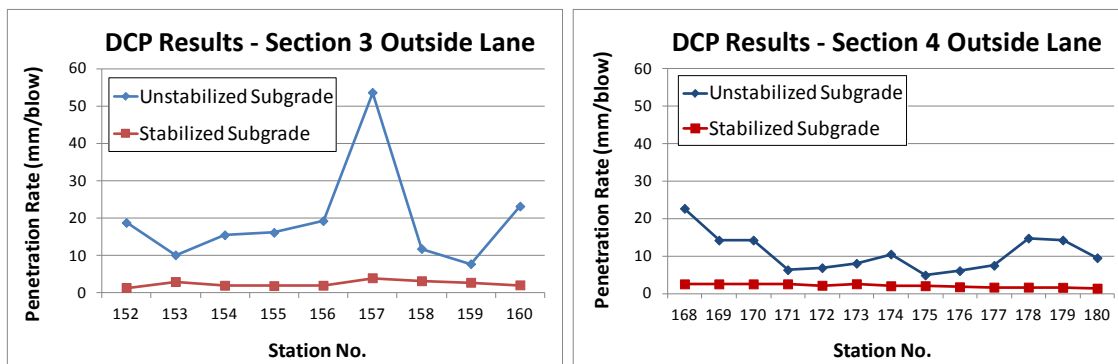
Figure 25. Change of PR after Subgrade Stabilization.

24

ERODIBILITY TEST USING HWTD

During construction, subgrade and subbase materials were stabilized and tested to meet the 7-day compressive target strength. Stabilization of this nature also increases erosion resistance of subgrade and subbase materials compared to an untreated or unstablized condition. Therefore, lab molded cement treated subbase and subgrade materials as well as field cores of cement treated subgrade were tested to study the increments of erosion resistance of subgrade and subbase materials.

Sieve Analysis

Samples were sieved according to the Texas Department of Transportation (TxDOT) method. Table 1 and Figure 26 show the aggregate size distributions of the samples.

Table 1. Sieve Analysis for Subgrade and Subbase Aggregates.

Sieve Number	Sieve Size (inch)	Sieve Size (mm)	Subgrade (%)	Subbase (%)
1 ¼	1.25	31.75	0	4.5
⅞	0.875	22.6	0	18.5
⅜	0.375	9.5	0	25.5
# 4	0.187	4.76	7.5	12.9
# 10	0.0787	2.0	15.4	12.5
# 40	0.0165	0.42	16.3	12.6
# 100	0.0059	0.149	39.2	7.6
# 200	0.0029	0.074	12.3	3.6
Pan	-	-	9.3	2.3
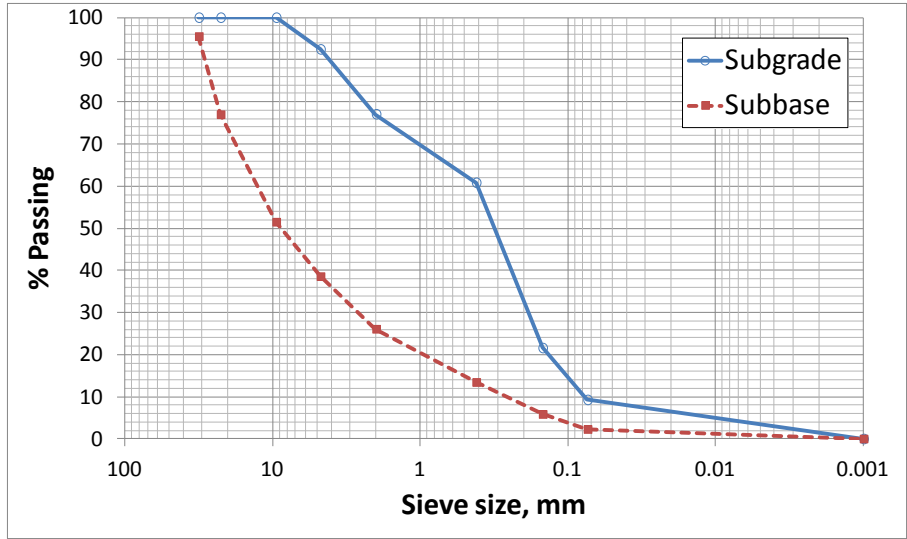
Figure 26. Sieve Analysis Results of Subgrade and Subbase Aggregates.

Optimum Moisture Content and Compaction

Optimum moisture contents (W_{OPT}) to compact samples are determined as Figure 27 shows. Subgrade W_{OPT} using the mix containing 6 percent cement was 10.3 percent while Subbase W_{OPT} using the mix containing 4 percent cement was 8.2 percent.
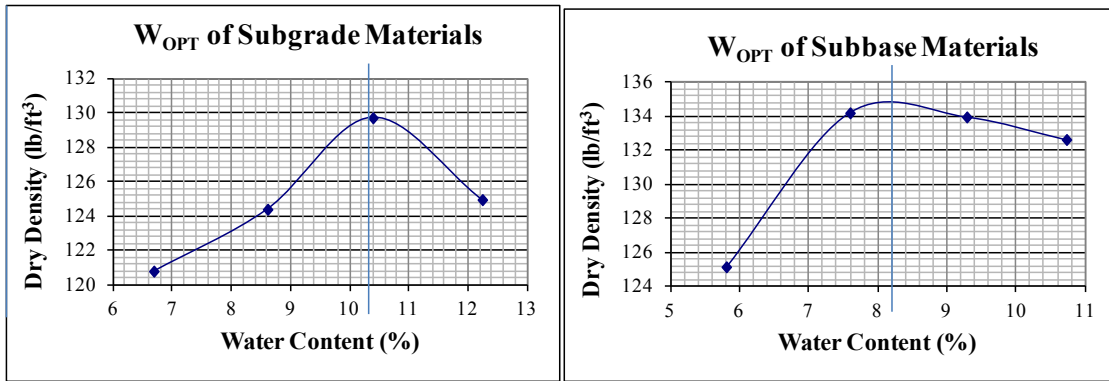
Figure 27. Optimum Moisture Contents of Subgrade and Subbase Aggregates.

Sieved subgrade materials were stabilized with different cement contents of 4, 6, 8, and 10 percent cement at optimum moisture content by weight, and subbase materials were stabilized with 2, 4, 6, and 8 percent of cement contents. Changing optimum moisture contents of the samples with different cement contents followed the same rule in the TxDOT test method "Tex-120-E, Soil-Cement Testing" as shown in Equation 3.2.

% molding water = % optimum moisture from M/D curve + 0.25 (% cement increase)   (3.2)

Where:
% cement increase = difference in cement content between curve and other cement contents.

All samples were prepared according to the test method Tex-120-E and compacted according to the test method "Tex-113-E, Laboratory Compaction Characteristics and Moisture-density Relationship of Base Materials," using a 10-lb hammer, with an 18-inch drop, at 50 blows/layer in a 6 × 6-inch mold (with 5-inch disk insertion at the bottom). All samples were cured for 28 days under 100 percent relative humidity conditions except for the untreated (0 percent cement treated) samples. Maximum aggregate size for molding subbase sample was determined as ⅜ inch based on the result of the previous TxDOT project 0-6047 (*2*).

EROSION TEST DEVICE

The erosion test incorporates the use of the HWTD, which allows for water to transport material that has been abraded due to mechanical wear (and to some extent hydraulic shear action) generated by slab movement under an applied load along the interface between the slab and the surface of the base layer. The configuration of the test device is the same as normally used with the HWTD except for the multi-layering of the test sample shown in Figure 28. The test configuration consists of a 1-inch-thick subbase material placed on a neoprene material below a 1-inch-thick jointed concrete cap (modification of the HWTD sample mold may allow for thicker subbase layers). The test configuration is such that it allows for testing either a laboratory compacted specimen or a core sample obtained from the field. A 158-lb wheel load is applied to the test sample at a load frequency of 60 rpm up to 10,000 load repetitions under selected moisture conditions typically at a temperature of 70°F. Measurements consist of the depth of erosion at 11 locations versus the number of wheel load passes. In most cases, maximum deflection occurs at measuring points # 5, 6, or 7. Shear stress for the HWTD configuration can be calculated using Equation 3.3.

$$\tau_{e-p} = \chi\tau_b + (1-\chi)\tau_u$$

(3.3)

and using beam theory:

$$\tau_i = \frac{V_s\left\{1-\left[\frac{2(h_c - x_{na})}{h_i}\right]^2\right\}}{h_i b \frac{E_{base}}{E_c}}$$

(3.4)

Where:

τ_i= partially (*p*), bonded (*b*), or unbonded (*u*), shear stress, (psi).

χ = degree of partial bonding (as a function of the coefficient of friction (μ) where 0 = unbonded and 1 = fully bonded.

V_s = shear load (158 lb).

h_c = thickness of the concrete cap.

h_i = effective unbonded (*u*) or bonded (*b*) thickness.

x_{na} = distance to the neutral axis.

E_i = elastic modulus of concrete cap (*c*) or subbase (*base*) layer, (psi).
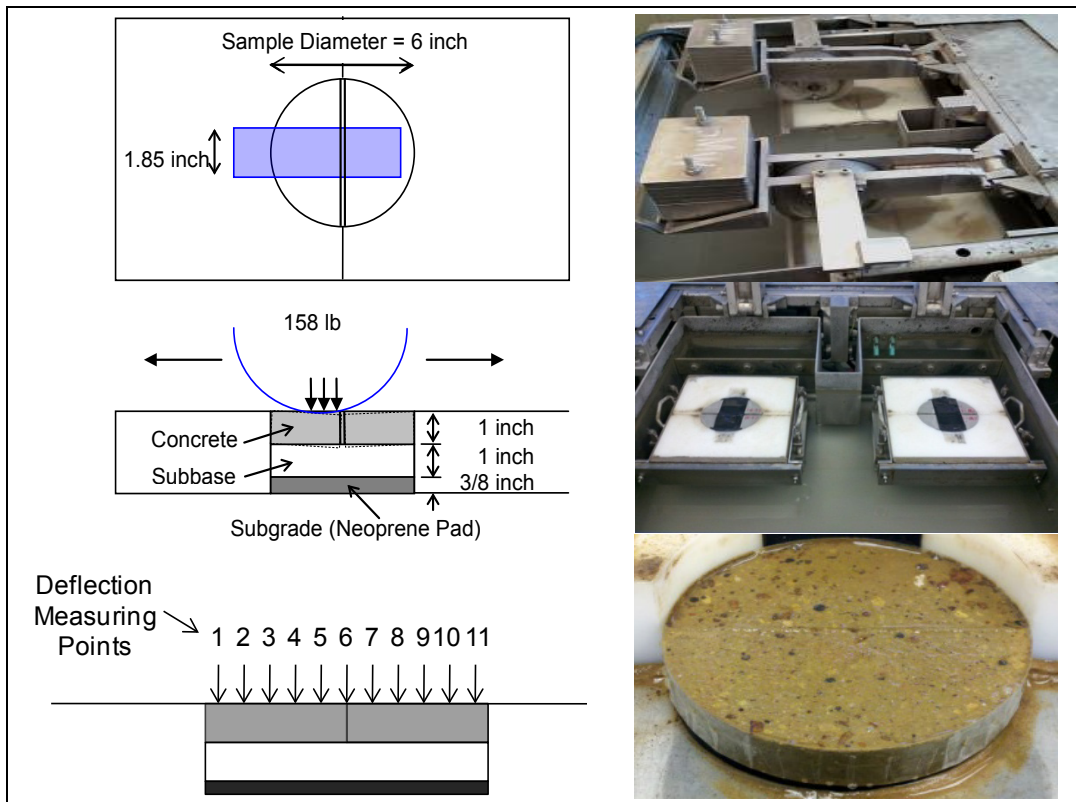
Figure 28. Erosion Test Using Hamburg Wheel-Tracking Device.

Using plate theory the shear stress is determined for field conditions as:

τe-p = interfacial shear stress (FL^{-2})

$$= \left(\frac{\partial \delta_{L_i}}{\partial X}\right)_{e-p} \frac{E_{sb}}{2(1+\upsilon)}\left(\frac{1}{\psi}\right)$$

δ = loaded deflection, (L)

$$= \frac{\delta^* P}{k \ell^2}$$

δ^* = dimensionless deflection

$$\frac{\partial \delta_{L_i}}{\partial X}\bigg|_e = \left(\frac{\partial \delta^*}{\partial x}\right)_{e-p} \frac{P}{L^* k \ell^2_{e-p}}$$

X = distance from the point of loading along the diagonal from the corner or from the edge of the slab

$$X = \frac{X}{L^*}$$

$$L^* = \frac{W}{2} \text{ (slab edge)}; = \frac{W}{\sqrt{2}} \text{ (slab corner)}$$

W = slab width (L)

$$\frac{\partial \delta^*}{\partial x} = b + 2dx + fy$$

b, d, f = edge or corner coefficients as a function of load position

$$y = \frac{h_{e-p}}{\ell}$$

E_{sb} = subbase modulus (FL^{-3})
ν = subbase Poisson's ratio
ψ = Load transfer factor = $a_i(LTE) + 1$
a_i = 0.03 for edge loading; 0.07 for corner loading
LTE = load transfer efficiency (%)

EROSION TEST RESULTS – LAB MOLDED SAMPLES

Figure 29 and Figure 30 show the average of 11 erosion depths across the sample erosion profile relative to HWTD load repetitions for lab molded cement treated subgrade (CTSG) and cement treated base (CTB) samples. The rate of erosion was initially high at the start of the test but decreased with time as the erosion progressed. Early research suggests that the hydraulic shear stress is higher when the void between concrete and the subbase surface is small. (Phu and Ray [3] indicated [at a constant slab deflection speed] that if the void is larger than 0.04 inch [1 mm] the rate of erosion will diminish with an increase in void depth.) Test results show a fluctuation of erosion depth with the number of loading most likely due to relatively large aggregates being dislocated by pumping action while small fines are more uniformly transported hydraulically through the joint. Erosion depths of CTSG samples in Figure 29 were higher than those of CTB samples in Figure 30 as expected, since CTSG has more erodible fines than CTB.
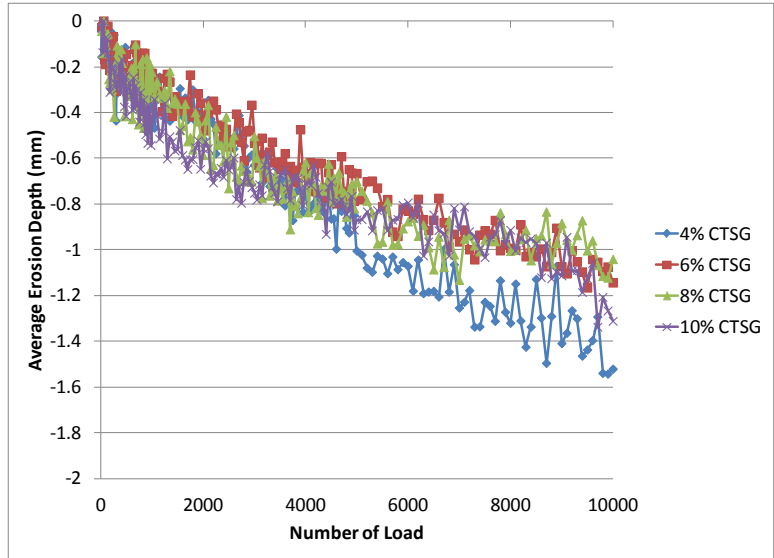
Figure 29. Average Erosion Depth of CTSG Using HWTD.
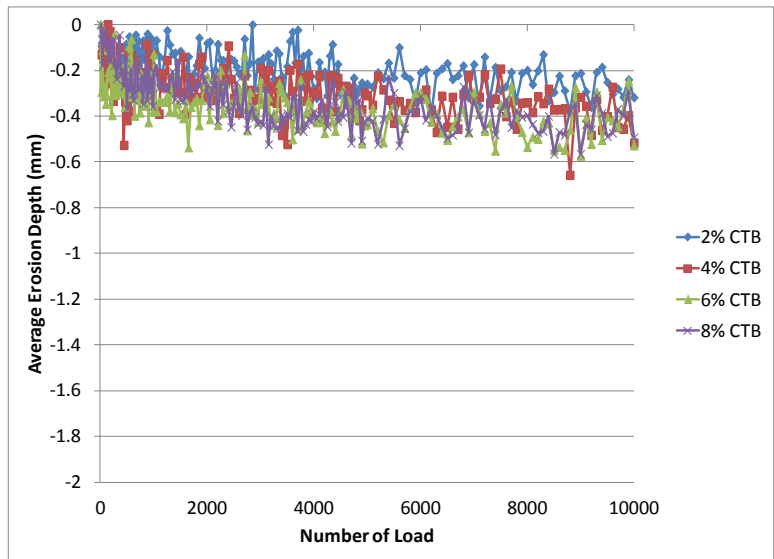
Figure 30. Average Erosion Depth of CTB Using HWTD.

Figure 31 and Figure 32 show the analysis of erodibility versus cement stabilization level. Test results of subgrade samples in Figure 31 show lower erodibility when cement content increases, but the test results of subbase samples in Figure 32 show no significant change with different cement contents since subbase aggregate has very low erodibility consisting of only a small portion of erodible fines, which results in a good resistance to erosion.
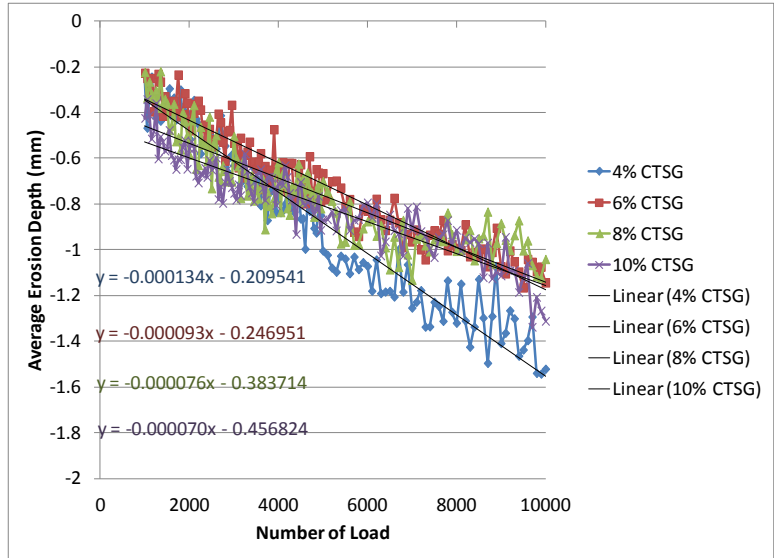
Figure 31. Erosion Rate of CTSG Using HWTD.
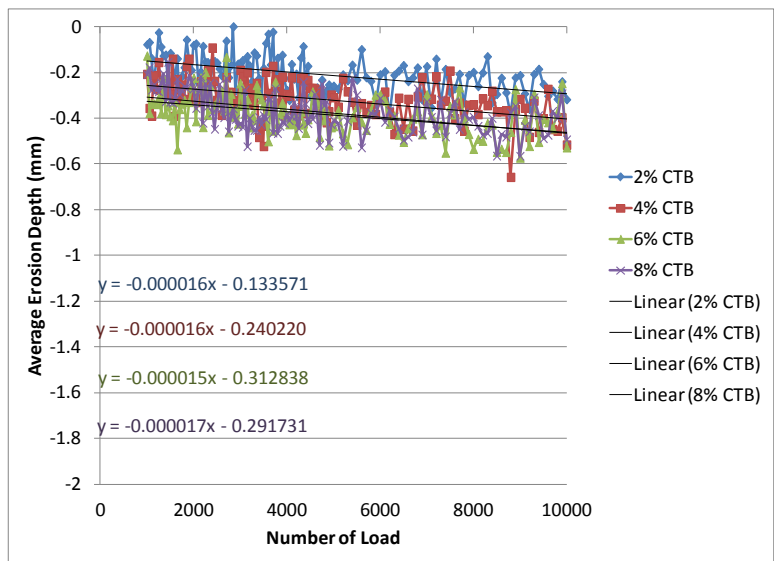
Figure 32. Erosion Rate of CTB Using HWTD.

Table 2 shows the mean erosion rate of CTSG and CTB using HWTD, and Figure 33 shows the regression model for the erosion rate of CTSG. Accordingly, more than 6 percent of the cement content is suggested for moderate erosion resistance if the subgrade layer would not have severe erosion based on the subbase design recommendation in Table 3 from TxDOT project 0-6037 (*2*). CTB materials are considered good erosion resistant materials for subbase design based on erosion rates measured by the HWTD test.

Table 2. Mean Erosion Rate Using HWTD.

CTSG Samples	Mean Erosion Rate (mm/10,000 load)	CTSG CTB Samples	Mean Erosion Rate (mm/10,000 load)
4% CTSG	1.34	2% CTB	0.16
6% CTSG	0.93	4% CTB	0.16
8% CTSG	0.76	6% CTB	0.15
10% CTSG	0.70	8% CTB	0.17
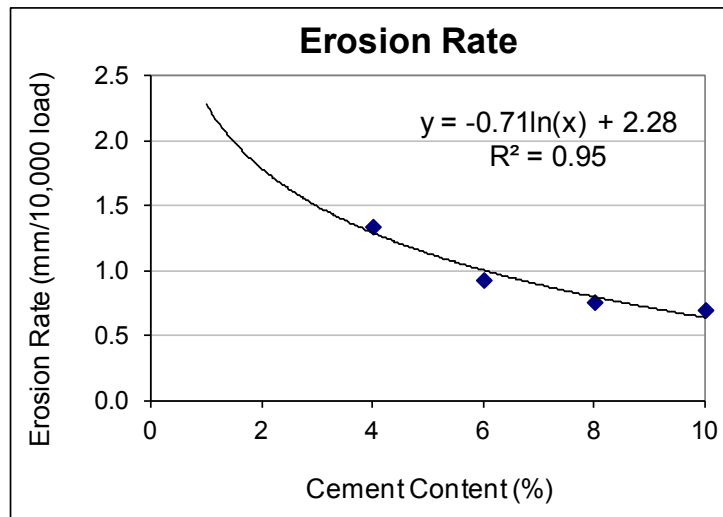
Figure 33. Regression Model of Erosion Rate of CTSG.

Table 3. Subbase Erosion Resistance Criteria in Design Factors (*2*).

Erosion Resistance	Mean Erosion Rate Using HWTD (mm/10,000 load)	Design Recommendation
Good	ER < 0.5	Acceptable
Moderate	0.5 < ER < 1	Add more stabilizer if frequently saturated condition
Poor	1 < ER	Add more stabilizer or change material type or gradation
Very poor	1.5 < ER	Change material type or gradation

EROSION TEST RESULTS – FIELD CORE SUBGRADE SAMPLES

Three subgrade cores and one AC (Type B) core from the construction field site were tested to demonstrate the evaluation of erosion resistance based on a field sample. Figure 34

shows average erosion depth versus load using HWTD, and Figure 35 shows the analysis result of erodibility.
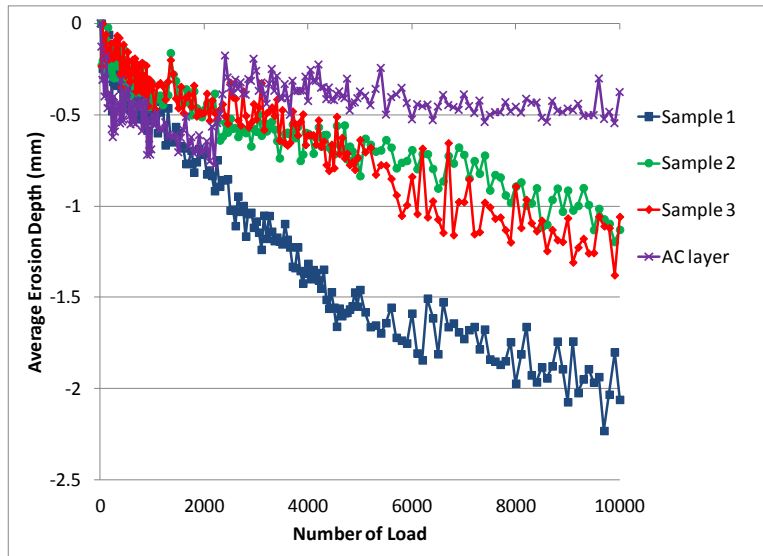
Figure 34. Average Erosion Depth of Core Samples from FM 1938.
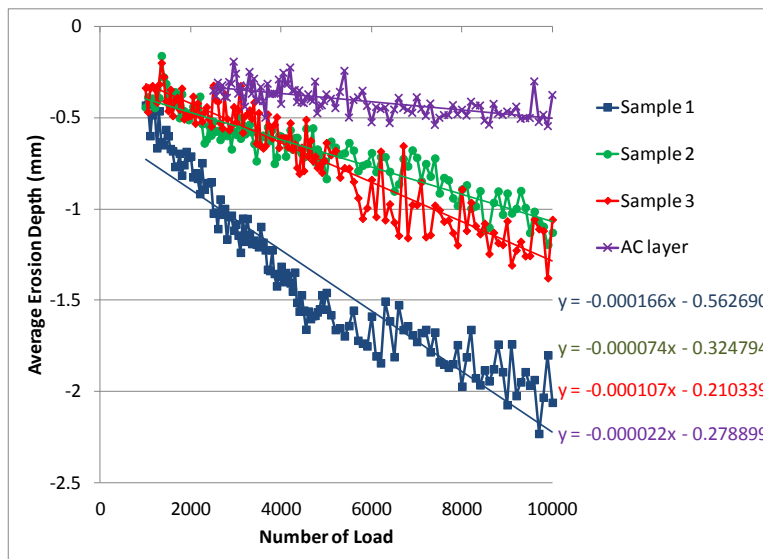
Figure 35. Erosion Rate of Core Sample from FM 1938.

Sample 1 showed very poor erosion resistance, and sample 2 showed moderate erosion resistance. Sample 3 showed poor erosion resistance as shown in Table 4 based on the subbase design recommendation. These different results were possibly caused by irregular cement allocation and mixing during cement stabilization in the field. The cement content of each sample can be back-calculated based on lab sample test results and regression model as shown in Figure 36 and Table 4. Design cement content for subgrade stabilization is 4.5 percent, and the corresponding erosion rate is 1.2 mm/10,000 load. AC core showed good erosion resistance as

33

anticipated. As indicated earlier, the cement stabilized subgrade is used underneath the subbases; none of the concrete will be placed directly on cement stabilized subgrade. However, the results are interesting in that it shows finely graded materials can still be erosion susceptible even with rather high cement contents.

Table 4. Erosion Rate and Estimated Cement Content of Field Cores.

Sample ID	Mean Erosion Rate Using HWTD (mm/10,000 load)	Erosion Resistance	% of Cement
Sample 1	1.66	Very Poor	2.4%
Sample 2	0.74	Moderate	8.7%
Sample 3	1.07	Poor	5.5%
AC	0.22	Good	N/A
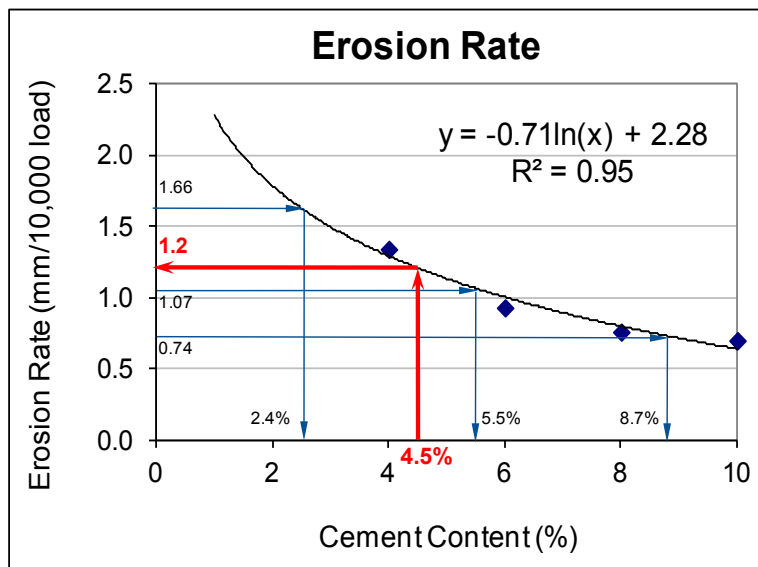
Figure 36. Estimated Cement Content of Cored CTSG Sample.

SUMMARY

Erosion testing using the HWTD was conducted to evaluate the cement stabilized subgrade and subbase samples from the FM 1938 CRC pavement construction area. The erosion resistance of the cement treated subgrade materials was increased along with more cement in the sample while the erosion rate of subbase material was not changed significantly by cement content since subbase materials have a very low percentage of erodible fines. Cored cement stabilized subgrade samples showed a range of erosion rates because of irregularity of cement stabilization in the field.

REFERENCES

1. Webster, S.L., R.H. Grau, and T.P. Williams. "Description and Application of the Dual Mass Dynamic Cone Penetrometer. Instruction Report GL-93-3," Department of Army, Waterways Experiment Station, Corps of Engineers, Vicksburg, Mississippi. 1992. p. 50.

2. Youn su Jung, Dan G. Zollinger, Byoung Hooi Cho, Moon Won, and Andrew J. Wimsatt. "Subbase and Subgrade Performance Investigation and Design Guidelines for Concrete Pavement," Research Report 0-6037-2. Texas Transportation Institute, The Texas A&M University System, College Station, TX. Submitted December 2011.

3. Phu, N.C., and M. Ray. "The Hydraulics of Pumping of Concrete Pavements." Bulletin de Liaison des Laboratoires des Ponts et Chaussees, Special Issue 8, France. July 1979. pp. 15–31.

CHAPTER 4 EVALUATION OF PCC PAVEMENT STRUCTURAL RESPONSES

Various gages were installed in concrete slabs and the data downloaded on a periodic basis. Various gages, including vibrating wire strain gages, relative humidity (RH) sensors, thermo-couple wires, concrete displacement gages, and steel strain gages, were installed in the slabs to measure in-situ drying and plastic shrinkage, coefficient of thermal expansion (CTE), and other pertinent parameters of the in-situ concrete and steel.

INSTALLATION OF VARIOUS GAGES

Steel and concrete strains and stresses were measured by various gages as described above. Figure 37 shows various gages installed in the field.
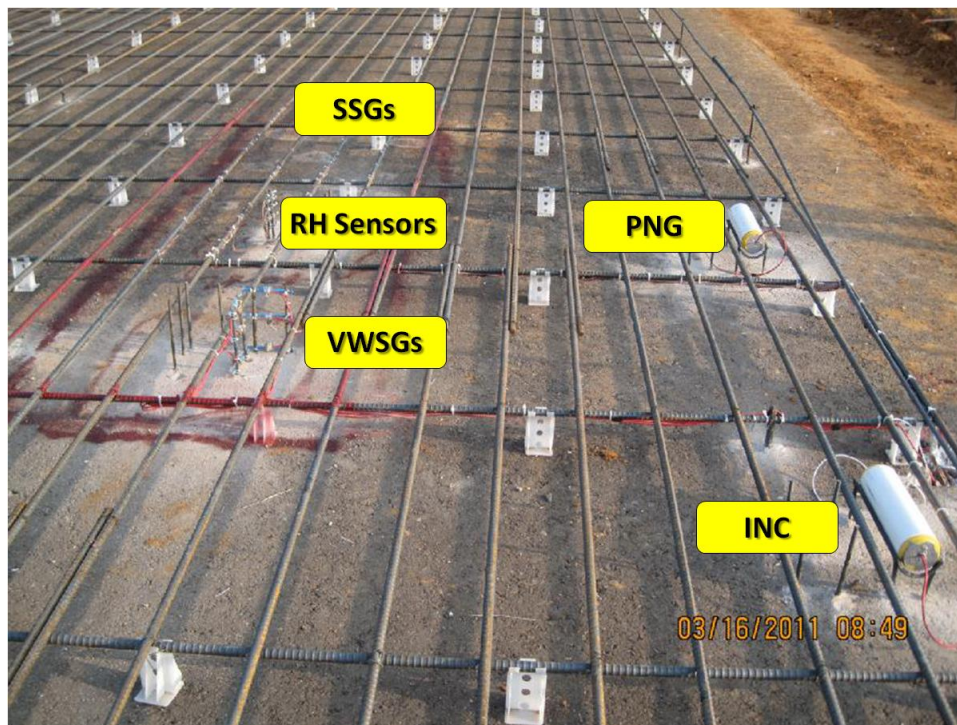
Figure 37. Various Gage Installations.

Figure 38 shows vibrating wire strain gages (VWSGs) installed in the longitudinal and transverse directions at three different depths (1.25 inches, 4.25 inches, and 8 inches from the concrete surface).

VWSGs	Depth [in]
Trans_Bot	8.00
Trans_Mid	4.25
Trans_Top	1.25
Long_Bot	8.50
Long_Mid	4.25
Long_Top	1.25
PNC	4.50
INC	4.50
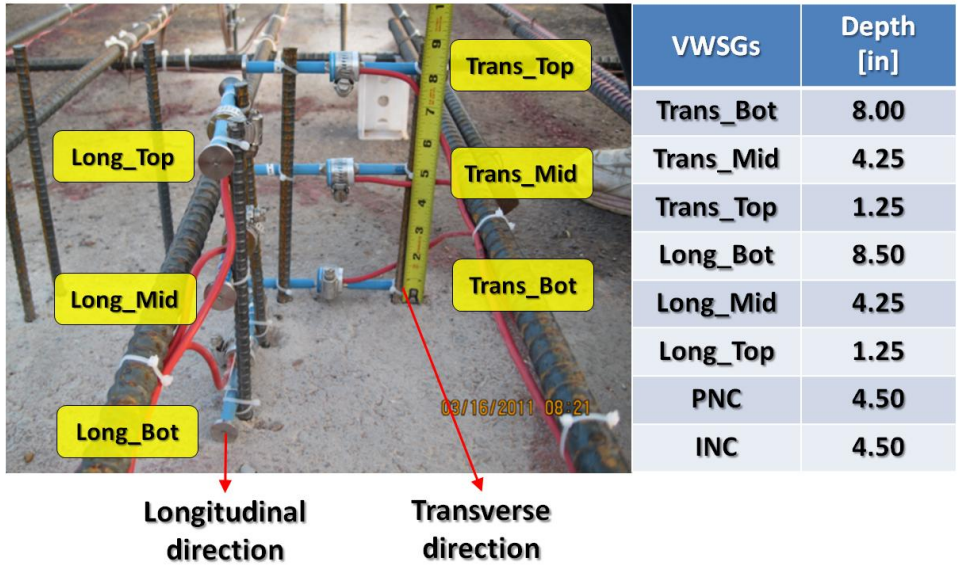
Figure 38. Vibrating Wire Strain Gages.

RH sensors were installed to measure relative humidity variations at five different depths (1 inch, 2 inches, 3 inches, 4.25 inches, 6 inches, and 8.5 inches from the concrete surface) as shown in Figure 39.

Figure 39. RH Sensors.

38

The installation of non-stress cylinders (NC) and concrete displacement gages are shown in Figure 40 and Figure 41, respectively.
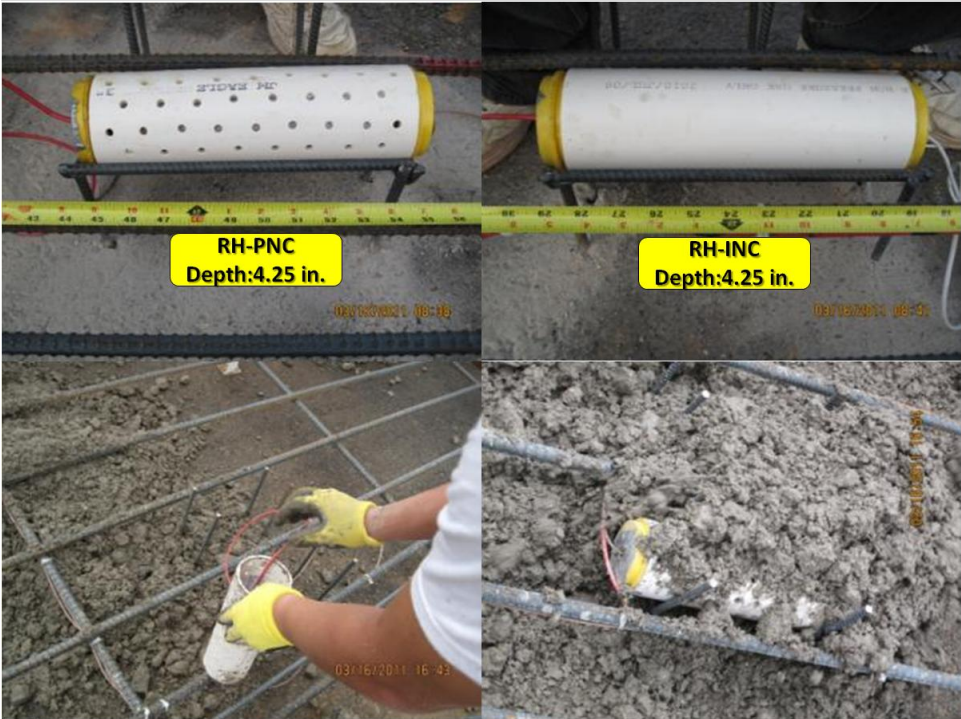
Figure 40. Non-Stress Cylinders.

Figure 41. Concrete Displacement Gage.

Laboratory testing was done for the evaluation of concrete properties including setting of concrete, compressive strength, flexural strength, and drying shrinkage. Concrete was placed on August 8, 2011, for the second section and on March 15, 2011, for the fourth section. The information on concrete setting times is illustrated in Table 5, Figure 42, and Figure 43.

Table 5. Setting of Concrete.

Test Section	Concrete Placement	Initial Set [min]	Final Set [min]
2nd	08/08/2011	303	357
4th	03/15/2011	402	539
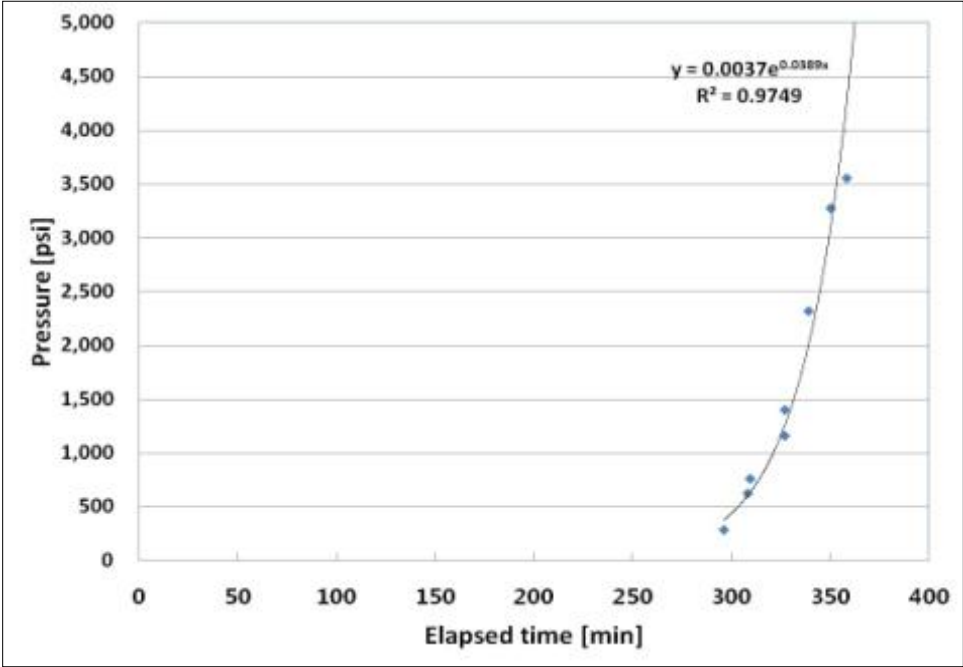
Figure 42. 2nd Section Concrete Setting.
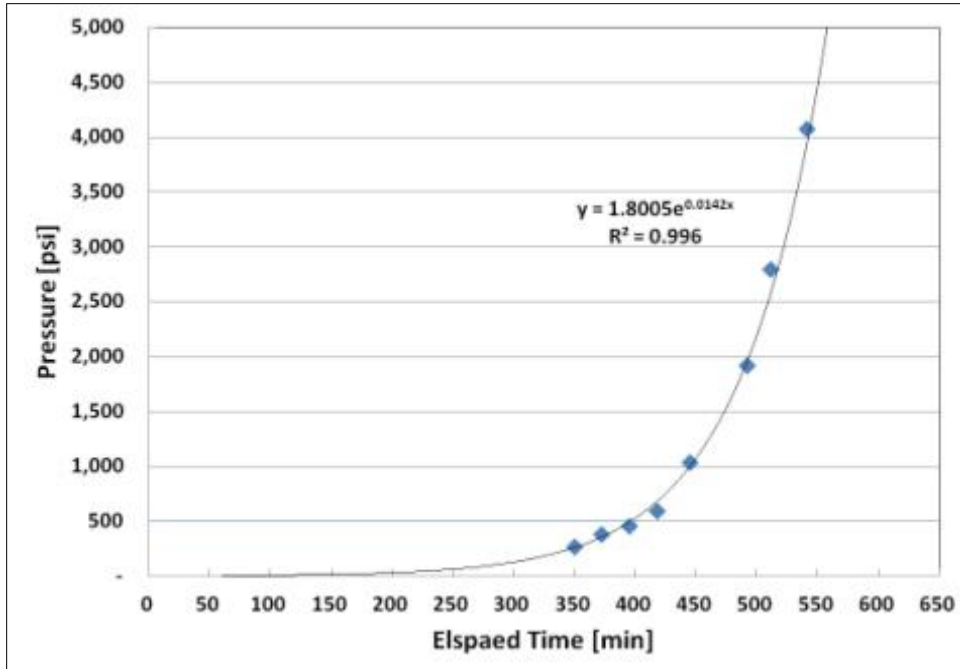
Figure 43. 4th Section Concrete Setting.

The results of compressive strength measured at 1, 3, 5, 7, 14, 28, and 56 days and flexural strength measured at 3, 7, and 28 days are shown in Figure 44–Figure 4747.
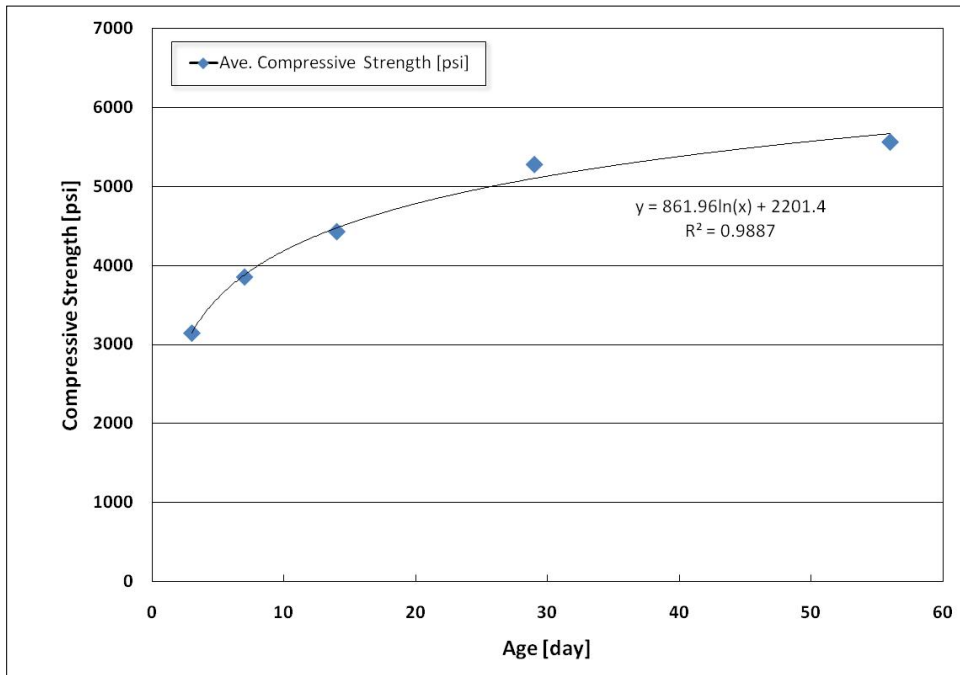
Figure 44. 2nd Section Concrete Compressive Strength.
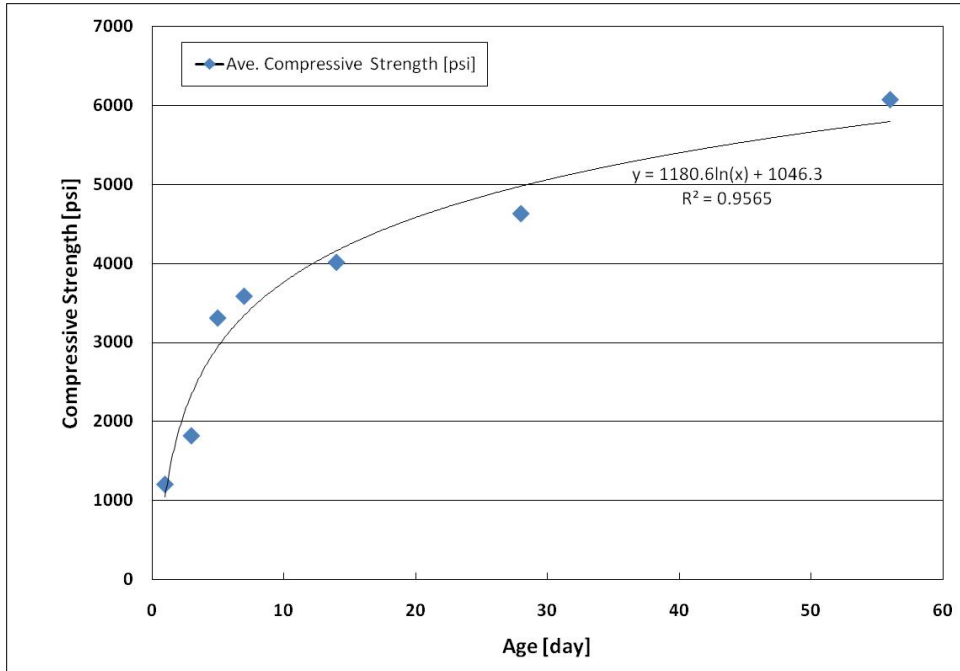
Figure 45. 4th Section Concrete Compressive Strength.
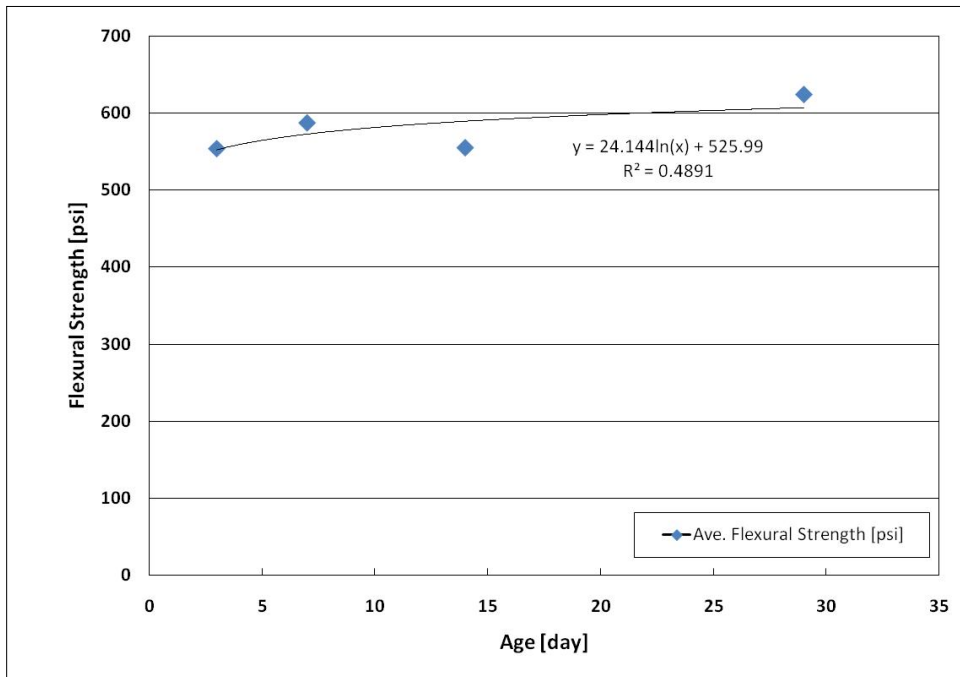
Figure 46. 2nd Section Concrete Flexural Strength.

42
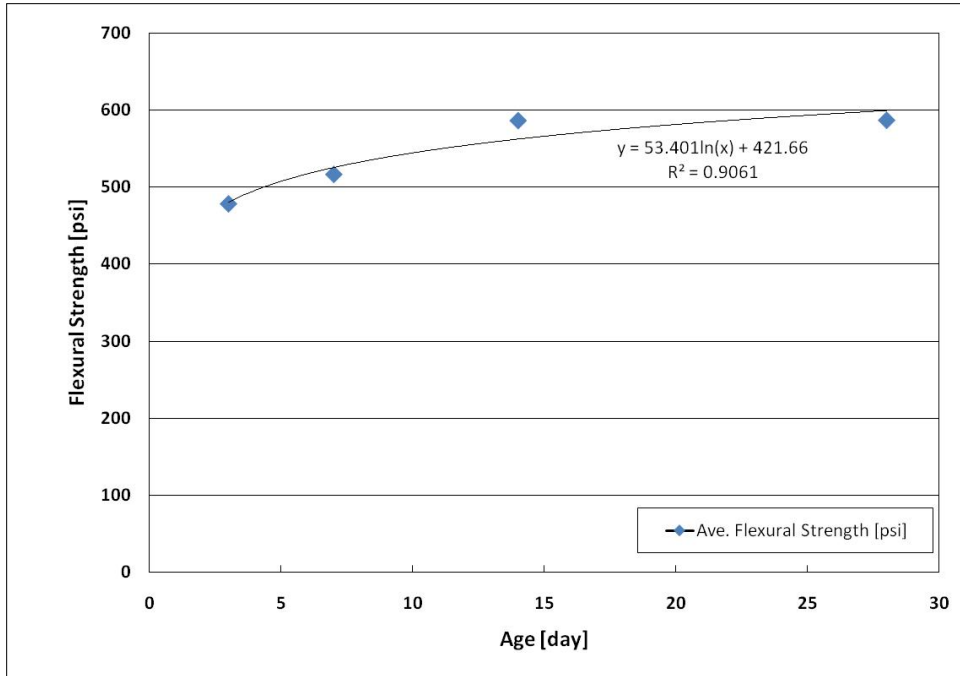
Figure 47. 4th Section Concrete Flexural Strength.

In-situ coefficient of thermal expansion (CoTE) of concrete was measured by using the concrete strain and temperature data from non-stress cylinders. As shown in Figure 48, CoTE value of 4.54 microstrain/ºF was obtained.
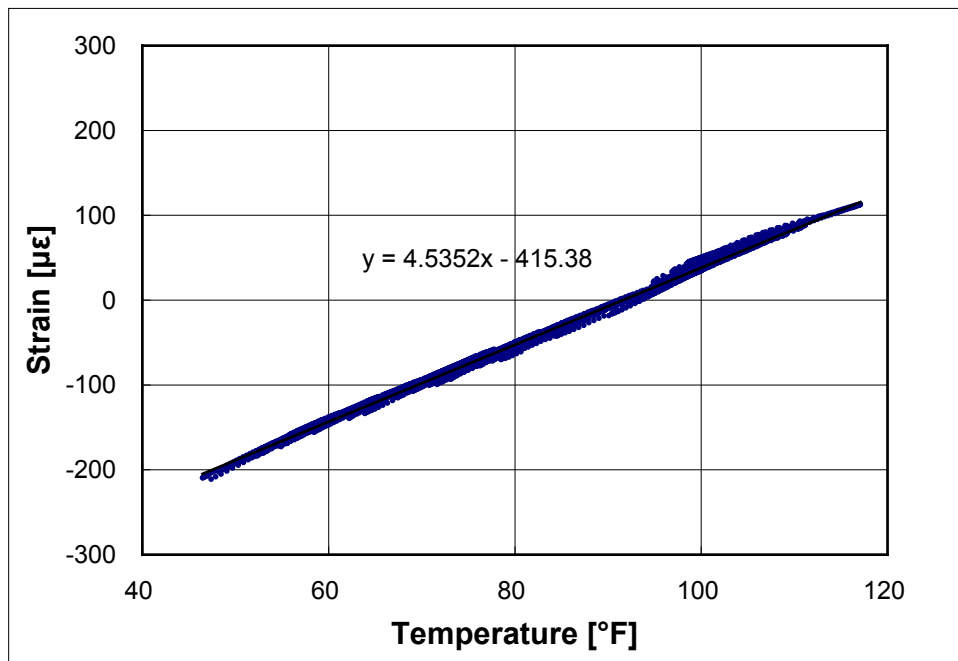
Figure 48. In-situ CoTE.

Long-term in-situ drying shrinkage can be evaluated from the concrete strain data in the non-stress cylinders as shown in Figure 49. It shows that the drying shrinkage is quite small. The NCs were installed at the mid-depth of the slab, which could explain low drying shrinkage in the concrete.
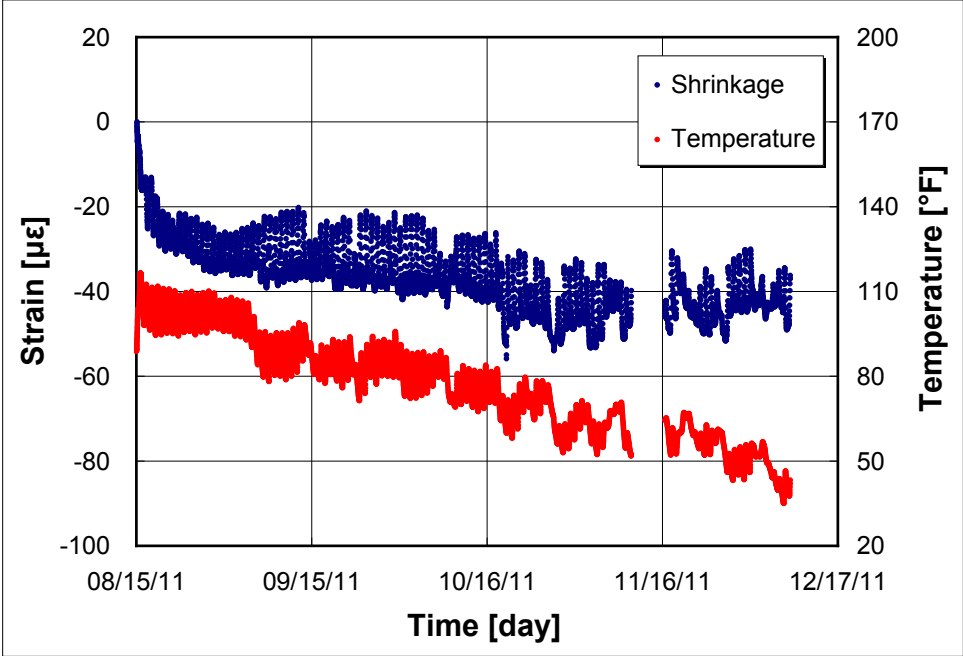
Figure 49. In-situ Concrete Drying Shrinkage.

Zero-stress temperature (ZST) for each subsection was analyzed, and the results are shown in Figure 50–Figure 52. In the analysis, strains due to stresses were isolated from total strains by subtracting thermal strains.
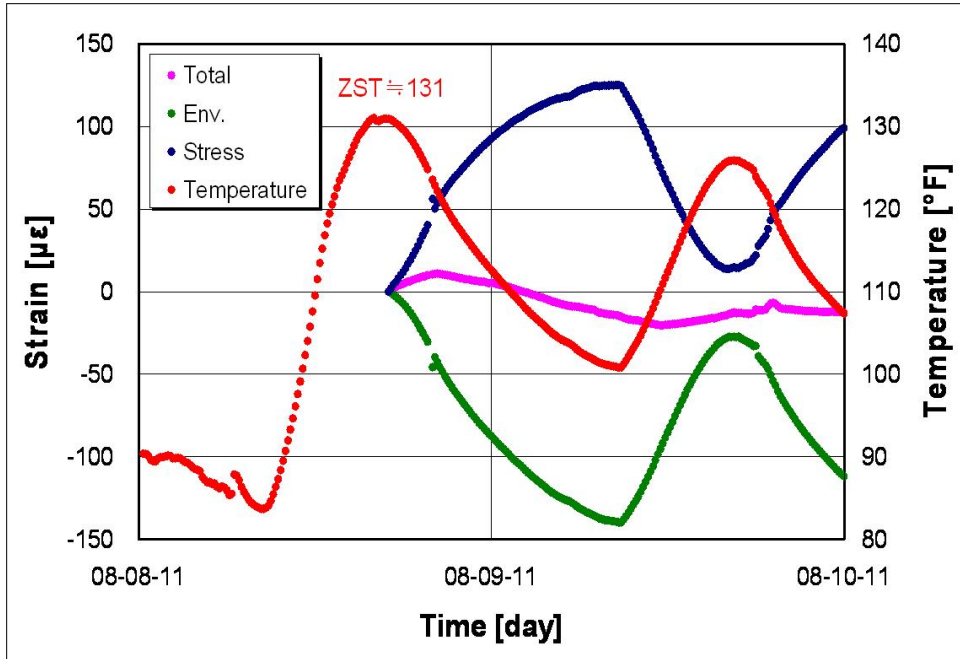
Figure 50. 2nd Section Zero-Stress Temperature.
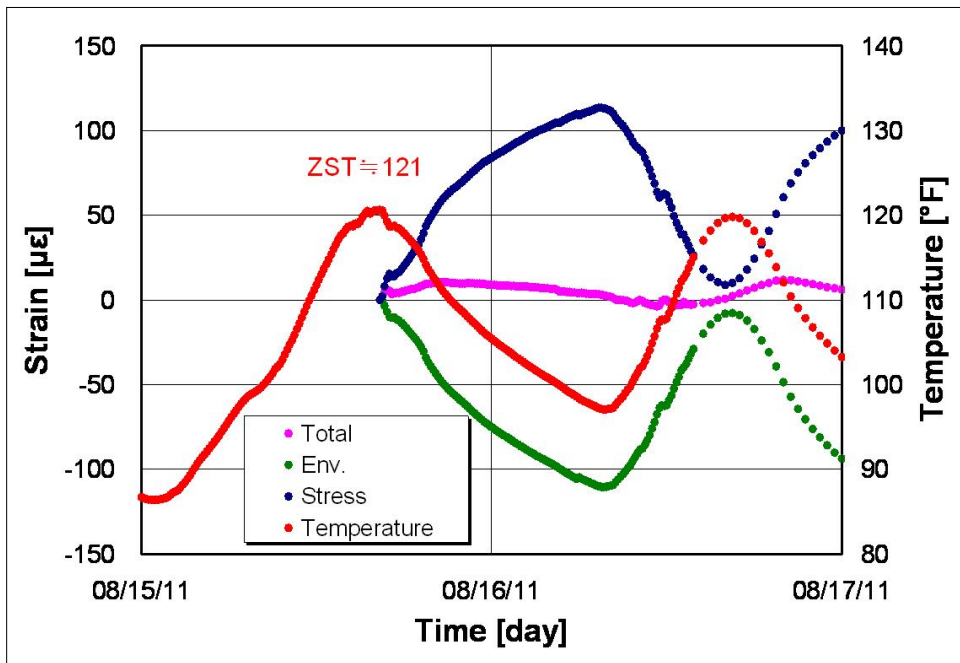
Figure 51. 3rd Section Zero-Stress Temperature.
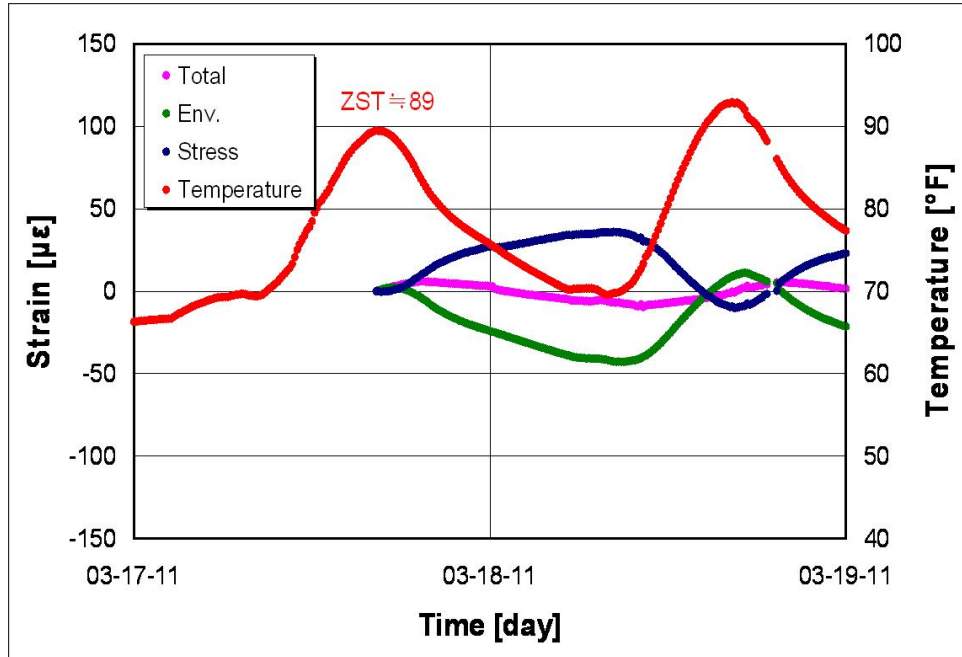
Figure 52. 4th Section Zero-Stress Temperature.

EVALUATION OF SUBBASE FRICTION

In this project, two distinctive base types were used: Type D hot mix and nonwoven geotextile. The frictional characteristics of those two base types were evaluated using the concrete prisms as shown in Figure 53.
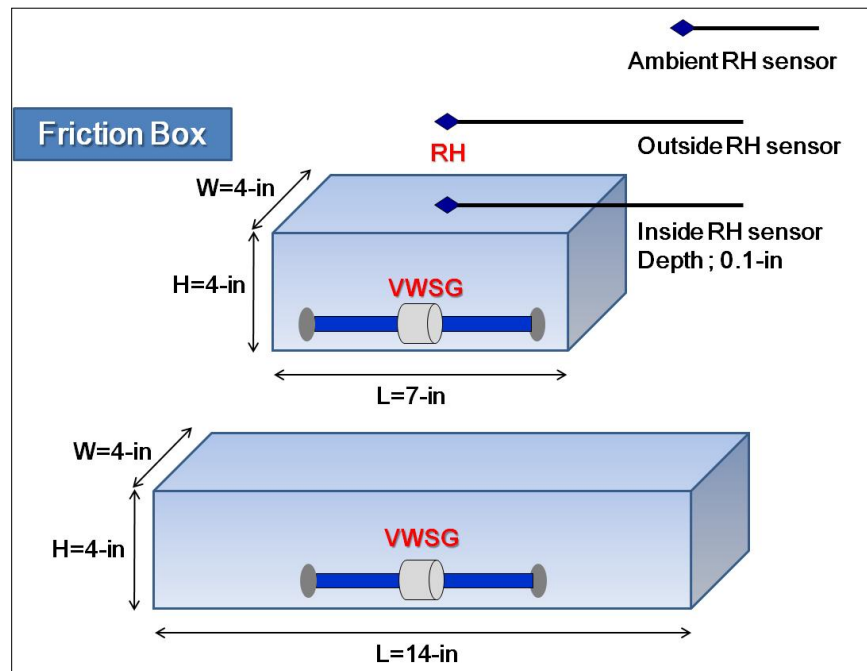
Figure 53. Concrete Prisms for Friction Evaluation.

46

Prisms with 4 inches×4 inches×7 inches and 4 inches×4 inches×14 inches with vibrating wire strain gages and RH sensor embedded were cast on two different subbase types as shown in Figure 54.

Figure 54. Concrete Prisms Cast at Field.

Figure 55 shows the concrete strain variations in the concrete prisms on nonwoven geotextile are much larger than those on Type D hot mix surface. It indicates that the friction on Type D hot mix surface is larger than on nonwoven geotextile. With less friction, restraints from subbase will be smaller and concrete prisms can move more freely. Figure 56 shows transverse crack spacing distributions in the second and third sections. Nonwoven geotextile was used in the third section. Figure 56 shows that the portion of crack spacing larger than 10 ft is greater in the third section than in the second section. Higher restraint caused by hot mix surface produced a higher stress level in concrete resulting in more transverse cracks or cracks with shorter crack spacing.
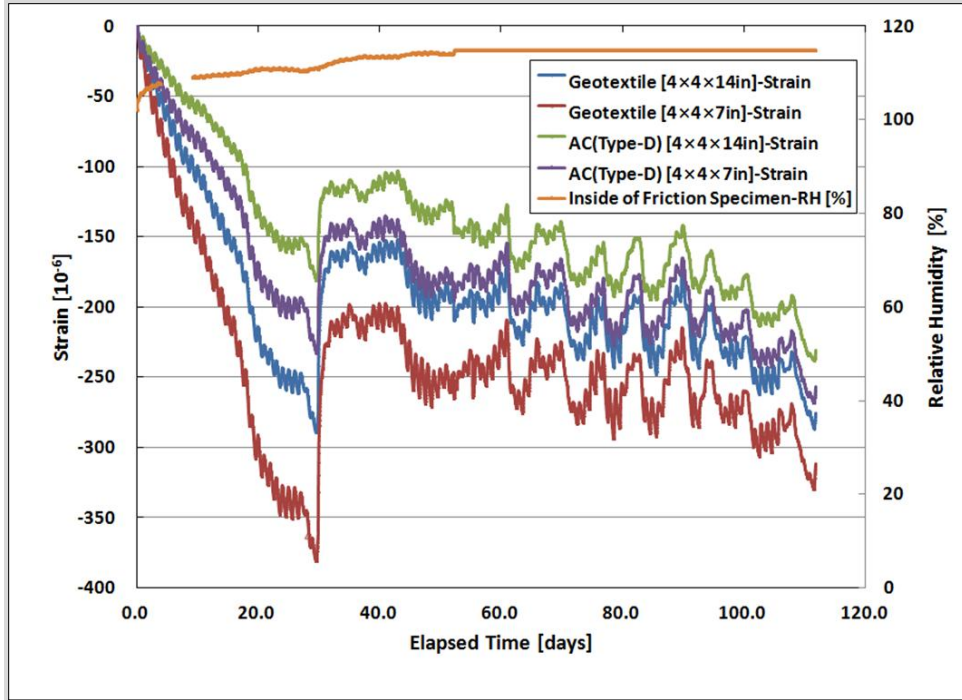
Figure 55. Concrete Prisms Strain.
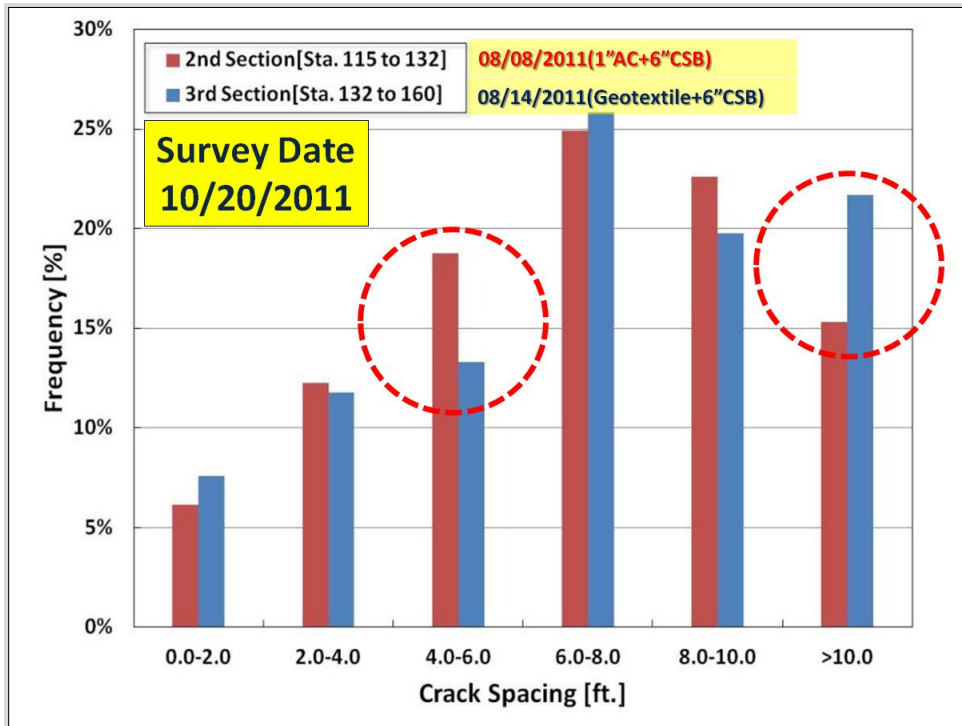
Figure 56. Transverse Cracking Pattern.

48

EFFECT OF BASE STIFFNESS ON CONCRETE CURLING

Variations in warping and curling due to subbases with different stiffness were measured by vertical concrete displacement gages. As shown in Figure 57, daily vertical movements at the edge of pavement became smaller as the daily temperature variation became small.
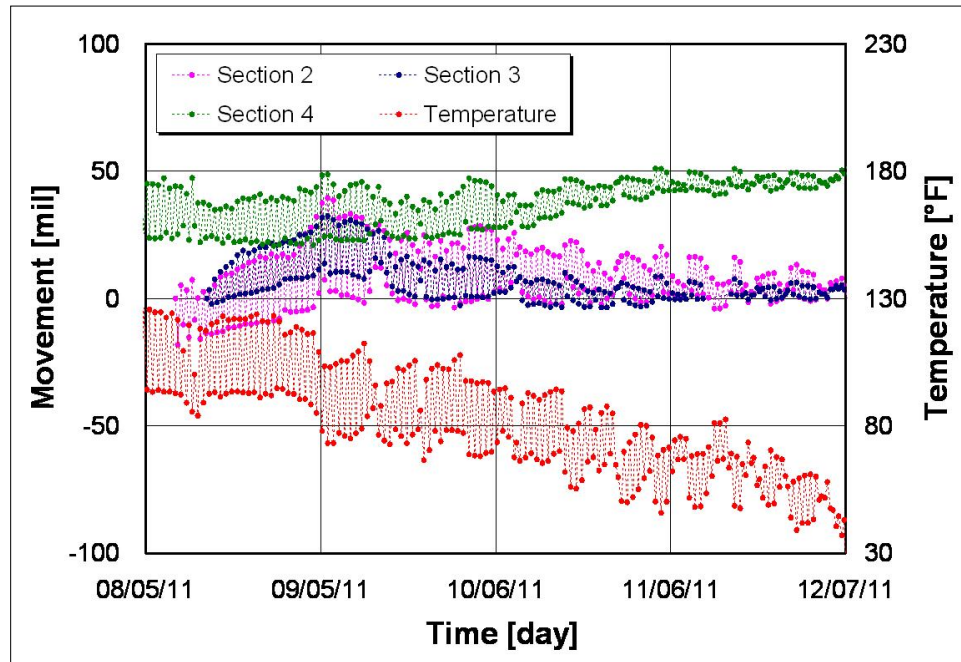
Figure 57. Vertical Movement.

Daily vertical movements at different test sections were compared with the *k*-values obtained by the AREA back-calculation method and PBT testing as shown in Figure 58 and Figure 59. The numbers in Figure 58 represent daily maximum and minimum movement values. Figure 59 illustrates good correlation between daily vertical movements and dynamic *k*-value obtained by the AREA method. As expected, daily variations in vertical movement increase with *k*-value.

49
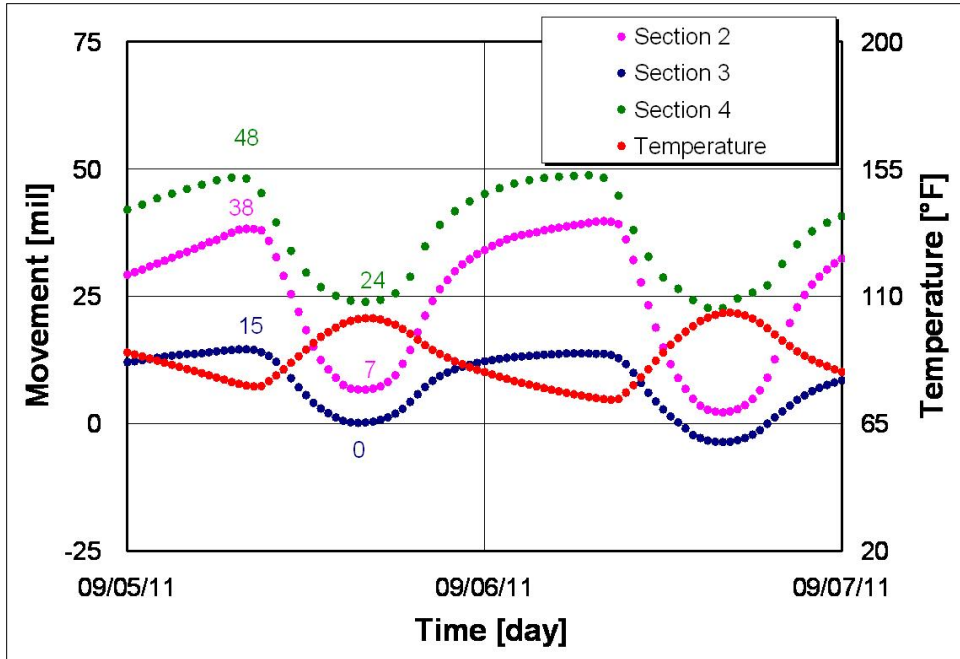
Figure 58. Daily Vertical Movement.
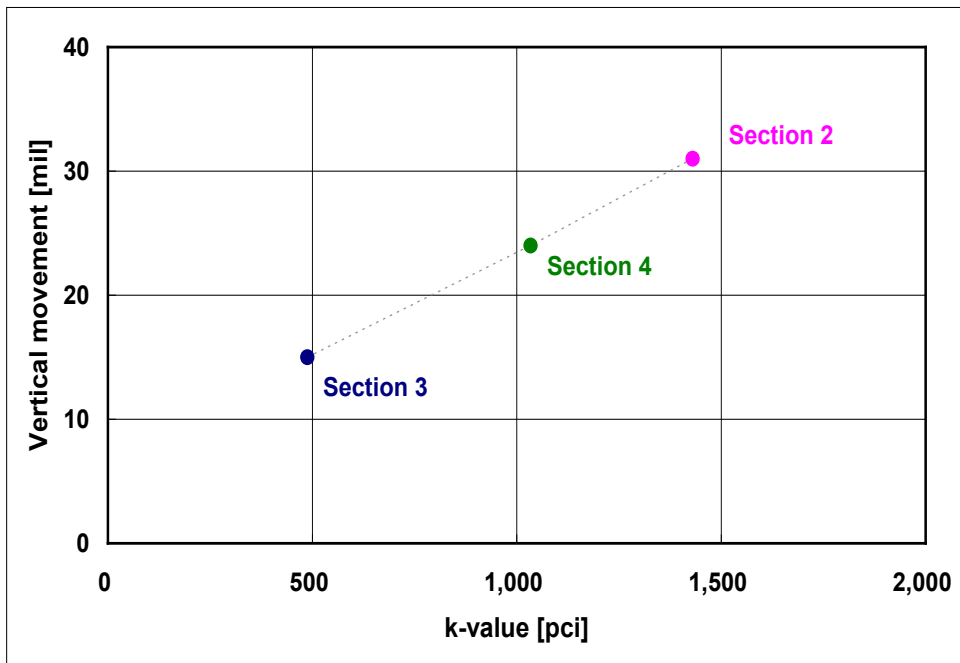
Figure 59. Daily Vertical Movement Variation vs. *k*-Value (AREA).

CONCLUSIONS

In this study, concrete pavement behavior due to environmental loading (temperature and moisture variations) was evaluated with various gages. Base frictional characteristics of two base materials—asphalt and nonwoven geotextile—were evaluated with concrete prisms. The findings from this study can be summarized as follows:

1. Drying shrinkage at the mid-depth of the slab was quite small.
2. Base friction of nonwoven geotextile was smaller than that of asphalt layer. Smaller friction in nonwoven geotextile section resulted in larger transverse crack spacing.
3. Base stiffness has substantial effects on slab curling due to temperature variations in the concrete slab.

CHAPTER 5 EVALUATION OF CONCRETE CURING EFFECTIVENESS USING CONCRETE ABRASION TESTING

INTRODUCTION

The large surface area-to-volume ratio of a concrete pavement, as a major difference in comparison to most other concrete structures, makes concrete paving highly susceptible to moisture loss through evaporation (*1*). Under the influence of certain field conditions, including a variety of combinations of temperature, relative humidity, solar radiation, and wind, excessive early-age water evaporation could occur at the surface of concrete pavement during construction. These climatic effects may induce detrimental impacts, i.e., high porosity, delamination (leading to spalling), and loss of strength that in the long-term eventually affects the quality of concrete pavement smoothness and riding quality (*2*).

To mitigate early-age moisture loss, application of a variety of curing technologies on the surface of concrete pavement has been widely used to minimize evaporation (*2*). Among the several methods of curing, liquid membrane-forming curing compounds are the most widely used to cure concrete pavements. As the curing compound is directly related to the curing performance, a technology for evaluating the effectiveness of the curing compound is indispensable.

However, the present methods for assessing the curing effectiveness are mostly non-existent, even though American Association of State Highway and Transportation Officials T 155 (AASHTO T 155 1997) and the American Society of Testing and Materials (ASTM C 156) describe a procedure to characterize the water retention capability of a curing compound. Inherent limitations are prevalent (*1*).

In this effort, an innovative approach was used based on measured relative humidity over time as an indication of concrete curing quality using the ATEK Concrete Maturity Meter (ACMM) device. A detailed view of this device along with a support plate is shown in Figure 60. Figure 61 shows a schematic view of the support plate, which consists of two chambers—one is sealed and the other is filtered through the top via the curing medium sprayed on a thin layer of mortar resting on a perforated surface of that chamber. Both chambers rest on bare concrete (since it is placed prior to the application of the curing compound) and provide a sampling space that is sufficiently large to be sampled by the relative sensors within the housings.

The sealed chamber represents near perfect curing conditions where the filtered chamber is subject to the vapor pressure trapped to the extent possible by the sprayed curing membrane and thus represents a measure of the quality of curing provided to the concrete surface. The chilled mirror sensors are the most suitable type of sensor to measure the relative humidity at the RH levels that develop within the sampling chambers.

| **Figure 60. ACMM System.** | **Figure 61. Schematic View of the System Support Plate.** | **Figure 62. ASTM C944 Abrasion Test Equipment.** |
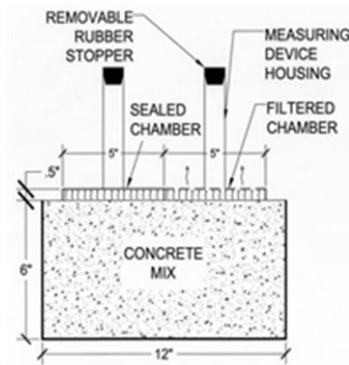
The RH measurements in both chambers were recorded for three days, as well as the sample moisture loss, which was recorded by using a high accuracy weighing scale throughout the test. At the same time, the dielectric constant (DC) was measured on the surface of the hardening concrete as an indication of the water content inside the hardened concrete. After three days, samples were tested for their abrasion strength based on ASTM C 944 as shown in Figure 62. Only the top ¾ inch of the surface of the samples was utilized in determining the abrasion strength of the concrete.

The present standard test, ASTM C 156-98, "Standard Test Method of Water Retention by Concrete Curing Materials," has some inherent limitations in assessing the curing effectiveness of concrete particularly under field conditions. A different approach was taken where abrasion strength of the surface concrete was related to an effectiveness index (EI). This index is based on relative humidity measures over time as means of assessing curing effectiveness. Also, moisture loss of concrete mortar and dielectric constant measurements of hardening concrete were taken to supplement RH measures. Samples were made using two different water to cement (w/c) ratios and were applied with two different curing compounds at two different rates of application. The utility of the test data to assess concrete curing compound effectiveness was evaluated.

MATERIALS AND METHOD

Concrete materials for the curing specimens consisted of ASTM Type I Portland cement and ASTM C 33 concrete sand. Mixture proportions followed those given in Table 6. Two different w/c ratios were used and test mixtures are prepared under laboratory conditions.

Table 6. Mixture Proportion.

Mixture	w/c	Unit Weight (lb/ft^3)		
		Water	Cement	Sand
	0.4	15.38	38.45	105.75
	0.43	16.53	38.45	102.69

Mortar preparation and mixing was carried out using an electrically driven mechanical mixer according to ASTM C 305, Standard Practice for Mechanical Mixing of Hydraulic Cement Pastes and Mortars of Plastic Consistency.

The research considered two different curing compounds in order to generate different levels of curing quality. The classifications of the curing compound samples are listed in Table 7. Type 2 denotes white-pigmented curing compounds. Class B denotes the solids in the compounds are resin-based.

Table 7. Classification of Curing Compounds to Be Tested.

Designation Name	Type	Comments
A	Type 2–Class B	Normal Resin-based
Lithium	Lithium-based	

Two levels of application rate were used in this project together with two types of the curing compounds and two levels of w/c ratio resulting in three main effects to be evaluated from the data collected during the testing program. As a result, eight samples were made and replicated. Due to the time constraint, only four test combinations were repeated. Tests were carried out in the environment of 32°C and 50 percent relative humidity with no wind. The design variables are listed in Table 8, and the factorial combinations are shown in Table 9.

Table 8. Different Levels of the Designs.

Variable	Unit	High Level	Low Level
Name of the curing compound		Class B	Lithium
Application rate of compound	ft^2/gallon	120	220
w/c of concrete mixture		0.40	0.43

Table 9. Factorial Testing Combinations.

Test #	w/c	Application Rate, ft²/gallon	Curing Compound	Repetition Done
1	0.4	120	Class B	Yes
2	0.4	220	Class B	In Progress
3	0.43	120	Class B	Yes
4	0.43	220	Class B	In Progress
5	0.4	120	Lithium	No
6	0.4	220	Lithium	No
7	0.43	120	Lithium	No
8	0.43	220	Lithium	No

Once the tests were finished, the RH results obtained from ACMM device were transferred and used to determine an effectiveness index that is based on a moisture-based maturity model. Equation 5.1 shows a moisture modification factor developed for the purposes of accounting for the effect of moisture on strength gain:

$$\beta_H = \left[1 + (7.5 - 7.5H)^4\right]^{-1}$$ (5.1)

Where:
β_H = moisture modification factor.
H = humidity of concrete.

The moisture modification factor represents the influence of moisture upon the rate of hydration. It is suggested that the temperature-based maturity may be adjusted by incorporating the moisture modification factor into the Nurse-Saul maturity function as (*3*):

$$M_H = \beta_H \cdot \sum_0^t (T - T_0).\Delta t = \frac{\sum_0^t (T - T_0).\Delta t}{1 + (7.5 - 7.5H)^4}$$ (5.2)

Where:
M_H = moisture-based maturity at age t of concrete.
T = average temperature of the concrete during time interval Δt.
T_0 = datum temperature with a value of $-10°C$.

In this project, the curing effectiveness index was characterized by the moisture-based maturity model, and the effectiveness index is then calculated by the following equation:

$$EI = \frac{M_f - M_a}{M_s - M_a}$$

(5.3)

Where:

M = equivalent age of the filtered curing condition.
M_s = equivalent age of the sealed curing condition.
M_a = equivalent age of the ambient curing condition.

This EI was used as an indication of the curing effectiveness throughout the experiment.

RESULTS AND DISCUSSION

Moisture loss results were recorded by using a high accuracy weighing scale by checking the weight periodically; results are shown in percentages, which were calculated from the weight loss of the sample at 12, 24, and 48 hours after placement divided by the sample original weight. The results shown in Figure 63 were the average of two samples if a test combination was repeated; the error bars are shown where applicable to represent the standard error for the repeated tests.
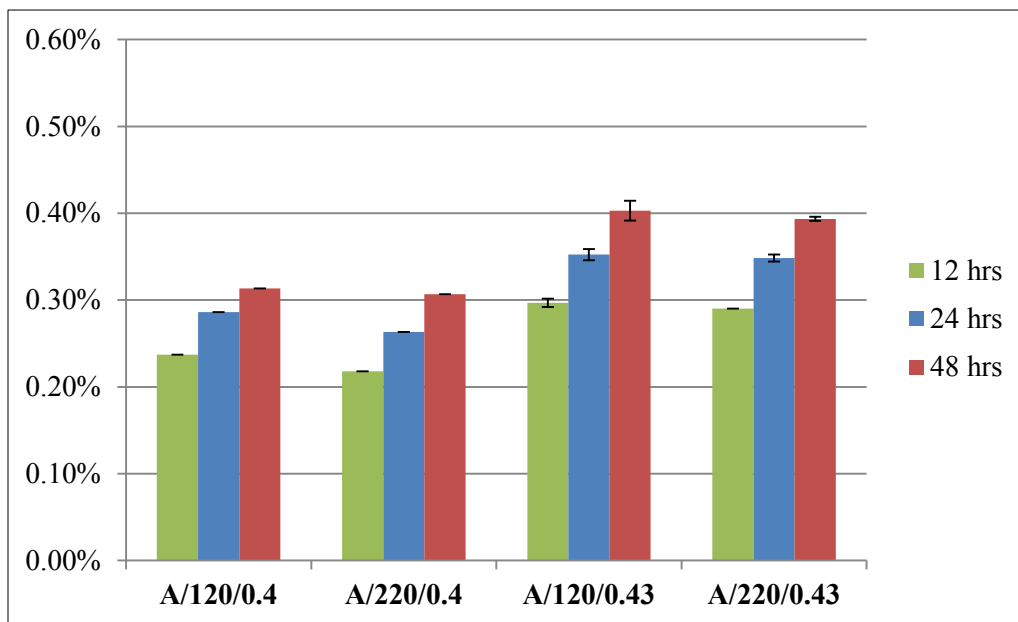
Figure 63. Moisture Loss Results for Curing Compound A.[1]

---

[1] **Class A/120/0.4** iIn this figure the sample was cured with a Class A curing compound at a rate of 120 ft^2/gallons at a 0.4 w/c ratio.

Based on the results shown in Figure 63, samples with higher w/c ratio (0.43) always had a higher percentage of moisture loss than the samples with lower w/c ratio (0.4) regardless of the application rate or the curing compound used. This phenomenon could be due to a greater amount of bleeding water that was available at the surface in the higher w/c ratio samples than in the lower ones, which led to higher evaporation within the first 12 hours, considering that the differences of the moisture loss between the first 12 hours and 24 hours for all the samples were smaller than that of the first 12 hours.

Also, it was observed that at the same w/c ratio, a higher application rate was not always effective in limiting evaporation compared to samples with a lower application rate for the Class B curing compound. Samples prepared with a rate of 220 ft^2/gallon had comparable moisture loss results as the samples prepared with a rate of 120 ft^2/gallon. This phenomenon seems to indicate that a rate of 220 ft^2/gallon was high enough to maintain the moisture at a similar level as that experienced with a rate of 120 ft^2/gallon, which meant that the higher rate of application did appear to improve the retention of water in the samples.

The measurements of dielectric constant were also performed for each of the samples, which were correlated with the water content within the samples. Figure 64 shows the DC for each sample over the experiment, and the trend line of each DC curve was also plotted. The greater the DC value the greater the water content.
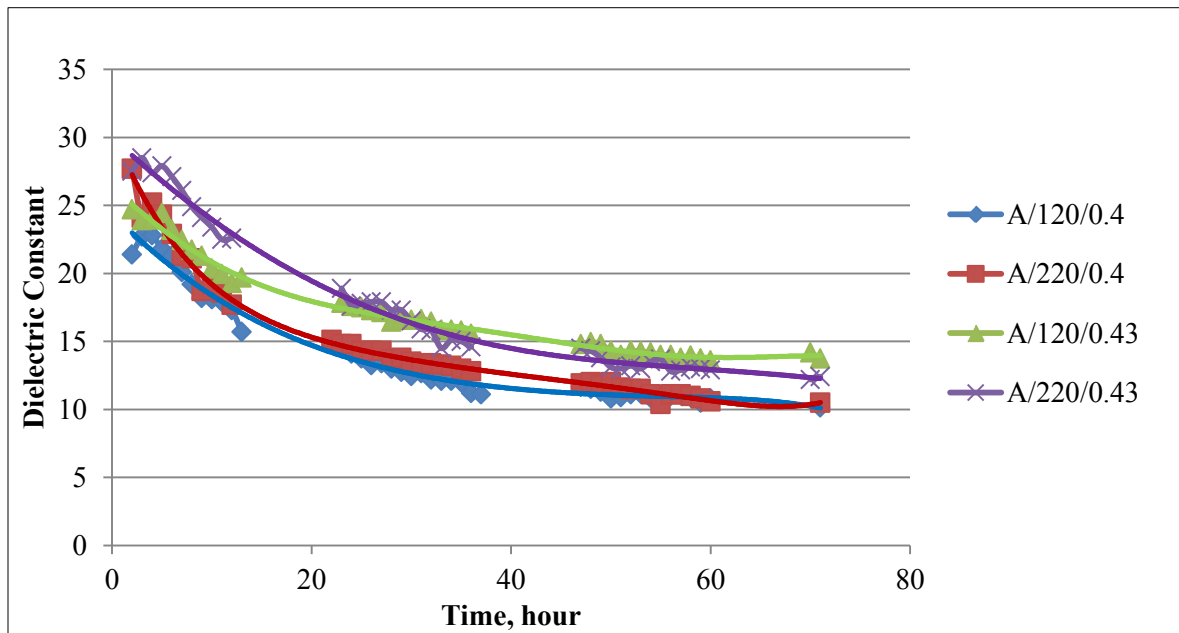
Figure 64. Dielectric Constants of the A Samples.

The results for DC indicated that the water content for samples made with a 0.43 w/c ratio were higher than the samples made with a 0.4 w/c ratio at the same application rate. Although the differences are small, samples made at a 0.43 w/c ratio with the higher application rate (120 ft^2/gallon) had higher DC values than samples made with a lower application rate (220

ft^2/gallon) after about 30 hours. This effect may be due to a higher rate of bleeding associated with a lower rate of application. Although this trend was not apparent in the moisture loss data it may be a result of the effect of the curing compound, where samples with the higher application rate retained moisture more effectively (with less bleeding) than the samples with the lower rate of application. For the samples at a 0.4 w/c ratio, the differences between the DC readings for the lower and upper rates of application were very small.

Based on the ACMM device, RH data of sealed and filtered chamber within the plate were measured, and EI was calculated and is shown in Figure 65. The values of EI were determined at 72 hours of curing. Also, the abrasion testing, which serves as an indication of curing quality, was conducted at an age of 72 hours (3-day age) and is summarized in Figure 66.
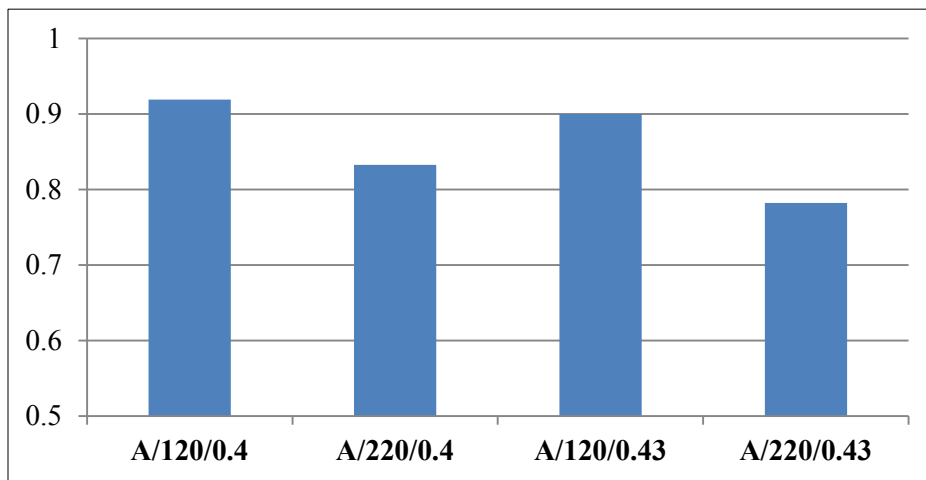
Figure 65. Effectiveness Index for Curing Compound A Samples.
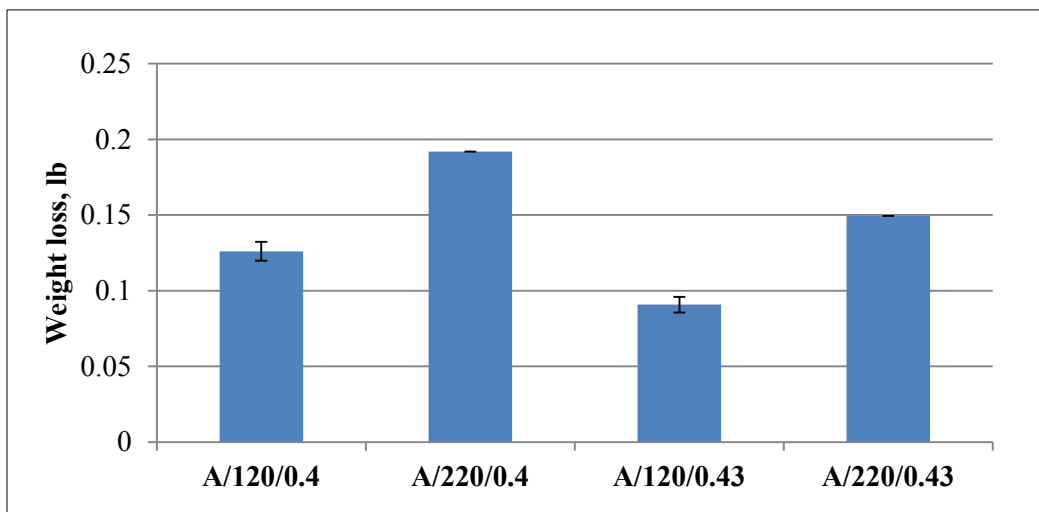
Figure 66. Abrasion Test Results for Curing Compound A Samples.

The EI and the abrasion test results were determined at a concrete age of three days; the results shown in the preceding figures showed a good correlation. For both 0.4 and 0.43 w/c

59

ratios, samples tested with a higher application rate (120 ft^2/gallon) exhibited higher EIs, indicating a better curing effectiveness compared to those made with the lower application rate (220 ft^2/gallon). The abrasion test results indicated the same level of correlation, where samples made with the higher application rate (120 ft^2/gallon) lost less weight, exhibiting a better curing quality than the samples made with the lower application rate (220 ft^2/gallon) which exhibited a greater amount of weight loss.

The ASTM C 156-98 moisture loss data did not appear to be entirely useful in evaluating curing quality. That is, when the application rate of a certain curing compound exceeds a certain amount, increasing the application rate may not be helpful to decrease the moisture loss. In this case, the Standard Test ASTM C 156-98 would not be useful even if the curing quality was improved by increasing the application rate. On the other hand, the EI did a better job in the same situation; the increased application rate did show a significant effect on improving EI, which indicated a better curing quality. Also, the abrasion test served as a better reference as it directly measures the surface strength of cured concrete in comparison to the surface concrete curing quality.

RESULTS AND DISCUSSION FOR LITHIUM SAMPLES

For moisture loss, test results of samples cured with lithium are shown in Figure 67. The samples with higher application rate (120 ft^2/gallon) showed less moisture loss compared to the samples with lower application rate (220 ft^2/gallon) for both 0.4 and 0.43 w/c ratios, especially during the first 12 hours. This seems to indicate that samples with the higher application rate had better curing quality for lithium curing.
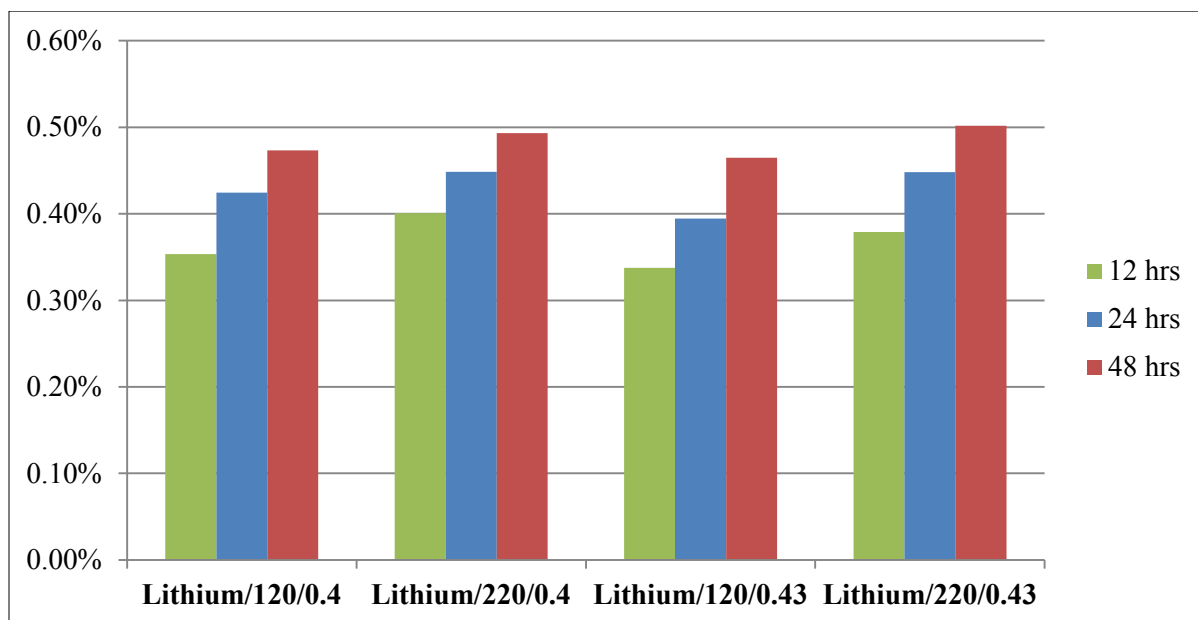
Figure 67. Moisture Loss Results for Lithium Cured Samples.

DC results shown in Figure 68 seemed to vary in comparison to the results shown in Figure 64; one sample with a lower application rate had higher DC values as expected. This variability is likely due to similar amounts of bleeding action that characteristically is associated with lithium curing membranes. The primary difference in the DC values appears to be mainly due to the initial w/c ratio.
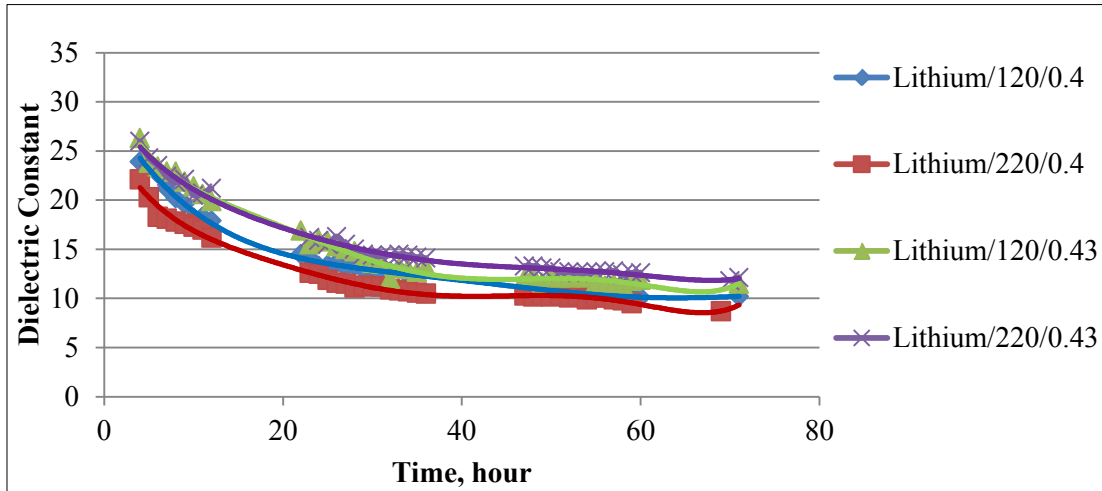
Figure 68. Dielectric Constants of the Lithium Samples.

Based on the results shown in Figure 69 and Figure 70, the 0.4 w/c ratio samples with a higher application rate led to higher EI and lower abrasion weight loss which indicates the higher application rate results in better curing quality. However, for the 0.43 w/c ratio samples, sample Lithium/120/0.43 showed lower EI but had a similar weight loss in the abrasion test compared to sample Lithium/220/0.43.
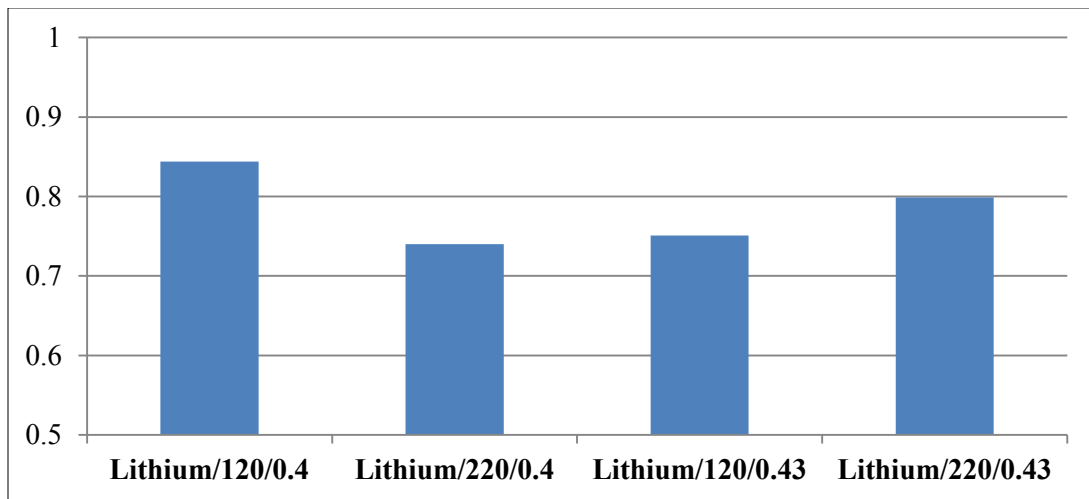
Figure 69. Effectiveness Index for Lithium Samples.

61
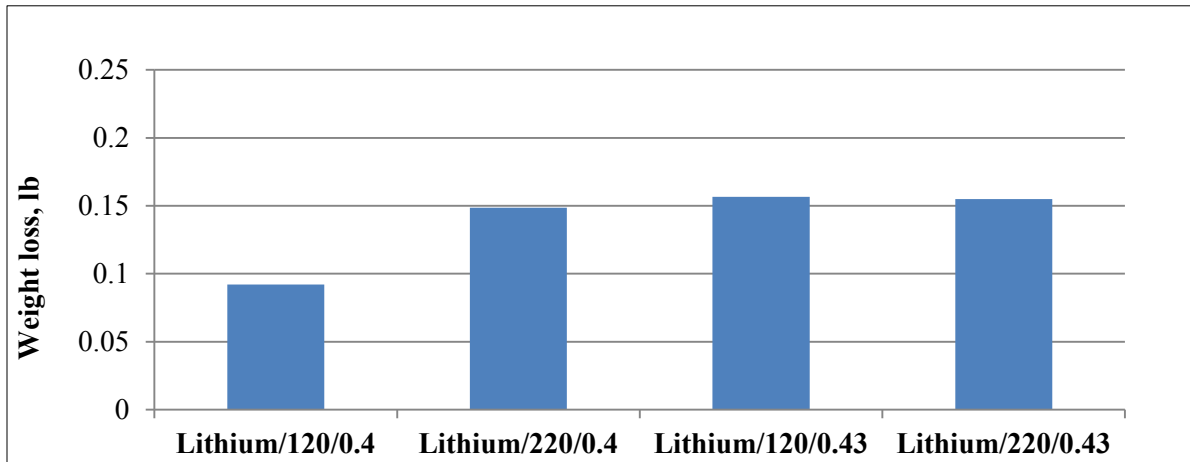
Figure 70. Abrasion Test Results for Lithium Samples.
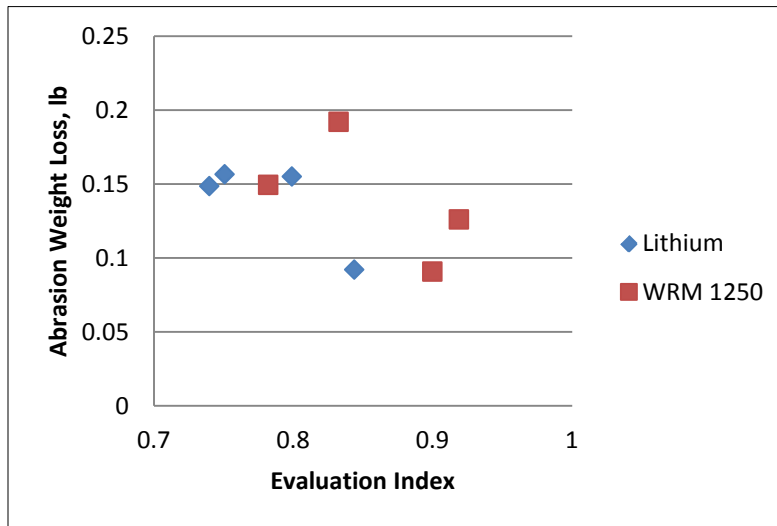
Figure 71. Correlation of EI to Abrasion Testing.

The EI correlated reasonably well with the abrasion test and DC, as shown in Figure 71. The greater the EI, the lower the loss was due to abrasion. The lithium compound also indicated a greater quality of curing, at least from the abrasion test results. Moisture loss data alone were much less distinctive (and in some cases contradictive) with respect to similar correlations.

FIELD TESTING

Several years ago during construction of SH 130 near Hutto, Texas, a small test section of curing quality was placed to examine its effect on the development of the cracking pattern. The pavement section was 12 inches thick and contained approximately 0.61 percent steel reinforcement using #6 bars. Curing compound consisting of the WRM 1250 placed at the

standard rate of 180 ft^2/gallon was compared against a section of pavement cured with the WRM 2250 product at the same rate of application. As can be seen in Figure 72, the higher quality curing compound actually resulted in a closer cracking pattern which may be due to a higher degree of porosity resulting from the bleeding effect that is likely not prevalent under the lower quality WRM 1250 product.
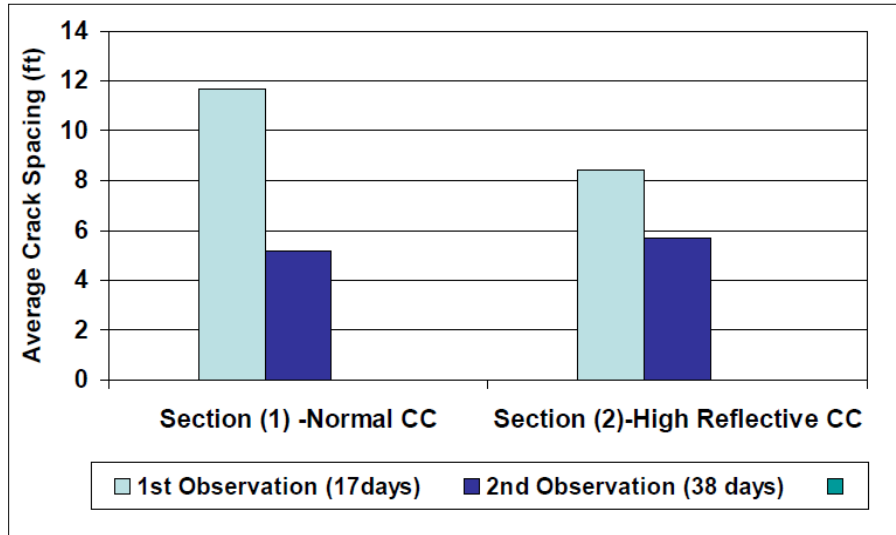
Figure 72. Effect of Curing Quality on Crack Development in CRC Paving (WRM 1250 vs WRM 2250) on SH 130.

Cracking patterns for the FM 1938 project are shown in Figure 73 for lithium and high reflective resin cure (HRRC) compound (i.e., WRM 2250) for SB Sta 104 to 106 and Sta 117 to 119. This pavement utilized a limestone aggregate, but as can be observed, the effect between the two types of curing compound is similar with respect to the final cracking pattern. However, the lithium compound did not affect the development of cracking as the HRRC compound had, as shown in Figure 72, due to the delayed effect of the lithium curing compound on total moisture loss.
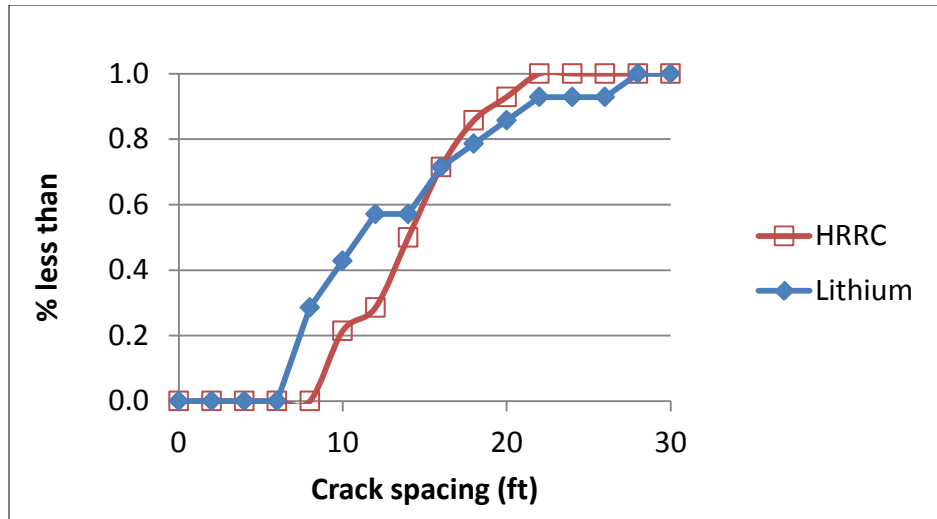
**Figure 73. Cracking Patterns of Lithium and HRRC (WRM 2250)
Cured Section on FM 1938.**

A small curing study was carried out in April 2011 in Victoria, Texas, on CRC paving using gravel aggregate. The resulting cracking patterns comparing WRM 1250 to lithium cure are shown Figure 74; the pavement section was 10 inches thick and contained approximately 0.6 percent steel. The crack pattern is similar to the cracking pattern achieved in the FM 1938 project, which is interesting due to the fact the paving consisted of gravel aggregate. Perhaps more noteworthy was the reduced amount of chipping that resulted in the lithium cured segments in comparison to the resin cured sections. As can be observed in Figure 74, the lithium curing reduced chipping, which is manifest as small chips of mortar breaking free of the gravel aggregate on the surface of the pavement. This distress type has little to do with the CoTE of the aggregate and more to do with the bond capacity of the coarse aggregate.
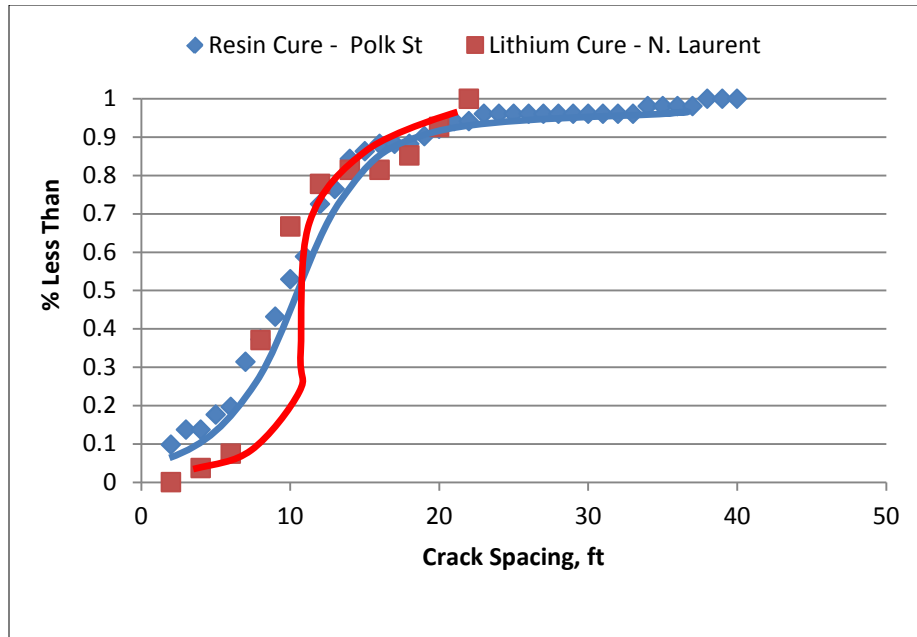
Figure 74. CRC Paving Crack Patterns in Victoria, Texas.

In addition to the effect of curing, base type and interface resistance effects were also manifest in the cracking patterns observed on the FM 1938 project as shown in Figure 75. The base type from Sta 115 to 132+00 was a 1-inch ACP over a 6-inch CSB. The base type from Sta 132 to 160+00 was a 6-inch CSB with a nonwoven geotextile, and the base type from Sta 160 to 205+00 was a 4-inch ACP. In comparison, the nonwoven geotextile affects the development of the cracking patterns by lengthening the average crack spacing by approximately 18 inches. Of great interest is the effect on the structural capacity of the pavement section. Using the FWD data, the effective slab thickness and the interfacial resistance were back-calculated (*4*) and illustrated in Figure 77. Clearly, the fabric significantly reduces the structural capacity of the pavement section by reducing the effective thickness and the interfacial resistance, which may in fact negatively impact the erodibility of the pavement section.

Figure 75. CRC Paving in Victoria, Texas, Showing Reduced Chipping and Spalling in the Lithium Curing Sections.
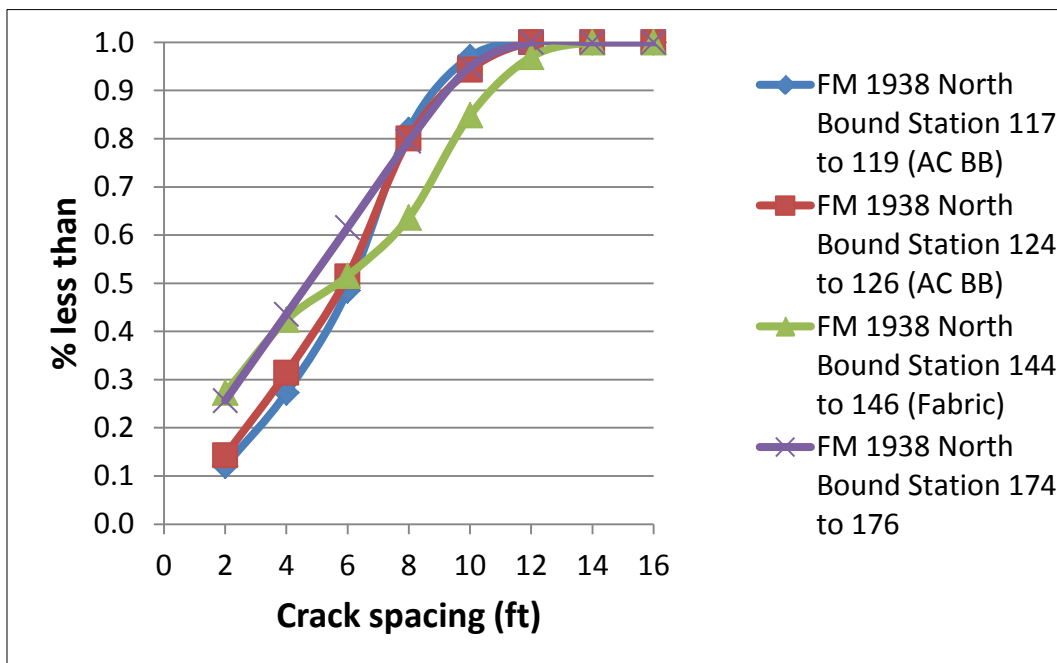
Figure 76. Cracking Patterns Manifest in FM 1938 CRC Paving.
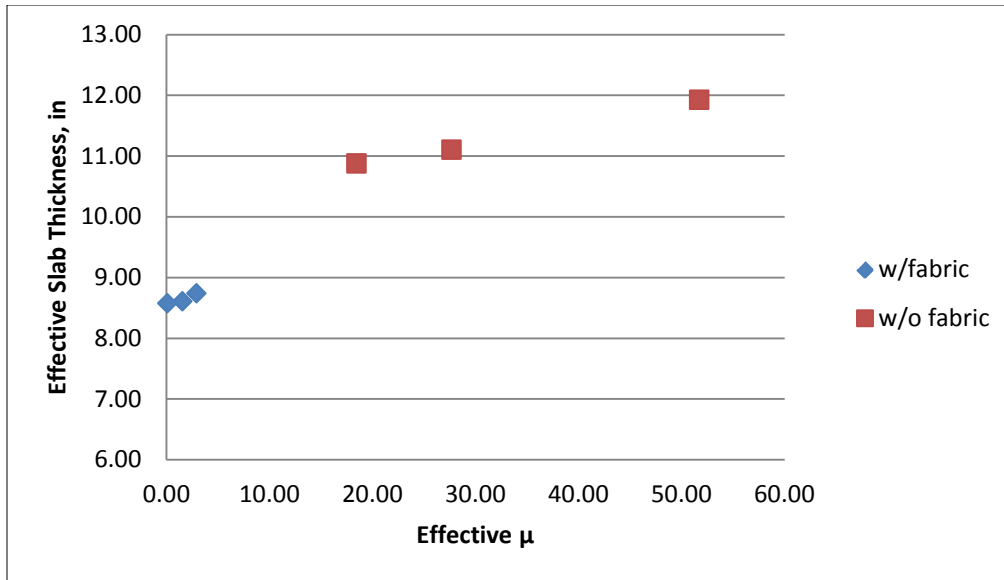
Figure 77. Effective Slab Thickness Back-Calculated from FWD Data – FM 1938.

CONCLUSION

The proposed curing compound evaluation protocol not only considered the moisture loss throughout the maturing process of concrete but also introduced the relative humidity, surface abrasion strength, and water content of cured concrete samples to assess the curing compound effectiveness. More importantly, EI showed good correlation with the abrasion test and DC data even with limited experimental results. The new protocol shows some promise as a means of evaluating the curing compound effectiveness.

REFERENCES

1. Ye, Dan. "A new performance-based approach to ensure quality curing during construction." Journal of Materials in Civil Engineering, Vol. 22. No. 7. 2010. pp. 687–695.

2. Ye, Dan, Anal K. Mukhopadhyay, and Dan G. Zollinger. "Laboratory and Field Evaluation of Concrete Paving Curing Effectiveness." Project FHWA/TX-10/0-5106-3. September 2009.

3. Jin Hoon, Jeong. "Development of a moisture-modified maturity model for Portland cement concrete pavements." The Baltic Journal of Road and Bridge Engineering, Vol. 3. No. 1. 2008. pp. 5–13.

4. Zollinger, Corey, Dan G. Zollinger, Dallas Little, and Adel Godiwalla. "Innovative Approach to Pavement Rehabilitation Analysis and Design of Runway 15L-33R at George Bush Intercontinental Airport in Houston, TX." Proceedings, Eighth International Conference on Concrete Pavements, Vol. 3. Colorado Springs, CO, August 14-18, 2005. pp. 1101–1119.

CHAPTER 6 NOISE AND SKID RESISTANCE DATA

TxDOT personnel collected noise and skid resistance data on FM 1938 using equipment owned by the department. The researchers reviewed these data; the results of the review are in this chapter.

NOISE TESTING RESULTS

Figure 78 shows the results of the noise testing.
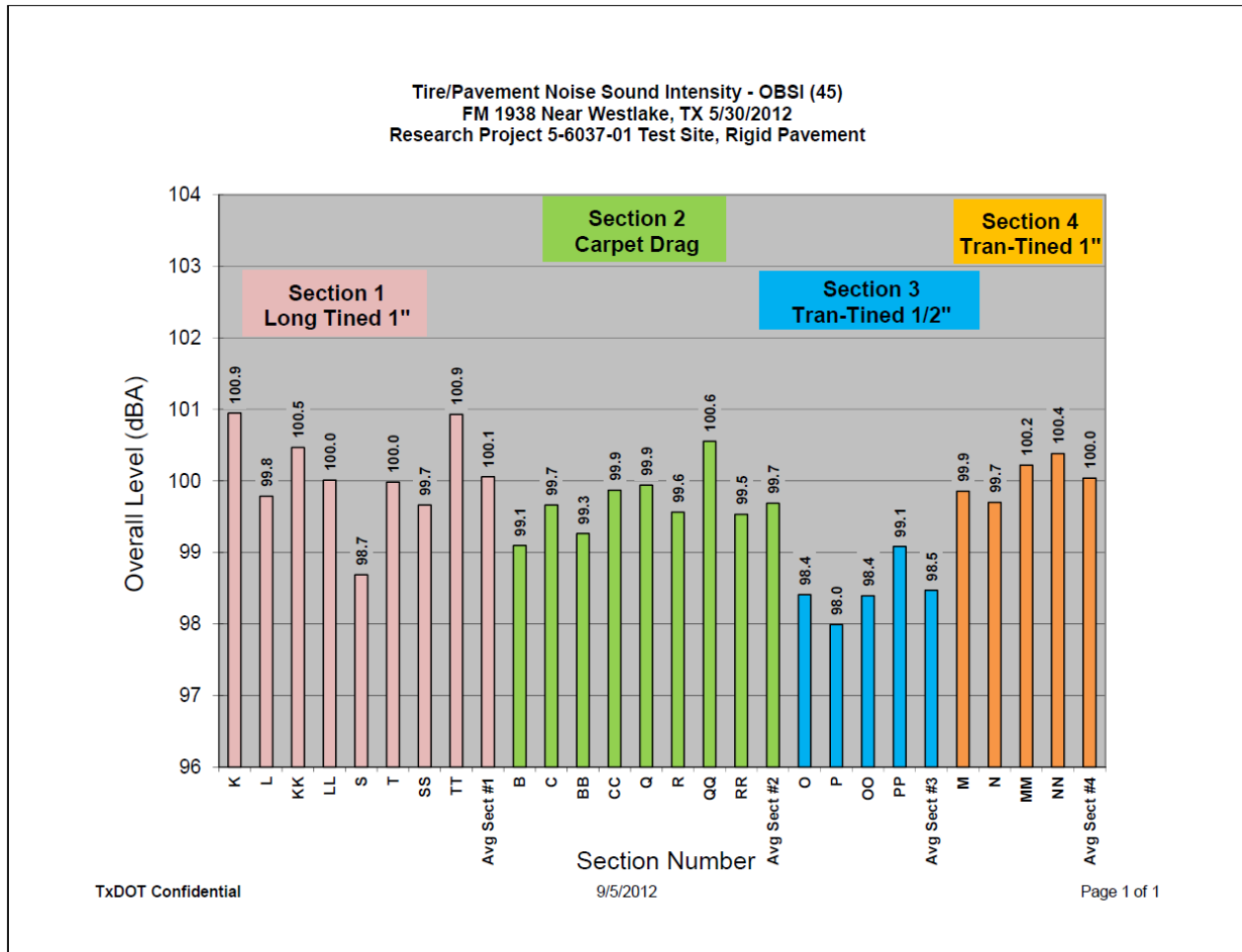
Figure 78. Noise Testing Results, FM 1938.

TxDOT personnel collected the data at 45 mph. As can be seen in Figure 78, Section 3 (transverse tines at ½-inch spacing) has the lowest noise level. However, Section 1 (longitudinal tines) was not opened to traffic during this testing; the researchers expect that this noise level will decrease after it is exposed to traffic loading.

69

SKID RESISTANCE TESTING RESULTS

TxDOT personnel were only able to collect skid resistance data on Sections 2, 3, and 4 during this project using a smooth tire. The results are as follows:

- For Section 2 (Carpet Drag), TxDOT personnel collected two datapoints, both with values of 23.
- For Section 3 (Transverse tined with ½-inch spacing), TxDOT personnel collected two dataponts. One value was 46, the other was 44.
- For Section 4 (Transverse tined with 1-inch spacing), TxDOT personnel collected two datapoints, both with values of 50.

As can be seen, Section 2 (Carpet Drag) had the lowest skid resistance value. Section 4 (transverse tined with 1-inch spacing) had the highest skid resistance value.

CONCLUSIONS AND RECOMMENDATIONS

In terms of noise level, Section 3 (transverse tines at ½-inch spacing) had the lowest noise level. However, Section 1 (longitudinal tines) was not opened to traffic during this testing; the researchers expect that this noise level will decrease after it is exposed to traffic loading.

In terms of skid resistance, Section 2 (Carpet Drag) had the lowest skid resistance value. Section 4 (transverse tined with 1-inch spacing) had the highest skid resistance value.

The researchers recommend that TxDOT personnel collect noise and skid resistance data on Section 1 after at least three months of traffic loading on Section 1.

CHAPTER 7 DEVELOPMENT AND EVALUATION OF AN OPTIMIZED AGGREGATE GRADATION

INTRODUCTION

The goal of this study is to provide a mixture design that needs a minimum amount of cement content for pavement concrete to be used on FM 1938 near Ft. Worth, Texas. The reduction in cement content was achieved by using different aggregate gradations. The methods used are outlined in Part 2. In Part 3, the maturity curves were developed for the final design mixtures as inputs for the ConcreteWorks computer model that predicts the long-term performance of the pavements.

DEVELOPMENT OF AN OPTIMIZED GRADED CONCRETE

Aggregates occupy 70–85 percent of concrete by mass or 60–75 percent by volume for typical concrete mixtures (*1*). Aggregates affect the fresh properties of concrete such as workability and unit weight. Aggregate also affects the hardened properties like compressive stress, permeability, electric resistance, and durability (*1*).

It is desirable to minimize the paste content in concrete mixtures. A minimum cement paste in a mixture creates concrete with a lower initial cost and improves the sustainability of the material by minimizing the carbon footprint. In addition, there are benefits to minimizing the concrete's shrinkage and compressive strength as well as improving its workability.

With optimized graded concrete it is common to maximize the volume of aggregate and minimize the volume of paste. This can be done to different degrees with variable materials and for multiple applications. One technique that is commonly used is to optimize the packing or gradation of the aggregate. There is not a lot of guidance in the literature on how to obtain these mixtures. The subject of this chapter is the development of the mixture using several common tests.

The gradation of aggregate is classified into: well or dense, uniform, gap, and open graded (*2*).

The classification that is thought to be the most desirable is well-graded. Gradation of aggregate according to the known aggregate methods of Power 0.45, Haystack, and the Shilstone Coarseness Chart can help in selecting the appropriate gradation (*3*).

Another way to think about the gradation of the aggregates is to try to minimize the void content or to maximize the density of the aggregates in a mixture. A way this is done is using the dry rod unit weight of rock and sand materials as per ASTM C 29/C 29M.

Objectives of Research

In this study the mixture design followed the procedures outlined by Koehler and Fowler (*4*). The first step in this procedure is to choose the aggregate gradation. Next, choose the paste

content so that the mixture can meet the constructability, durability, and strength needs of the in-place concrete. For this work much of the effort was focused on finding mixtures with satisfactory constructability. To ensure durability the research team prescribed limits on w/c ratio strength, and air content of the final mixtures. After the aggregate gradation was chosen the paste in the mixture was systematically reduced while also using a mid-range water reducer (WR) to change the paste viscosity. A series of paste volumes and viscosities were investigated until a satisfactory performance was found. Finally the research team verified the results with strength testing. It would be desirable to also investigate the durability of these mixtures. However, this was not possible with the resources on this project.

Aggregate Properties

Fresh and hardened concrete properties are affected by aggregate properties that vary by the source. These properties, characteristics, and standard tests can be summarized as shown in Table 10.

Table 10. Aggregate Properties.

Characteristic	Significance of the Characteristic	Requirement
1- Shape & texture	Affect the workability	ASTM C 295 ASTM D 3398
2- Resistance to abrasion	Index of aggregate quality	ASTM C 535 ASTM C 779
3- Grading	Affects the workability of fresh concrete, minimize the cement content	ASTM C 117 ASTM C 136
4- Bulk density (dry unit weight)	Affects the mix design calculations	ASTM C 29
5- Specific gravity	Affects the mix design calculations	ASTM C 128 ASTM C 127
6- Absorption	Affects the water to cement ratio	ASTM C 70 ASTM C 127 ASTM C 128 ASTM C 566
7- Compressive & flexural of strength	Acceptability of fine aggregate failing other tests	ASTM C 39 ASTM C 78
8- Aggregate constituents	Affects the amount of deleterious and organic materials in aggregate	ASTM C 40 ASTM C 87 ASTM C 117
9- Resistance to alkali	Affects the volume change	ASTM C 227 ASTM C 289

Aggregate Gradation

Aggregate gradation can be defined as the frequency of a distribution of the particles sizes (*5*).

Types of gradations: Arrangement of particles with the effect of shape, textures, and angularity will lead to a certain type of gradation depending on percentage used of different aggregate sizes. FHWA classified the types of gradation as following:

1. Well graded (dense). This is thought to occur when the gradation curve is near the maximum density on the Power 45 plot. Most HMA mix design tends to approach this line (*2*). The arrangement of particles as shown in Figure 79a, shows grain-to-grain contact, low void content, and high density.
2. Gap graded. It is aggregate with little or no intermediate sized particles. Using this kind of gradation will lead to segregation (*2*). Figure 79b shows the particle arrangement, which has no grain-to-grain contact, higher void content, and lower density.
3. Open graded. This gradation of aggregate contains a small amount of small particles. The blend has voids between big particles that are not filled with the missed small sizes (*2*). Arrangement of this grade has grain-to-grain contact, high void content, and low but variable density, as illustrated in Figure 79c.
4. Uniformly graded. Most of the aggregate particles are the same size in this gradation, with steep shape (*2*), as shown in Figure 79d. The arrangement in this type of gradation has grain-to-grain contact, high void content, and low but variable density.
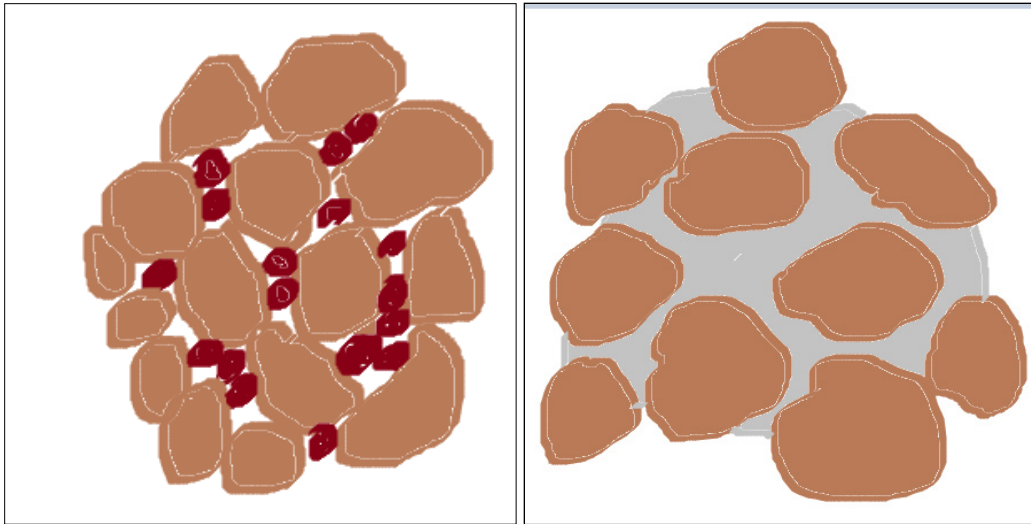
a) Well graded   b) Gap graded
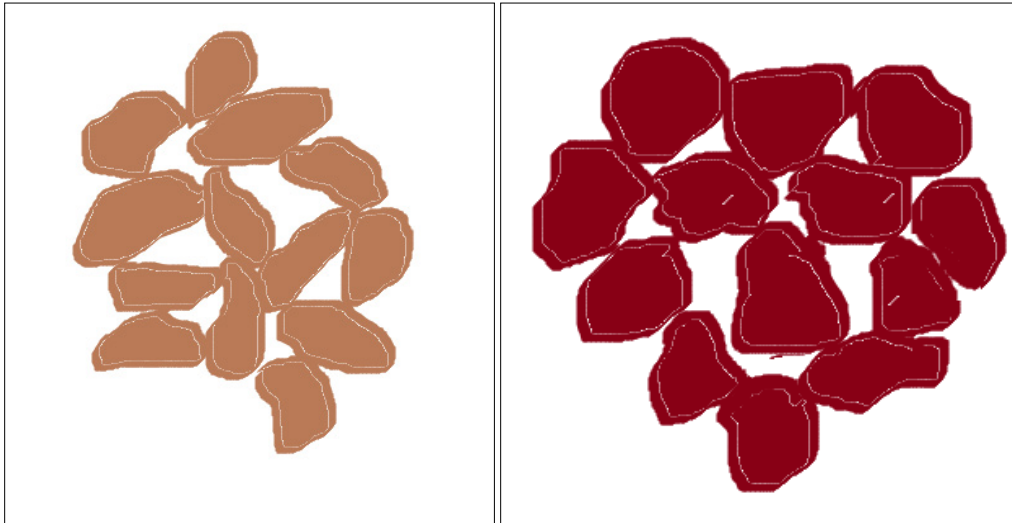
c) Open graded   d) Uniform graded

Figure 79. Aggregate Particle Arrangement in Different Gradation Curves.

The idea of changing the aggregate gradation in such a way that leads to best results regarding decreasing the void ratio is not a new concept. Many efforts have been made over the last century to optimize the aggregate gradation in order to get a lower void ratio which would result in less cement or cementitious content in the concrete mixture (*3*).

The gradation of aggregate affects the properties of the concrete like strength, modulus of elasticity, shrinkage, and creep (*6*). There is an optimal packing of the aggregates that would theoretically require less mortar. However, attention should be kept to obtain a sufficient workability.

74

Fine aggregate gradation is also important as it impacts the workability more than the coarse aggregate. Aggregate with fine aggregate gradation near sieve passing No. 50 and 100 may suffer problems in workability and bleeding due to high surface area (*7*). The finer aggregate, passing No. 100, has the bigger specific surface area that contributes to more cement paste demand (*8*).

Methods of optimizing aggregate gradation can be summarized in the following sections.

Maximum Density of Aggregate

This method was first researched by Fuller and Thompson (*9*). Later they found this curve was not necessary given the maximum density or even the maximum strength of concrete, because the interaction between aggregate particles with water and cement is not the same as the aggregate particles packed alone. Based on this concept, Tolbot and Richart established the maximum density equation (*9*):

$$P = \left(\frac{d}{D}\right)^n \tag{7.1}$$

Where:
P = amount finer than (d) size.
d = particle size.
D = maximum particle size.
n = exponent governing the distribution of the particle sizes.

The n value was set as 0.5 by Fuller to achieve the maximum density, but this value led to mixtures with reported poor finishing. This value was adjusted by Good and Lufsey in 1965 to 0.45 for asphalt mixtures (*10*). Figure 80 shows a typical Power 0.45 curve.
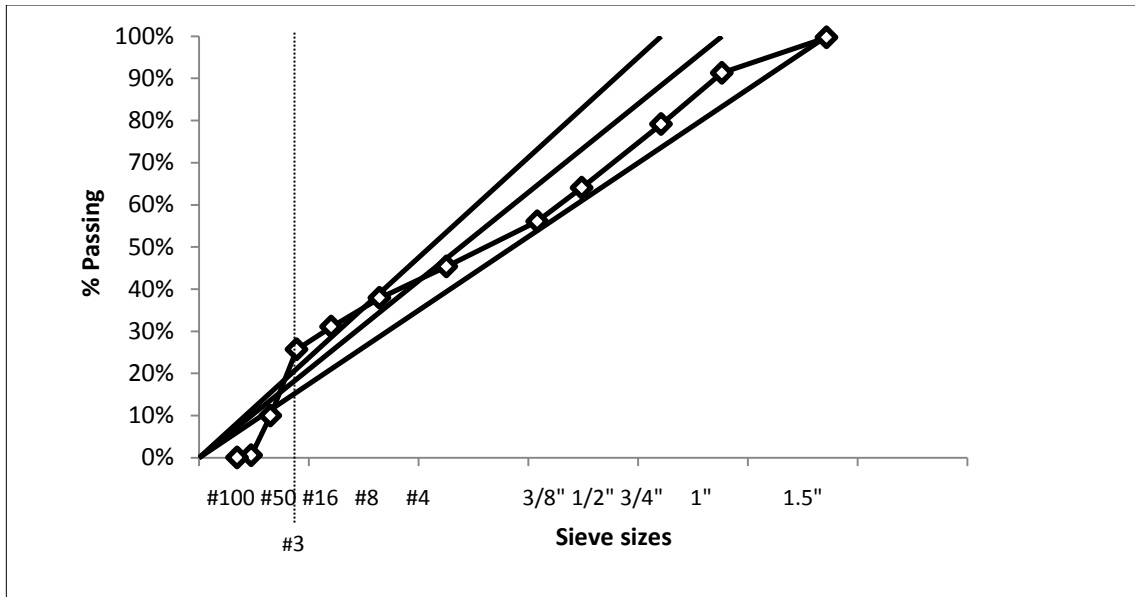
Figure 80. Typical Power 0.45 Chart.

The horizontal axis represents the sieve size divided by the maximum particle diameter raised to the 0.45 power, while the vertical axis represents the percent passing.

Fineness Modulus (FM)

This method was developed by Abrams in 1918. He found that there is a relation between the aggregate gradation and the water demands. The concept is to reduce water content to get higher concrete strength by maximizing the fineness modulus (*11, 12*).

Fineness modulus, according to ASTM C 125, is an aggregate index computed by dividing the sum of percent retained on specified sieves over 100. Specified sieves for coarse aggregate size are; 3, 1.5, ¾, and ⅜ inch, while the specified sieves for fine size aggregate are No. 4, 8, 16, 30, 50, and 100, which is the minimum limit. Limits of fineness modulus of sand are typically between 2.3 and 3.1 (ASTM C 33). A higher value of FM correlates to a bigger average aggregate size. The method takes into account the volume of mixed particles. In determining the aggregate proportions or quantities per unit volume (cubic yard), the method depends on the fineness modulus of fine aggregate with respect to dry unit weight of coarse aggregate and the maximum size of coarse aggregate (*11*).

Results from Table 11 suggest that as we increase the fineness modulus of a certain maximum size of coarse aggregate we will need less coarse aggregate. Additionally, for a certain fineness modulus of fine aggregate we will need more coarse aggregate as we increase the maximum size of coarse aggregate.

Table 11. Percent of Bulk Volume of Coarse Aggregate according to ACI 211.

Nominal Max. Size (inch)	Bulk Volume of Coarse Aggregate with Respect to Fineness Modulus of Fine Aggregate			
	2.4	2.6	2.8	3.0
3/8	0.5	0.48	0.46	0.44
½	0.59	0.57	0.55	0.53
¾	0.66	0.64	0.62	0.60
1	0.71	0.69	0.67	0.65
1.5	0.75	0.73	0.71	0.69
2	0.78	0.76	0.74	0.72
3	0.82	0.80	0.78	0.76
6	0.87	0.85	0.83	0.81

Specific Surface Area of Aggregate

In 1918, Young found that the specific surface area of aggregate would have an impact on the water demand of the concrete mixture (*13*). The less the specific surface area, the lower the amount of water required to obtain a certain workability. Later, in 1954, Newman and Teychenné found that if the gradation of a combined aggregate changed so that the total specific surface area changed, the concrete properties changed as well. If that change in aggregate grading kept the specific area constant, a mixture with similar properties was produced (*14*).

Another method based on Newman and Teychenné and developed by Ken W. Day assumes that the particles are spheres. Specific surface area is a good method to design the mixture. The negative side is that this method overestimates the effect of finer particles. Ken W. Day published a modified specific surface area table in which we can correlate every sieve size by a modified number. This table overcomes the problem of overestimation of the fine particles' effect on concrete workability and other properties (*15*).

Table 12. Modified Specific Surface Area according to Day (*15*).

Sieve Fraction	Day-Modified SS Values	Approx. True Specific Surface (cm^2/gm)	Surface Modulus
20mm	2	1	1
20–10	4	2	2
10–4.75	8	4	4
4.75–2.36	16	8	8
2.36–1.18	27	16	16
1.18–0.6	39	35	32
0.600–0.300	58	65	64
0.300–0.150	81	128	128
<0.150	105	260	256

The above table can be used for individual aggregate size, and the obtained results can be used to determine the combined specific surface area directly according to the following equation (*15*):

$$SSca = [SSf \times Sand\% + SSc \times \% (1-Sand\%)] / 100 \qquad (7.2)$$

Where:
SSca = specific surface area of combined aggregate.
SSf = specific surface area of sand (fine aggregate).
SSc = specific surface area of coarse aggregate.

Shilstone Method

The traditional methods such as fineness modulus will not give a clear indicator of effect of aggregate gradation on workability because different gradations may have the same fineness modulus. According to Shilstone the gradation of the aggregates is a very important parameter to determine the workability of the mixture (*16*). So these methods will not give a good indication of concrete workability. Shilstone recognized this and published papers about his work in Saudi Arabia. Shilstone's ideas show that one can obtain a desired workability by changing the aggregate proportions instead of changing the water content in the mixture (*17)*.

The Shilstone method is a volumetric-based method. The main two parameters in his method are coarseness and workability factor. Coarseness factor is the percent of cumulative retained on sieve size ⅜ inch (9.5 mm) over percent retained on sieve number 8 (2.36 mm). The higher the coarseness factor, the more coarse aggregate content is in the mixture. Zones are classified into five main areas according to the mixture workability and its suitability in construction type. Figure 81 shows the Shilstone Coarseness Chart.
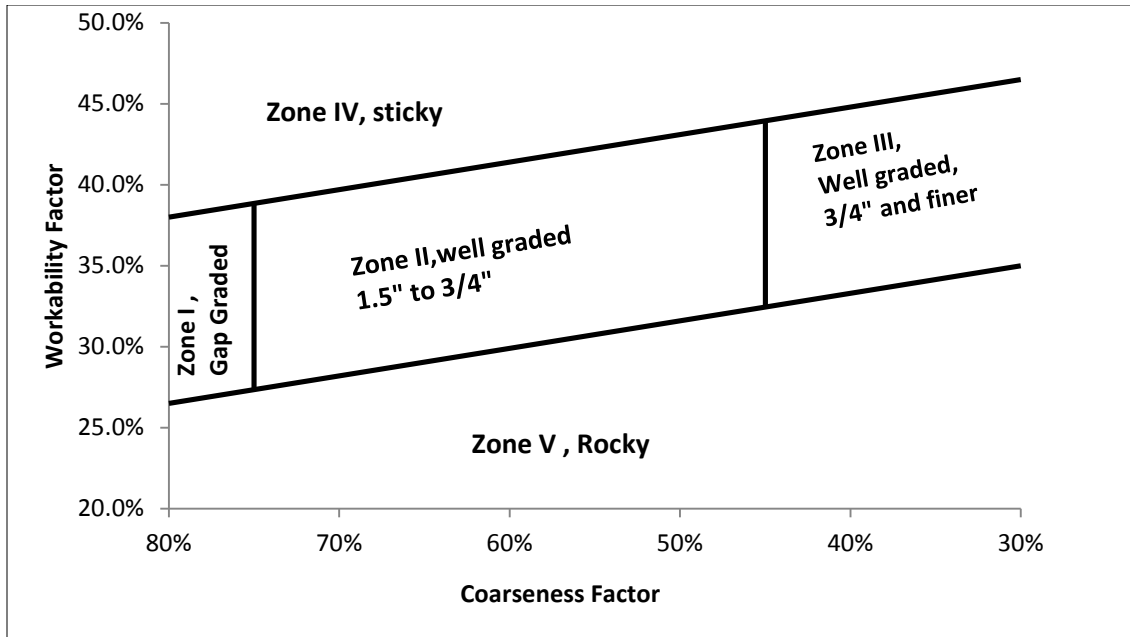
Figure 81. Shilstone Coarseness Chart.

This method is currently used by many state DOTs because of its ease of use. It is also called the coarseness factor chart. Coarseness factor (which represents the horizontal axis) is computed through the equation:

$$CF = Q/I *100\ (\%) \tag{7.3}$$

Where:
Q = cumulative % retained on sieve ⅜ inch (coarse size aggregate).
I = cumulative % retained on sieve #8 (intermediate size aggregate).

In the vertical axis researchers plot the workability factor values. This can be determined from the following equation:

$$WF\% = W \times 2.5(C-564)/94 \tag{7.4}$$

Where:
C = cementitious material content (lb/cy).
W = % passing #8 sieve.

By increasing the amount of the intermediate or fine aggregate size, the blend will be finer and the coarseness factor will decrease in value. Also, increasing the amount of coarse aggregate will increase the coarseness factor.

79

In the adjusted Shilstone graph, the coarseness factor ranges between 30 percent and 80 percent. Regarding the workability factor in which is a combination of binder content and passing the fine sieve #8, one would locate the point up or down on the graph according to workability as shown in Equation 7.4.

Percent Retained, (8–18) Graph

The main objective of this graph is to keep gradation in a haystack shape. The percent retained from sieve No. 30 through a sieve less than the nominal maximum aggregate size should be within the range of 8 percent and 18 percent (*9*). For a floor slab Holland recommended extending the range of (8–18) to (6–22) when it is hard to find intermediate aggregate sizes (*18*).

The 8–18 Chart, or Percent Retained Chart, is often used to show details of the aggregate gradation, by showing details of the percent retained for every sieve size. The main goal of this method is to limit the maximum and minimum amount of aggregate to an upper limit of 18 percent retained and minimum of 8 percent retained on sieve #30 (*19*). According to this method the perfect grade would be the gradation that has grains retained by weight within the 8–18 percent zone especially for the intermediate size. Figure 82 shows an example of this chart.
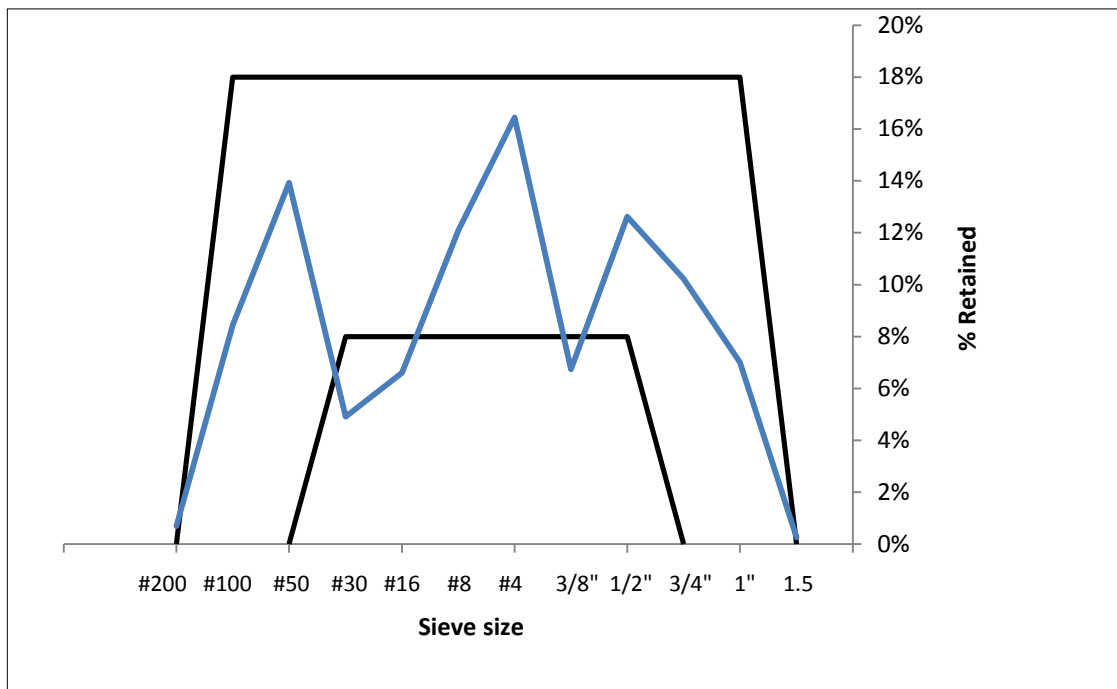
Figure 82. Example of an 8–18 Chart.

Aggregate Bulk Density

Aggregate Dry Pot Unit Weight

The voids between aggregate affect the mixture design by reducing or increasing the paste volume required to fill the cavities between the particles. Void ratio describes how tightly or loosely the aggregate particles are packed. Voids increase with increased aggregate size. Void ratios are also affected by the shape, angularity, and texture of particles. All of these parameters are included in ASTM C 29 (*20*) to determine the dry pot unit weight of aggregate. In this test a metal mold with known weight and volume is filled with aggregates to one third, and then this layer is compacted evenly by 25 strokes from a tamping rod. A second layer will fill the mold to two thirds with leveling and compacting by tamping rod without allowing the rod to penetrate to the first layer. A final layer will fill the mold to overflowing, and the same procedure is applied to level the final surface with a plate so that the level of the compacted aggregate is the same as the level of the mold edge. After weighing the mold with aggregate, the dry unit weight of the aggregate can be calculated according to the equation:

$$M = (G - T) / V \qquad\qquad (7.5)$$

Where:
M = bulk density of the aggregate.
G = mass of the aggregate plus the measure.
T = mass of the measure.
V = volume of the measure.

Packing Modulus

Packing is the ratio of the particle volume to the total volume or the complementary of the porosity (packing equals one minus porosity). Packing is another approach to aggregate optimization to get denser concrete with minimal amount of cementitious material, which results in less shrinkage and creep with more strength and durability (*21*). In 1907, Fuller and Thompson studied the effect of the distribution of particles on concrete properties by changing the distribution of the packing of constituent materials within the concrete (*22*). The packing theory by Furnas in 1931 stated an assumption that small particles fill out the cavities between big particles without disturbing the big particles' arrangement. His packing models have been developed based on spherical particle shape (*23*).

The basic packing model has been developed based on binary mixtures. The system has since been developed to multi-component mixtures (*24*). The basic packing formula is:

$$\text{Packing} = \text{Minimum}_{i=1}^{n}(\alpha i + (1 - \alpha i) \sum_{j=1}^{i-1} g(i,j)\emptyset i + \sum_{j=i+1}^{n} f(i,j) \emptyset j) \qquad (7.6)$$

Where:

α = mono disperses packing (packing for equally sized particles). This value is ranged between 0.6 and 0.64 for spherical shaped particles and can be less for non-spherical shaped aggregates.

$\emptyset$ = volume fraction of a mono material.

f (I,j) = interaction function for the wall effect and the effect of case of small particles close to larger particle size (cannot be packed dense as in bulk).

g (I,j) = interaction function for the case where small particles are so large that they cannot fit in cavities between larger particles without disturbing the packing of the larger particles (*24*).

The size of every material is divided into fractions. Mono packing will always be equal to or less than the packing of the whole material. The wider the distribution size within the material, the larger packing density can be obtained (*25*).

Materials

Materials Properties

All of the materials investigated were provided by Ed Bell Construction. These materials were the materials to be used on FM 1938 (see Table 13).

Table 13. Materials Properties and Requirements.

Material	Type & Source	Sp. Gr.	Requirements
1-Cement	Type l/Lehigh	3.1	ASTM C 150
2-Flyash	Class F/Martin Lake	2.5	ASTM C 618
3-Coarse Aggregate 1.5"	#57/Hanson	2.65	ASTM C 127, ASTM C 33
4-Intermediate Aggregate	⅜ inch/ Hanson	2.65	ASTM C 127
5-Sand	Hanson	2.65	ASTM C 128, ASTM C 33
6-Water	Tap water	1	ASTM C 1602
7-Water Reducer	DARACEM 55	1.28	ASTM C 494
8-Water Reducer	WRDA 35	1.2	ASTM C 494

Concrete Tests

The researchers ran the following tests on fresh concrete: slump according to ASTM C 143 (*26*), air content according to ASTM C 231 (*27*), unit weight according to ASTM C 138 (*28*), and the box test. The box test is a novel test method used to determine the workability of low slump concrete. Figure 83 illustrates the box dimensions and shape.
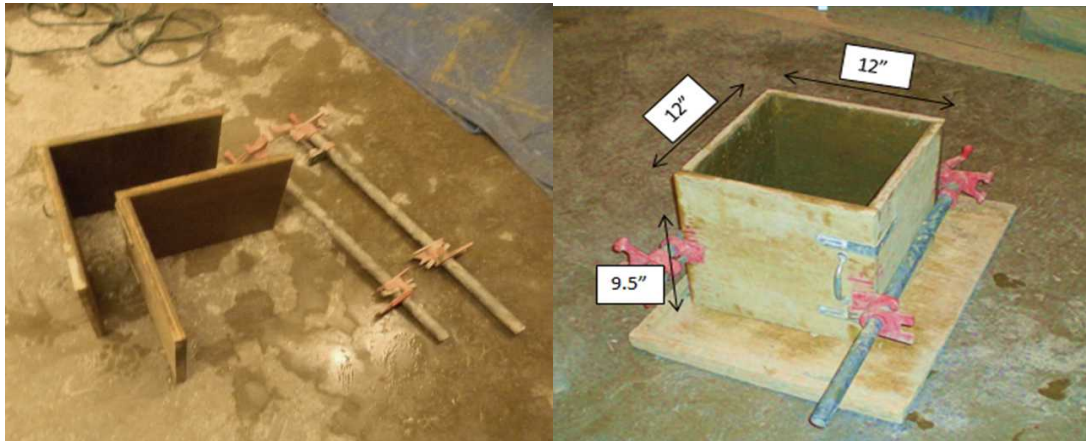
Figure 83. Box Test: Parts and Dimensions.

Procedure for using the box test:

1. Assemble the two parts of the box tightly, using clamps as in Figure 83.
2. Fill the box with 9.5 inches of unconsolidated concrete.
3. Vibrate with an electronic vibrator with a 1-inch diameter head with 1200 rpms. Insert the head for three seconds and remove after three seconds.
4. Loosen the two parts of the box and separate them gently.
5. If the obtained shape has a good straight edge with good top and only minor unfilled voids then the sample passes the test. If the shape has a slumped edge or significant voids on either the sides or the top, the sample is considered to fail the test.

a) Pass   b) Fail

Figure 84. Pass/Fail Conditions for the Box Test.

Concrete compressive strength was also measured according to ASTM C 39 (*29*) on hardened concrete samples for ages 7 and 28 days.

Methods

Aggregate Optimization

The basic start to optimize gradation is to combine two or three aggregates with different proportions and then investigate these proportions according to gradation methods associated with packing density of these combined aggregate. Obtained results will be used in the pavement mixture design.

Sieve Analysis and Combined Aggregate Gradation. The researchers completed the sieve analysis for the individual aggregate sizes as per ASTM C 136 (*30*). After completing the sieve analysis we computed the combined aggregate gradation according to ASTM C 136 specifications for chosen gradations according to the following equation:

$$P = Aa + Bb + Cc \tag{7.7}$$

Where:
P = combined percent passing of a given sieve.
A, B, C = percent passing for aggregate A, B, and C for each sieve.
a, b, c = relative percent of total aggregates A, B, and C.

The combined aggregate gradation will be used in the gradation methods.

Aggregate Gradation by Power 0.45. The maximum nominal aggregate size is one sieve size larger than the sieve that has less than 90 percent passing. In our case this size is 1 inch, as the first top sieve less than 90 percent passing is sieve ¾ inch. The nominal proportions of aggregate blends were investigated according to Power 0.45 to choose gradations

close to the max density line. This is the first step toward optimizing the gradation. Next the mixtures were varied systematically by 150 lb of each aggregate while holding the percentages of the other materials constant, and the values were observed. This was done to investigate the sensitivity of the values in the different aggregate gradation techniques. These values are plotted in Figure 85..
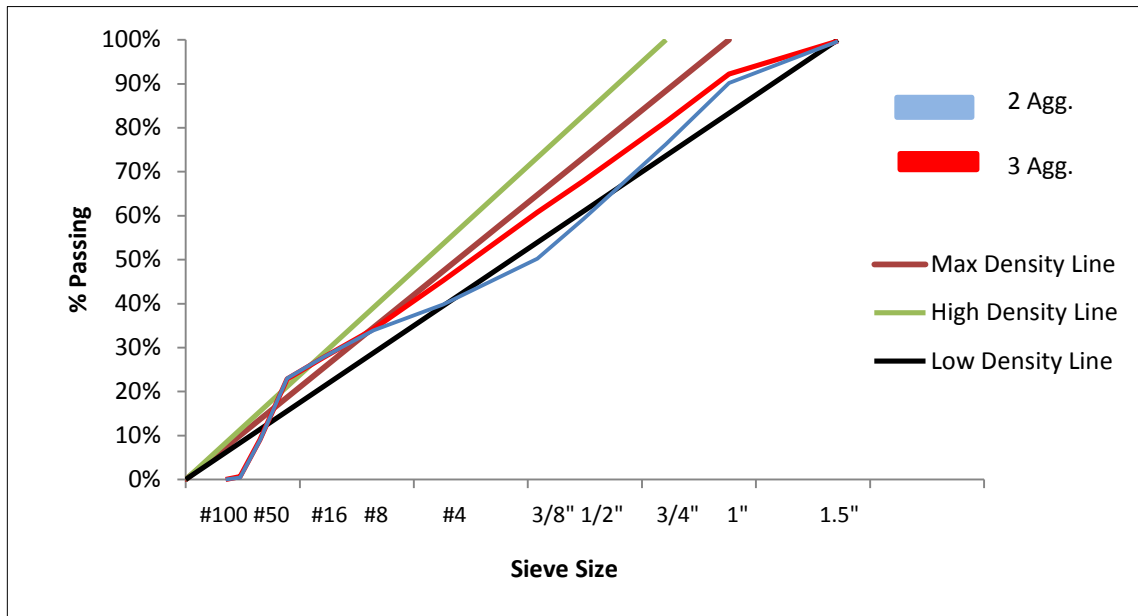
Figure 86. Two- and Three-Aggregate Blends in Power 0.45.

Percent Retained (Haystack Shape) Charts. The gradations of aggregate blends—either (G3, ⅜ inch, Sand) group or (G3, Sand) group—will be verified in a percent retained chart to identify gaps in the gradation as shown in Figure 86.
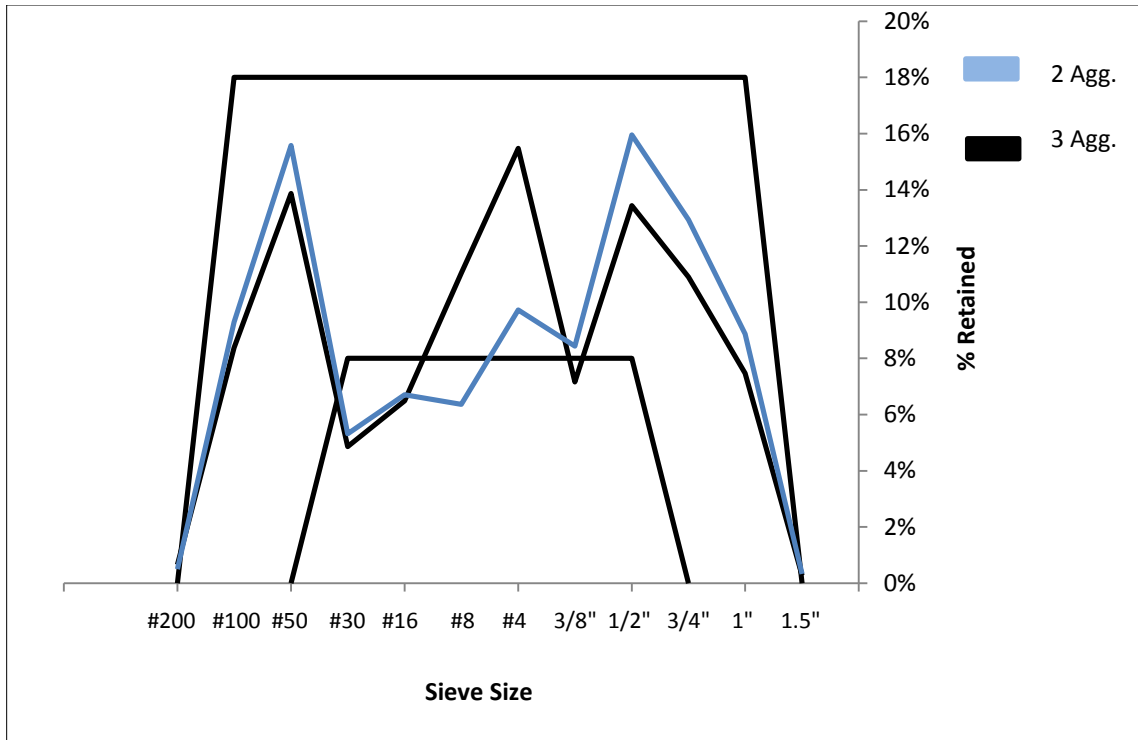
Figure 87. Percent Retained for Two- and Three-Aggregate Blends.

Shilstone Method. In this method a number of gradations were plotted in a Shilstone Chart while holding the cement binder fixed to observe the effect of the gradation. Figure 87 illustrates this case for the two groups of aggregate blends with the associated aggregate void ratio as determined by ASTM C 29. The points with the lowest voids content are shown in green. These points were used to establish the gradations for the concrete mixtures.
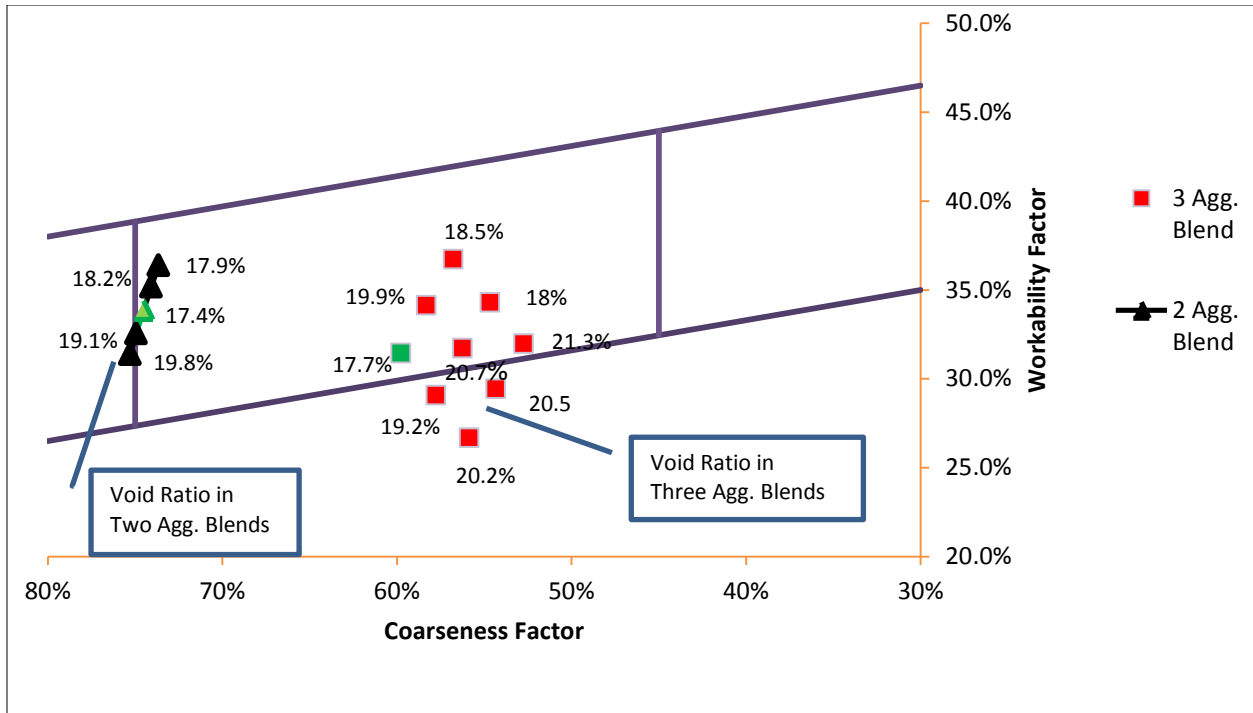
Figure 88. Aggregate-Void Ratio in Shilstone Chart.

Mixture Design

The main goal of mixture design is to reduce the cement content and get a good concrete workability with adequate strength. For a selected aggregate gradation a volume of paste, w/cm, was chosen. Concrete was produced with these materials, and properties like workability, the impact of the vibrator on the mixture, air content, and strength were examined. If satisfactory results were found for the mixture then the paste volume was decreased and the mixture was investigated again. At this point lower paste volumes were used with WRs to change the viscosity of the mixture until they were found to pass. This process was repeated until we found a concrete mixture with satisfactory performance and minimized paste volume.

Results

The sieve analysis for the percentage of aggregates passing different sieve sizes is shown in Figure 88.
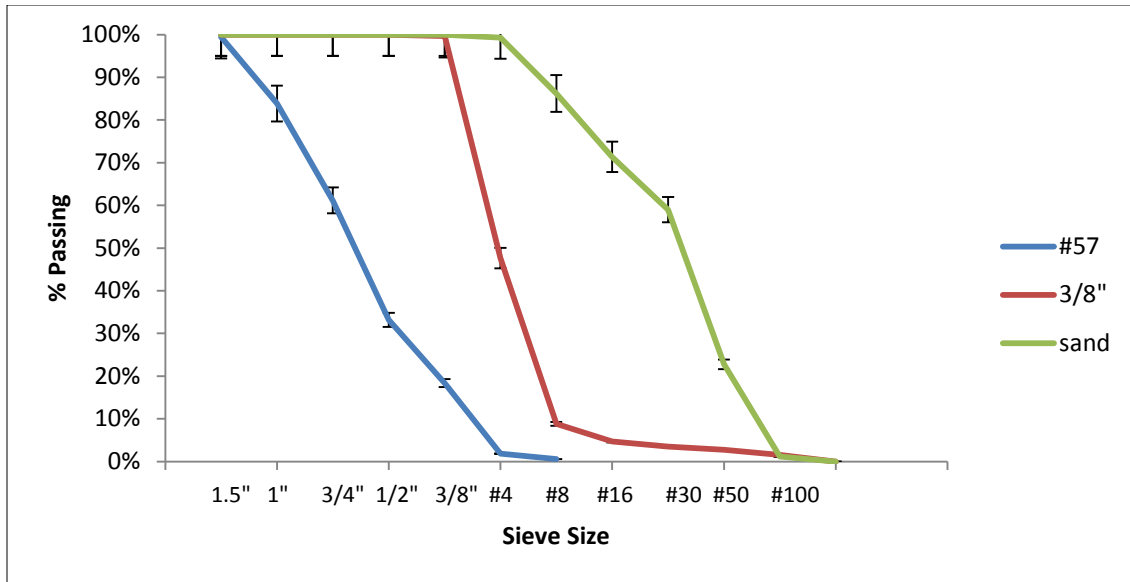
Figure 89. Gradation of Individual Texas Aggregate.

In the Power 0.45 method, the following gradations achieved the best results in approaching the dense line in three- and two-aggregate blends, respectively. Figure 89 shows the two gradations on the Power 0.45 Chart. Table 14 shows the best gradation.

Table 14. Best Gradation in the Power 0.45.

G3	⅜"	Sand
48%	14%	38%
58%	0%	42%

88
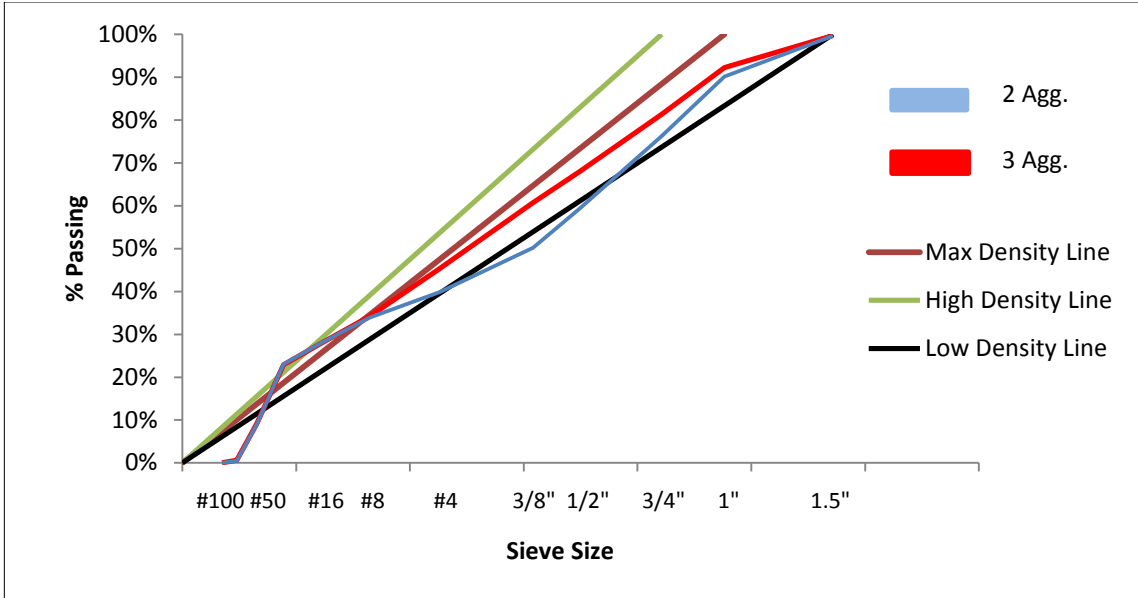
Figure 90. Good Gradations for Two- and Three-Aggregate Blends.

These mixtures are compared in Figure 90. The three-aggregate gradations showed acceptable results in percent retained graph with two separated valleys (one is a small valley shape). The two-aggregate gradations have two consecutive valleys. Figure 91 shows mixtures 10 and 18 in the Shilstone Chart. Table 15 lists the aggregate dry pot unit weight and void ratio results as per ASTM C 29. Table 16 lists the mixtures investigated for this study.
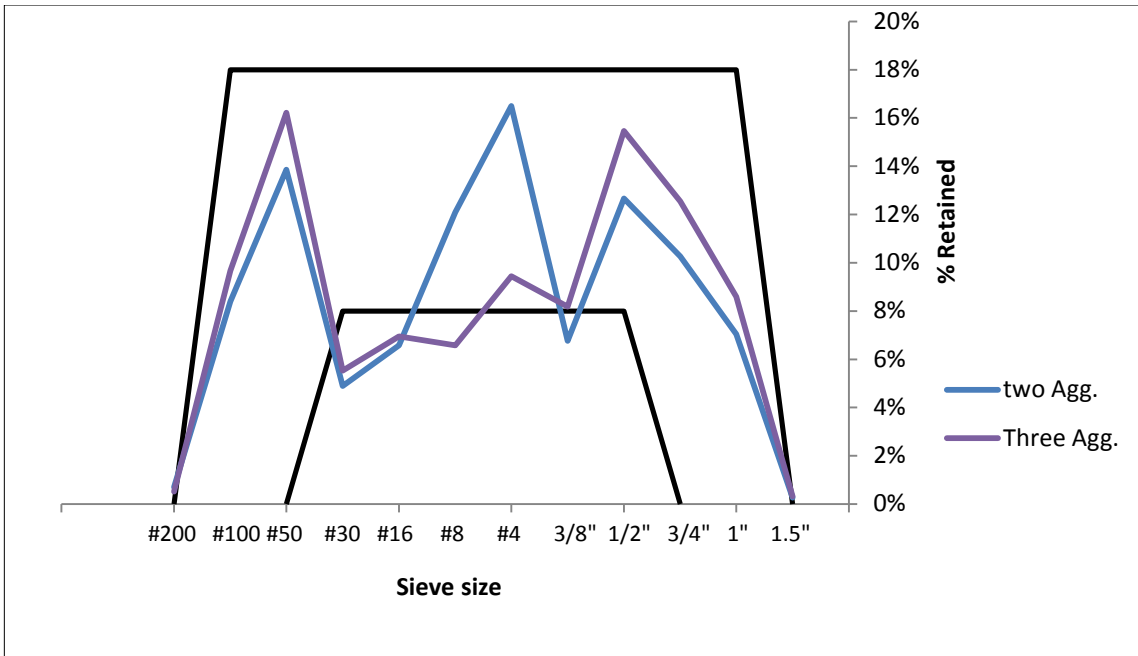
Figure 91. Good Gradations of Two- and Three-Aggregate Blends in (8–18) Chart.
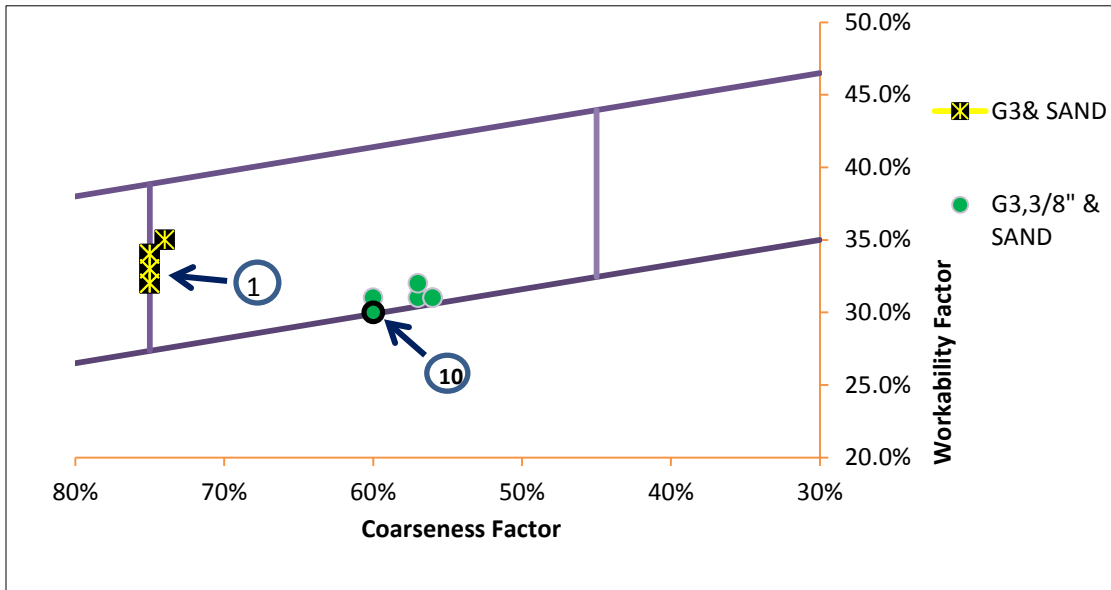
Figure 92. Mixtures 10 and 18 Shown on the Shilstone Chart.

Table 15. Dry Aggregate Unit Weight and Aggregate Void Ratio.

Blend No.	Aggregate Type & Size	Aggregate Percentage			Unit Weight (b/ft^3)	Void Ratio %
		G3	⅜"	Sand		
1	Grade 3	100%	0%	0%	100.85	39.0
2	⅜"	0%	100%	0%	106.00	35.9
3	Sand	0%	0%	100%	111.76	32.4
4	Grade 3 & ⅜"	88%	12%	0%	104.04	37.1
5	Grade 3 & ⅜"	86%	14%	0%	106.61	35.5
6	Grade 3 & ⅜"	81%	19%	0%	105.45	36.2
7	Grade 3 & ⅜"	76%	24%	0%	108.00	34.7
8	Grade 3 & ⅜"	75%	25%	0%	108.67	34.3
9	Grade 3 & ⅜"	74%	26%	0%	107.20	35.2
10	Grade 3 & ⅜"	72%	28%	0%	109.07	34.0
11	Grade 3 & ⅜"	70%	30%	0%	108.96	34.1
12	Grade 3 & ⅜"	68%	32%	0%	110.45	33.2
13	Grade 3 & ⅜"	67%	33%	0%	110.45	33.2
14	Grade 3 & ⅜"	66%	34%	0%	106.39	35.7
15	Grade 3 & ⅜"	65%	35%	0%	110.53	33.2
16	Grade 3 & ⅜"	64%	36%	0%	108.93	34.1
17	Grade 3 & ⅜"	62%	38%	0%	108.32	34.5
18	Grade 3 & ⅜"	57%	43%	0%	109.60	33.7
19	Grade 3 & ⅜"	52%	48%	0%	109.36	33.9
20	Grade 3 & ⅜"	48%	52%	0%	111.68	32.5
21	Grade 3, ⅜"/sand	48%	17%	35%	133.65	19.2
22	Grade 3, ⅜"/sand	48%	20%	31%	132.03	20.2
23	Grade 3, ⅜"/sand	48%	14%	38%	136.08	17.7
24	Grade 3, ⅜"/sand	45%	17%	38%	131.09	20.7
25	Grade 3, ⅜"/sand	45%	20%	35%	131.49	20.5
26	Grade 3, ⅜"/sand	45%	14%	41%	132.48	19.9
27	Grade 3, ⅜"/sand	42%	20%	38%	130.16	21.3
28	Grade 3, ⅜"/sand	42%	17%	41%	135.63	18.0
29	Grade 3, ⅜"/sand	42%	14%	44%	134.69	18.5
30	Grade 3, ⅜"/sand	46%	16%	38%	133.00	20.1
31	Grade 3/sand	61%	0%	39%	132.60	20.0
32	Grade 3/sand	60%	0%	40%	134.60	20.3
33	Grade 3/sand	58%	0%	42%	136.67	17.4
34	Grade 3/sand	57%	0%	43%	135.23	18.2
35	Grade 3/sand	55%	0%	45%	135.76	17.9
36	Grade 3/sand	59%	0%	41%	135.00	20.4

Table 16. Mixture Designs and Tests Results (the highlighted mixtures are the ones recommended for placement).

Mix #	Binder (sacks)	Fly Ash %	Percentage of Aggregate			w/c	Add Mixture		Dry U.W. (b/ft³)	Slump (in)	Box Test	Concrete Unit Wt. (b/ft³)	AIR%	Comp. (psi)	
			G3	⅜"	Sand		Type	oz/cwt						7 day	28 day
1	4.73	35%	46%	16%	38%	0.41	Daracem 55	11.9	11.9	0.25	Pass	148.6	2%	5239	6974
2	5	35%	45%	17%	38%	0.41	Daracem 55	4.5	4.5	0	Pass	148.8	5%	4711	6560
3	5	35%	45%	17%	38%	0.41	WRDA 35	6.2	6.2	0.5	Pass	147.2	5.5%	4187	5964
4	5	35%	45%	17%	38%	0.41	WRDA 35	5.1	5.1	0.25	Pass	147.4	5%	4058	6021
5	4.75	35%	45%	17%	38%	0.43	Daracem 55	1.9	1.9	0.5"	Fail	149.7	4.1%	4507	6378
6	4.75	35%	45%	17%	38%	0.45	Daracem 55	6.3	6.3	1.5"	Pass	148.8	4.6%	4152	5473
7	4.75	35%	45%	17%	38%	0.45	Daracem 55	6.3	6.3	1.5"	Pass	149.4	1.5%	5066	7554
8	4.75	35%	45%	17%	38%	0.45	MIRA 110	5.6	5.6	1"	Pass	148.4	4.2%	3248	4928
9	4.73	35%	48%	14%	38%	0.45	MIRA 110	4.0	4.0	1.25"	Pass	149	3.9%	3235	5052
10	4.5	35%	48%	14%	38%	0.45	Daracem 55	6.0	6.0	0.75"	Pass	148.5	4.4%	3624	5299
11	4.25	35%	48%	14%	38%	0.45	Daracem 55	10.4	10.4	0.5"	Fail	150.1	4.3%	4743	5785
12	5	35%	57%	0%	43%	0.41	Daracem 55	7.5	7.3	0.25	Fail	148.4	5.0%	4814	7228

Table 16. Mixture Designs and Tests Results (the highlighted mixtures are the ones recommended for placement) – cont'd.

Mix #	Binder (sacks)	Fly Ash %	Percentage of Aggregate			w/c	Add Mixture		Dry U.W. (b/ft³)	Slump (in)	Box Test	Concrete Unit Wt. (b/ft³)	AIR%	Comp. (psi) 7 day	28 day
			G3	³⁄₈"	Sand		Type	oz/cwt							
13	5.5	35%	59%	0%	41%	0.41	Daracem 55	4.5	4.5	1	Fail	148.2	5%	4797	6553
14	4.7	31%	60%	0%	40%	0.45	Daracem 55	3.3	3.3	4.5	Pass	148.3	4.8%	3240	4553
15	5.2	30%	61%	0%	39%	0.45	Daracem 55	3.2	3.3	7.25	Fail	143.4	7.5%	4369	5871
16	5	35%	58%	0%	42%	0.43	Daracem 55	7.7	7.8	1"	Pass	148.2	4.5%	4157	6131
17	4.75	35%	58%	0%	42%	0.43	Daracem 55	10.0	10.0	3/4"	Pass	148.1	4.8%	4279	6083
18	4.5	35%	58%	0%	42%	0.43	Daracem 55	13.3	13.4	1.5	Pass	142.3	8.6%	3902	5627

Discussion

Gradation Methods

Since the initial aggregate gradation was close to the maximum density line, this will produce mixtures that are rocky. In the Percent Retained (8–18 percent) graphs the results show two separate valleys in the three-aggregate blends—one of them is very small and can be ignored while the bigger one is under sieve #50, indicating a lack of that aggregate size in the aggregate blend. Under the chart rules, this blend is acceptable.

The curve of the two-aggregate blends shows two consecutive valleys under sieves #50 and #16. The valleys denote the lack of aggregate sizes #50 and #16, respectively. Under the rules of this chart the curve may be considered unacceptable because of the consecutive valleys. The final results of the mixture properties showed satisfactory performance.

The Shilstone Coarseness Chart illustrates the effect of modifying the aggregate gradation in a systematic manner and the resulting impact on the voids content. This is shown in Figure 87 when the void ratio is plotted with the observed gradations. The void ratios for the three-aggregate blends were varied. The minimum void ratio (17.7 percent) was lying in the well graded zone, close to the rocky zone as a result of using the gradation (48 percent G3, 14 percent ⅜ inch, 38 percent sand) in which we can observe the highest percentage of coarse aggregate compared with the other three-gradation blends. This percentage affected the value of the coarseness factor in the Shilstone Chart and shifted the point to the left of the points group.

In the mixture design we inserted the real value of the cement binder in the Shilstone equation, and the effect of the cement binder was clear on the three-aggregate blends as most points were shifted down toward the rocky zone but still in the well graded zone.

The points of the two-aggregate blends were not affected by much, but we can see an inclination toward the gap zone as we decreased the cement binder and increased the aggregate content.

Aggregate Packing Density

Higher results of aggregate dry unit weight have been obtained from blends of G3 with sand and from blends of G3, ⅜ inch, and sand. The gradations of aggregate that had been obtained by the aggregate methods showed the highest values of the associated dry unit weight. The good particle distribution led to a good packing of the aggregate particles with a minimum void ratio.

Mixture Designs

The researchers used the optimized aggregate gradations and varied the paste volume. We started with a certain amount of cement binder and checked the obtained fresh concrete

properties like workability, air content, and response to the vibrator. We increased the cement binder as we got a harsh mixture with low slump in the first mixture.

In the next steps reducing the cement binder was associated with increasing of the aggregate amount in the mixture for a certain aggregate percentage. The workability and the mixture viscosity were observed. The viscosity of the mixture observed by the box test gives us an indicator of the mixture's response to the vibrator.

More reduction in cement binder occurred by switching to aggregate gradation with high aggregate packing with minimum void ratio. This also was combined by increasing the water to cement ratio a bit. Increasing the water to cement ratio with a suitable amount of Mid-Range Water Reducer was necessary to provide a mixture neither harsh nor sticky.

Ultimately a mixture was developed that showed satisfactory performance for strength, had a reasonable w/cm and WR dosage, and was able to pass the box test. This mixture was recommended to Ed Bell Construction and used successfully in the construction of FM 1938. Reports from Ed Bell Construction suggest that the mixture developed was able to reduce costs by at least 10 percent and reduce cement consumption and therefore reduce the carbon footprint by 25 percent.

Conclusions

Reducing the cement binder in a concrete mixture has been the subject of many studies. This work used an optimization of the aggregate gradation to achieve this goal. Gradation curves varied according to particle distribution and packing. The particle distributions were improved by using the standard gradation methods in combination with voids content measurements.

The following observations were made from the work:

- The Power 0.45 Chart was a good tool for determining the initial guess of aggregate gradations.
- In the Percent Retained or 8–18 Chart we used gradations that did not meet their suggested criteria and achieved good concrete properties.
- In the Shilstone Coarseness Chart, for mixtures with three-aggregate blends the points were lying in the well graded zone and close to the rocky zone. The points of mixtures with two-aggregate blends were also lying in the well graded zone but close to the gap graded zone. Despite this issue, satisfactory performance was obtained from both mixtures.
- Determining the voids content of the aggregate mixtures is a useful method to modify the suggested gradations from other techniques.
- Using the optimized gradations when choosing the appropriate cement content, water to cement ratio, and chemical admixture led to good mixture design that reduced the amount of cement binder, acquired good compressive strength, and had a suitable workability for pavement works.

- The box test has been shown to be a useful tool to predict the ability of a concrete to be used with a concrete paver.
- Satisfactory results were obtained by using concrete mixtures with 4.5 sacks with a three-aggregate blend and 4.75 sacks with a two-aggregate blend. These mixtures resulted in cost savings of about 10 percent and a reduction in the carbon footprint by about 25 percent.

CONCRETE MATURITY

Overview

The maturity method is a useful technique to estimate concrete strength while minimizing physical testing. The aim behind this idea is to model the effect of different curing temperatures on concrete strength (*31*). The maturity method is widely used because of its simplicity and accuracy in prediction of concrete strength.

The maturity theory has two main aspects: the first is application of the method to estimate in-place concrete strength, as described by ASTM C 1074 (*32*), and the second is projecting long-term concrete strength by measuring the early age concrete strength, which is adopted by ASTM C 918 (*33*).

The study includes the effect of material proportions on concrete maturity with the associated compressive strength. The study also includes the projecting of long-term concrete strength by means of concrete maturity according to ASTM C 918.

ASTM C 1074 defines the maturity as "a technique for estimating concrete strength that is based on the assumption that samples of a given concrete mixture attain equal strength if they attain equal values of maturity index."

A.G. Saul defined the maturity as "concrete of the same mixture at the same maturity has approximately the same strength whatever combination of temperature and time goes to make up that maturity" (*31*). In other words, if we have the same maturity for two mixtures with the same mixture design, the strength of concrete will be the same regardless of the combination of time and temperature for these two mixtures.

Advantages and Disadvantages of Maturity Method

Maturity is an accurate method to predict concrete strength. According to ASTM C 1074, in the field this method should be accompanied with another testing method to double-check the concrete strength.

The maturity method saves time and money by allowing forms to be removed early, early age sawing of pavements, and allowing structures to be open to traffic earlier. This method also saves money by reducing the samples required to perform the test (*34*).

The negative side of the maturity method is that hydration must continue without ceasing; otherwise the predictions by the method will be incorrect. This method will not take into account

inadequate consolidation or insufficient curing. Every mixture has its own unique maturity. Strength maturity curves should be established for each mixture (*34*).

Maturity Index and Equivalent Age Factor

This method provides a procedure for estimating concrete strength by means of the maturity index or equivalent age factor. Maturity index is expressed in terms of the temperature-time factor (°C-hour or °F-hour) according to the Nurse-Saul Function. Another method to calculate the maturity is to use the Arrhenius equation. The data from this method are expressed in terms of equivalent age (days or hours). These equations are summarized below:

1 – temperature-time factor or maturity index by Nurse-Saul equation (*31*):

$$M(t) = \sum (T - T_0)\, \Delta t \tag{7.8}$$

Where:
M (t) = temperature-time factor at age t, (°C-hours) or (°F-hours).
Δt = a time interval, days or hours.
T = average concrete temperature during time interval, °C or °F.
To = datum temperature, °C or °F.

Now we must find the lowest temperature at which strength gain is observed. This temperature can be calculated according to the ASTM C 1074 method. This temperature was adopted by Saul to be 0°C and then later adjusted to a value of −10°C (*31*). Other researchers like Plowman recommended using −12°C (*35*).

The Nurse equation can be expressed in terms of equivalent age at a reference curing temperature:

$$t_e = ((T - To) / (T_r - T_0))\, \Delta t \tag{7.9}$$

Where:
te = equivalent age at a reference curing temperature. It represents the duration of the curing period at the reference temperature that would result in the same maturity as the curing period at different temperatures.
Tr = reference curing temperature.

2 – Arrhenius Equivalent age at a specified temperature by Hansen-Pederson (Arrhenius) (*36, 37*):

$$te = \sum e^{\wedge}((-E)/R\{1/(273+T)-1/(273+Tr)\})\Delta t \qquad (7.10)$$

Where:
te = equivalent age at a reference curing temperature Tr, days or hours.
T = average temperature of concrete during time interval Δt, °C.
Tr = reference temperature, °C.
E = activation energy, J/mol.
R = universal gas constant, 8.3144 J/ (mol K).
Δt = time interval, days or hours.

Maturity Equations for Estimating In-Place Concrete Strength

The concept of concrete maturity has been expressed in the equation of Saul and Nurse, and then many equations appeared after that. The maturity index has been evaluated in many equations. The equations for evaluating the maturity index are as following (*31*).

1 – Nurse-Saul is a linear equation which overestimates the maturity index for temperatures below 20°C and underestimates the maturity index (age conversion factor) for temperatures above 20°C (early age). The maturity index is:

$$te = \sum \alpha \, \Delta t \qquad (7.11)$$

$$\alpha = (T - T_0)/ (Tr - T_0) \qquad (7.12)$$

Where:
te = equivalent age factor.
T = average temperature °C or °F.
To = datum temperature (−10°C or 14°F).
Tr = reference temperature (20°C or 68°F).
Δt = time interval (½ hour–1 hour).
A = age conversion factor. It converts the curing interval Δt into equivalent curing temperature at the standard reference temperature (*31*).

N.J. Carino does not recommend using this equation because it overestimates the maturity index for temperatures less than 20°C. This means that for ages above six days this equation gives inaccurate results (*38*).

2 – Rastrup equation is an exponential equation which is based on physical chemistry. This equation states that the reaction velocity is doubled if the temperature is increased by 10°C (*39*).

$$te = \sum(2^{(T-Tr)/10}) \, \Delta t \qquad (7.13)$$

For high concrete temperatures this equation yields higher values (*40*).

3 – Weaver and Sadgrove is another nonlinear equation (*41*). This equation gives a better strength estimation for a low maturity value than Nurse-Saul does. But for later maturities the Nurse-Saul equation will give more accurate results (*42*).

$$te = \frac{\sum(T+16)^2}{1296} \, \Delta t \qquad (7.14)$$

4 – Freiesleben Hansen and Pederson (Arrhenius) is another nonlinear equation, expressed in terms of absolute temperature (*37*). The curve will depend on the value of the activation energy value, as follows, according to Freiesleben Hansen and Pederson:

$$te = \sum_0^t e^{\frac{-E}{R}\left[\frac{1}{273+T} - \frac{1}{273+Tr}\right]} \, \Delta t \qquad (7.15)$$

T≥20°C E=33500 J/mol

For T<20°C E=33500+1470(20−T) J/mol

This equation is developed from the Arrhenius equation. It gives the best estimation of strength among a wide range of temperatures (*43*).
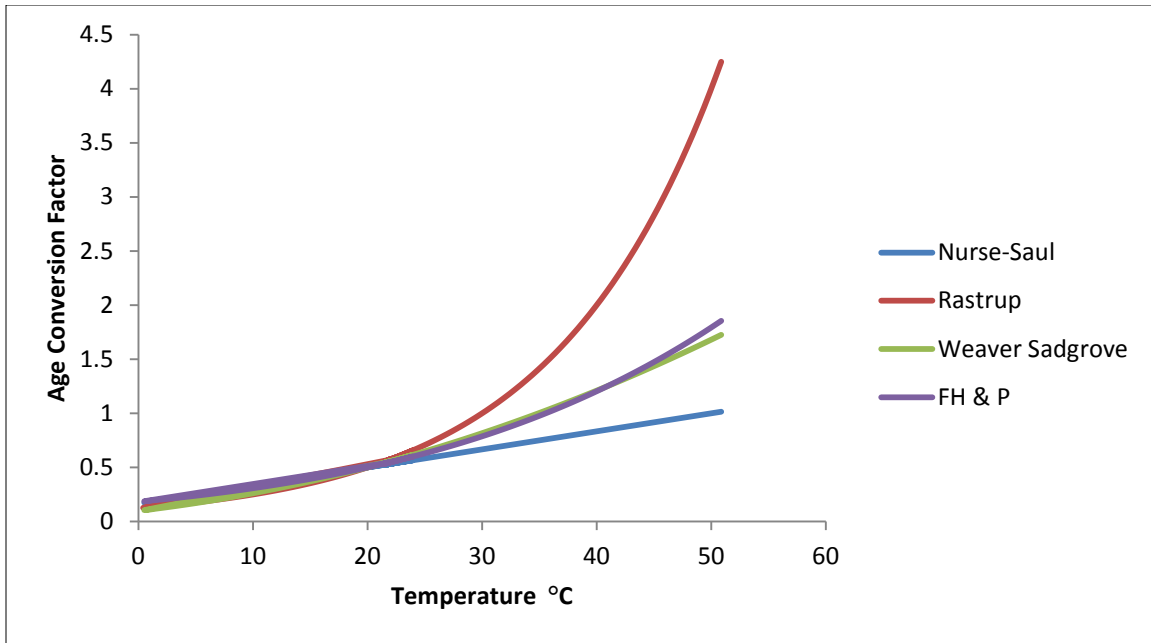
Figure 93. Comparison of Maturity Equations.

Figure 92 compares these equations for a certain mixture design and under different curing temperatures.

Maturity Equations for Predicting Strength

The previous section dealt with maturity as a means of estimating the in-place concrete strength depending on the hydration temperature history. Only one unique curve would represent the maturity-strength relation for a certain mixture. Any change in mixture design will lead to a different curve or relation (*44*).

The main strength–maturity equations can be classified as follows:

1 – Exponential equation, proposed by Nykanen in 1956 (*45*):

$$S = S\infty \, (1 - e^{kM}) \tag{7.16}$$

Where:
$S\infty$ = limiting strength.
S = compressive strength.
M = maturity index.
k = constant.

This equation uses a constant (k) whose value depends on the initial rate of strength development during the early age hydration. This is dependent on the water to cement ratio and the kind of cement used (*45*).

2 – Logarithm equation set by Plowman (*35*):

$$S = a + b \log(M) \tag{7.17}$$

Where:
a and b are constants.

Logarithm equations or linear equations adopted by the ASTM C 918 predict the long-term strength of concrete by measuring the early age strength. Logarithm of maturity index is represented on the horizontal axis, while the vertical axis is the concrete strength gained from 12 hours through 28 days or more. The constants (a) and (b) values are dependent on cement type and water to cement ratio used in the mixture. The drawback of this equation is the unlimited increasing strength value with respect to maturity index as it considers the relation as a line instead of curve (*46*).

3 – Lew and Reichard improved the Plowman equation to the following log-exponential equation (*47*):

$$S = \frac{K}{1 + D(\log(M-16.70))^{\wedge}b} \tag{7.18}$$

Where:
b and D are constants depending on cement type and water to cement ratio.
k = rate of strength also dependent on the water to cement ratio but less dependent on the cement type (*44*).

This improvement overcomes the negative side of the original logarithm equation by limiting the strength gain with increasing the maturity (*47*).

4 – Hyperbolic equation was proposed by Bernhardt in 1956 and developed by Chin (*48,49*). This theory was adopted by the ACI committee 229. The initial slope of the relation will control the shape of the hyperbolic curve (*49*):

$$S = M/(1/A + M/S\infty) \tag{7.19}$$

Where:

M = maturity index.

S∞ = limiting strength.

A = initial slope of strength maturity curve.

The equation above was later modified to account for the effect of early maturity on strength development in which the hyperbolic equation considered that the strength starts from maturity (M) =0, while real strength starts after the concrete has been set (*50*). Adding a shifting value of maturity to the previous equation solved this issue (*51*):

$$S = \frac{M\text{-}M_0}{\frac{1}{A} + \frac{M\text{-}M_0}{S\infty}}$$ (7.20)

Where:

M_0 = initial maturity in which strength starts > 0.

5 – Maturity-Heat of hydration equation, suggested by Freiesleben Hansen and Pederson to correlate the heat of hydration with maturity according to the following equation (*52*):

$$f = f_{cult}\ e^{-\left(\frac{\tau}{te}\right)^{\beta}}$$ (7.21)

Where:

f_{cult} = limiting strength (psi).

te = equivalent age (hour).

τ = time constant (hour).

β = shape parameter.

According to Carino, this equation can model gradual strength development during the setting period, and it is also asymptotic to a limiting strength (*38*). The time constant (τ) represents the time required to acquire 0.37 of the limiting strength. (1/ τ) represents the rate constant for this equation. The shape parameter (β) will affect the slope of the maturity curve (*38*).

Materials

Table 17 shows material properties used in this study and standard requirements.

Table 17. Requirements for Material Properties.

Material	Type	Sp. Gr.	Requirements
1-Cement	Type l/TX	3.15	ASTM C 150
2-Fly ash	Class F/Martin Lake	2.5	ASTM C 618
3-Coarse aggregate 1.5"	G3/TX	2.65	ASTM C 127, ASTM C 33
4-Intermediate aggregate	⅜"/TX	2.65	ASTM C 127
5-Sand	TX	2.65	ASTM C 128, ASTM C 33
6-Water	Tap water	1	ASTM C 1602
7-Water reducer	DARACEM 55	1.28	ASTM C 494
8- Air entertainer	DARAVAIR 1400	1.02	ASTM C 260

Maturity can be calculated by inserting thermocouples and recording temperature over time. Maturity then can be calculated by the Nurse-Saul equation or the Arrhenius equation. An interval of 30 minutes was chosen to acquire accurate results.

Mixture Designs

Table 18 lists the materials used and mixture designs. Table 19 lists the fresh and hardened concrete tests results.

The mixtures used were developed through the techniques explained in the chapter on optimized graded concrete. The first mixture had a total binder of 423 lb/yd^3, with a w/cm of 0.45. Class F fly ash represented 35 percent of the total cementitious materials. Coarse, medium, and fine aggregate sizes were used in the first mixture. In mixtures 2, 3, and 4 we increased the cementitious materials with a 0.43 water to cement ratio. The increasing of cementitious materials was needed to offset the loss of the intermediate-sized aggregate. The materials and quantities are the same in mixtures 3 and 4 but with increased water reducer in mixture 4.

Table 18. Mixture Designs and Results.

Mix #	Cement (lb/cy)	Fly Ash (lb/cy)	Binder (lb/cy)	G3 (lb/cy)	⅜" (lb/cy)	Sand (lb/cy)	Water (lb/cy)	w/c	AEA (Oz/cwt.) DARAVAIR	WR (Oz/cwt.) DARACE M	Slump (in)	Unit wt. (lb/ft³)	Air (%)
1	275	148	423	1626.8	467	1265.6	190.35	0.45	0.45	6.1	1.5"	147.6	5
2	290.2	156.3	446.5	1941	0	1395	192	0.43	0.32	10.2	1.5"	148.4	5.7
3	320.8	172.7	493.5	1886	0	1355	212.2	0.43	0.62	5.2	4.4"	144.3	6.9
4	320.8	172.7	493.5	1886	0	1355	212.2	0.43	0.50	9.2	3.4"	143.5	7.3

Table 19. Mixture Designs and Results.

Mix #	0.5 day Comp (psi)	σ (psi)	1 day Comp (psi)	σ (psi)	3 days Comp (psi)	σ (psi)	5 days Comp (psi)	σ (psi)	7 days Comp (psi)	σ (psi)	14 days Comp (psi)	σ (psi)	28 days Comp (psi)	σ (psi)	56 days Comp (psi)	σ (psi)

Compressive Strength & Standard Deviations for Different Ages

Mix #	0.5 day Comp (psi)	σ (psi)	1 day Comp (psi)	σ (psi)	3 days Comp (psi)	σ (psi)	5 days Comp (psi)	σ (psi)	7 days Comp (psi)	σ (psi)	14 days Comp (psi)	σ (psi)	28 days Comp (psi)	σ (psi)	56 days Comp (psi)	σ (psi)
1	480	19	1231	40	2661	31	3301	163	3603	18	4763	140	5857	166	6947	217
2	255	126	1776	16	3515	12	4090	51	4508	85	4704	65	6062	151	7075	93
3	404	13	1535	43	3147	120	3671	66	3891	129	3761	100	4677	94	5609	19
4	337	15	1613	54	3327	53	4100	147	4278	78	4754	71	5802	94	6678	131

Methods

Effect of Materials Proportions on Concrete Maturity

We prepared two mixtures with exactly the same proportions to observe the variation in the data. In our research we applied the same curing conditions and monitored temperatures for every mixture with respect to time to observe the effect of the materials proportions on the maturity-strength curve. We completed the following steps according to ASTM C 1074:

1. Molded the samples according to ASTM C 31 (*53*). Thermocouples were inserted into two samples to record the temperature over time.
2. Cured the samples in a moist room at a controlled temperature.
3. Performed the compressive strength test as per ASTM C 39/C 39M (*24*). The ages of testing were 12 hours, 1, 3, 5, 7, 14, 28, and 56 days, respectively.
4. Calculated the maturity index by the Nurse-Saul equation (temperature-time index) after observing the temperatures over time.
5. Plotted the relationship between the compressive strength and maturity index.

Predicting Later-Age Strength

In order to obtain the necessary parameters for ConcreteWorks, the following equations were used:

$$SM = Sm + b \ (\log M - \log m) \tag{7.22}$$

Maturity index for later age (M) can be established from the maturity-strength curve according to ASTM C 1074. We can determine the maturity index for the desired age directly from the graph. The maturity index can be plotted in log scale, and the slope of the best fit line from the regression analysis will determine the unknowns.

The Constants in Maturity-Strength Equations

Constants of the Logarithm Equation. The logarithm equation was adopted by ASTM C 918 to predict the concrete strength by maturity method.

$$S = a + b \log (M) \tag{7.23}$$

According to the specification of ASTM C 918, the constant (a) represents the intersection of the maturity-strength line (in log scale) with the vertical axis which represents the compressive strength, while the constant (b) represents the slope of the mentioned line.

Constants of Maturity-Heat of Hydration Equation. This equation was set by Freiesleben Hansen:

$$f = f_{cult} \, e^{-\left(\frac{\tau}{te}\right)^{\beta}} \qquad (7.24)$$

According to Carino the time constant (τ) represents the age at which the strength has reached 0.37 of the limited strength (Su) (*38*).

The first step is to establish the relation between the equivalent age and compressive strength. Equivalent age was determined by the Arrhenius equation.

$$te = \sum_{0}^{t} e^{\frac{-E}{R}\left[\frac{1}{273+T} - \frac{1}{273+Tr}\right]} \Delta t \qquad (7.25)$$

T$\geq$20°C E=33500 J/mol

For T<20°C E=33500+1470(20−T) J/mol

We calculated the equivalent age factor (te) according to the Arrhenius equation. We plotted the equivalent age-strength in log scale with the associated compressive strength. From the graph we can estimate the value of equivalent age corresponding to the 0.37 of the limited strength which represents the time constant (τ). The value of β (shape parameter) has been expressed depending on the main equation:

$$f = f_{cult} \, e^{-\left(\frac{\tau}{te}\right)^{\beta}} \qquad (7.26)$$

Simplifying the above equation into:

$$\beta = \ln (\ln f_{cult} - \ln f) / (\ln \tau/te)$$

Results – Effect of Materials Proportions on Concrete Maturity

The compressive strength of every mixture has been plotted with respect to the corresponding maturity. Figure 93 shows the results.
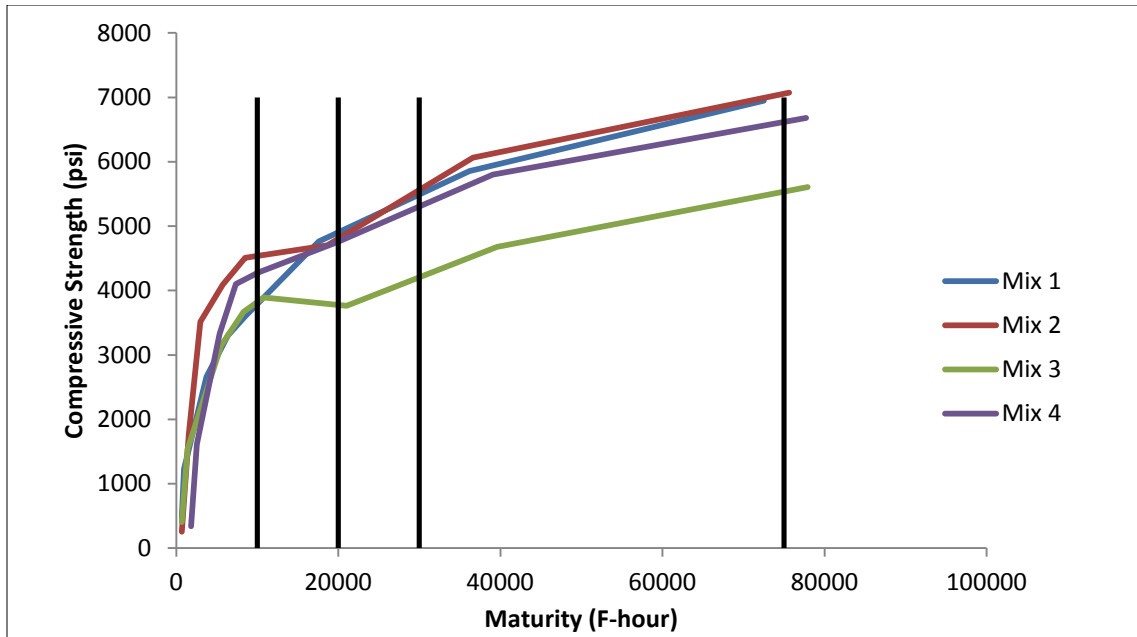
Figure 94. Zones of Maturity-Strength Development.

Figure 94 shows the maturity index in log scale with respect to the compressive strength for mixture 4. Mixture 4 was used to show the typical process. Table 20 shows the obtained values of the logarithm parameters. Figure 95 shows the maturity versus strength relationship for all mixtures. Figure 96 shows the (equivalent age-strength) curves for the mixtures. Table 21 provides the constants of the Logarithm and Hansen equations.
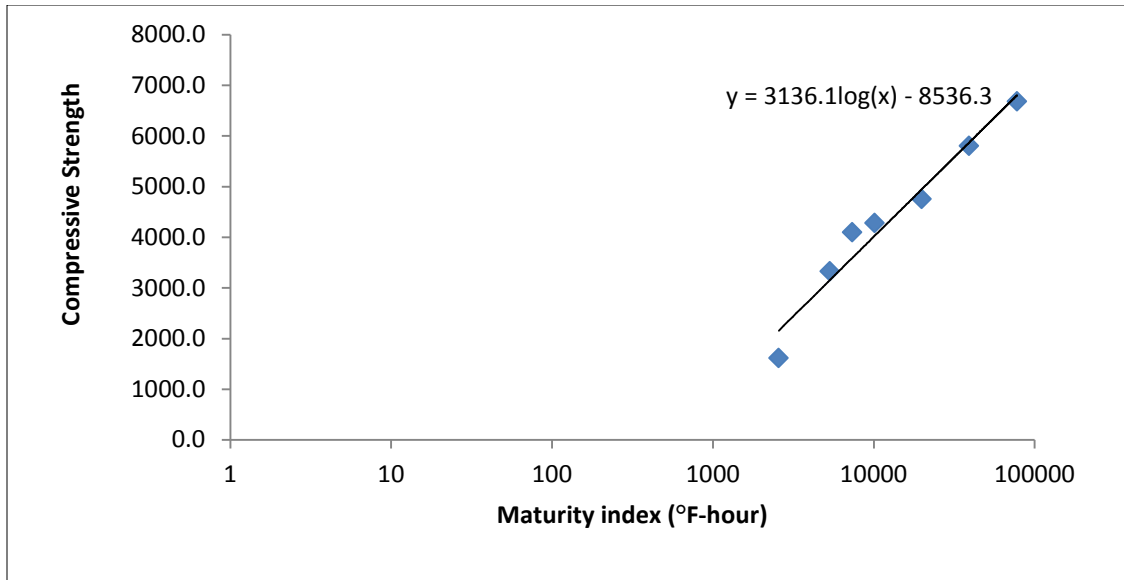
Figure 95. The Log of Maturity vs. Strength of Mixture 4.

Table 20. Predicted Strength Result.

b	Compressive Strength (psi)	Maturity (°F-hour)	Compressive Strength (psi)	
psi/°F/hour	Sm	M	Projected(SM)	Actual
3136.0	1272.0	1068.0	6174.0	5802.0
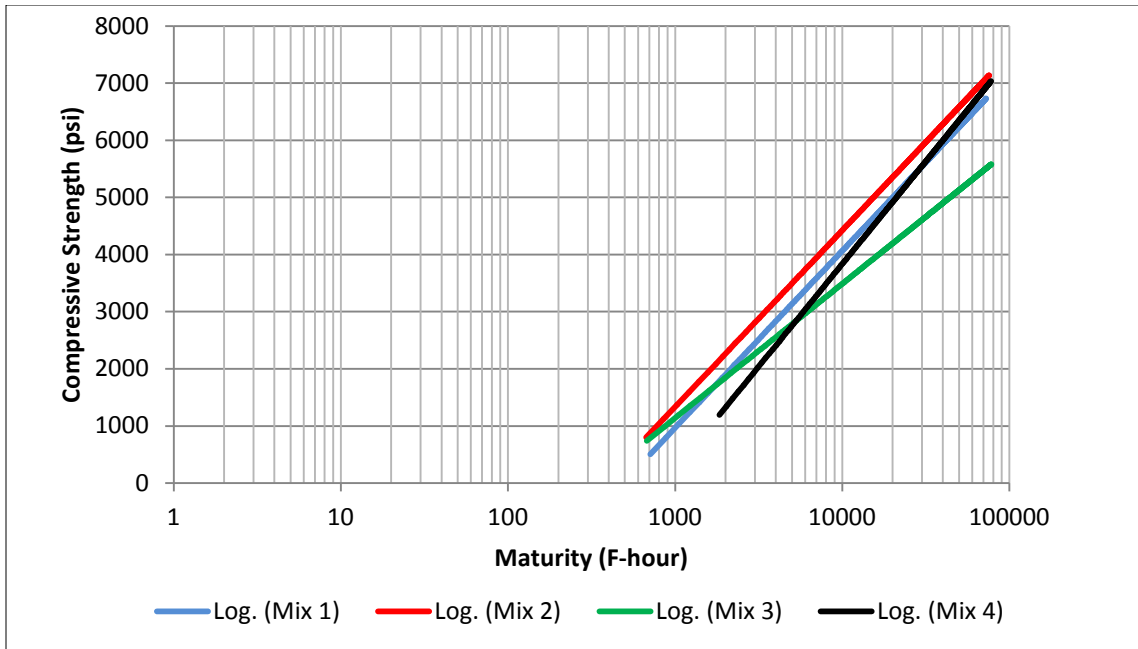
Figure 96. Maturity vs. Strength Curves.
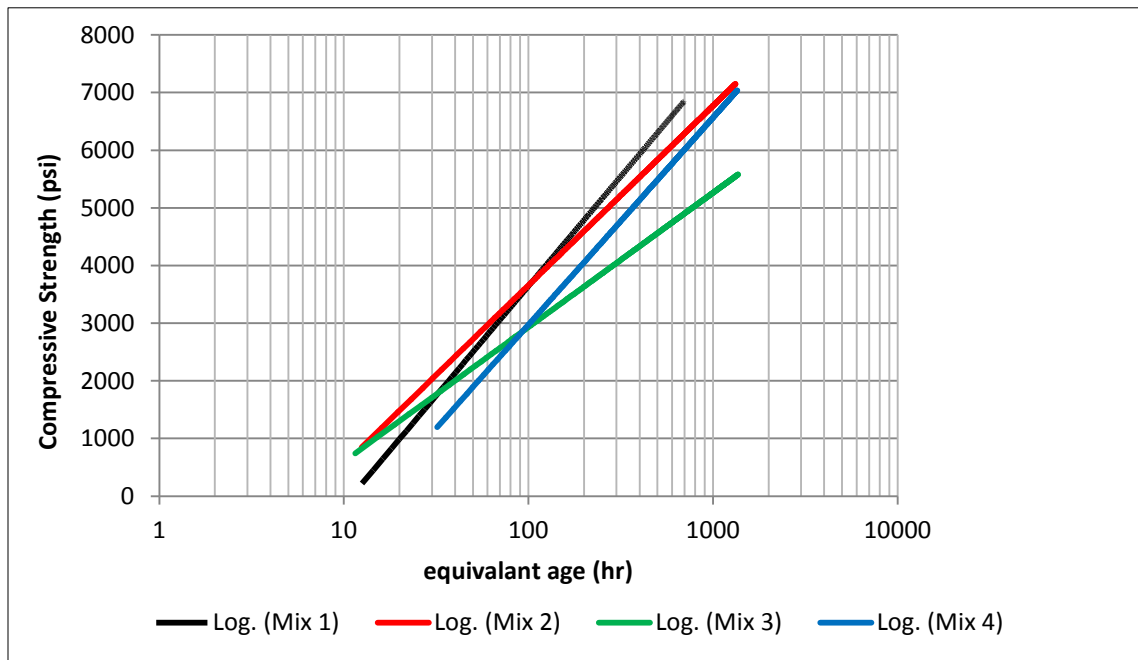
Figure 97. Equivalent Age Maturity-Strength Curves.

Table 21. Constants for Maturity Equations.

Mixture	Logarithm Equation		Hansen Equation	
	a (psi)	b (psi/°F/hour)	τ (hour)	β
1	−11,223	3802	30	0.99
2	−7936	3087	35	0.89
3	−5899	2344	55	0.59
4	−8536	3136	50	1.36

Effect of Materials on Maturity

The concrete maturity can estimate the in-situ concrete strength. This rate is affected by the curing temperature. In this study we held the curing environment fixed and observed the effect of the material proportions on maturity-strength curves. Some key observations were made:

- Mixture 1 used the minimum cementitious binder (423 lb/yd^3) but achieved a good compressive strength especially in later age. This high strength is likely caused by the use of an intermediate aggregate in the mixture.
- Mixture 2 had an increased binder content, water reducer dosage, reduced w/cm, and the highest compressive strength when compared at a comparable maturity index. The performance of this mixture was very close to the results from mixture 1.
- Despite mixture 3 using higher binder content it showed a lower strength gain than mixtures 1 and 2. Actually this mixture will require more time to achieve the desired strength compared with the other mixtures. This may be due to the reduction in water reducer from 10.2 oz/cwt in mixture 2 to 5.2 oz/cwt in mixture 3.
- Mixture 4 was the same as mixture 3 with a higher dosage of water reducer. This led to an improvement in the strength for a given maturity index. The water reducer is known to improve the strength with increased dosages.

Predicting Later-Age Strength

Predicting later-age strength by means of maturity depends on imperial equations. ASTM C 918 adopted the logarithm equation in establishing the maturity-strength relation. Results obtained were close to the measured strength. The slope of the line is important in projecting the strength. The slope of the line depends on the maturity-strength relation that has been plotted according to the ASTM 1074.

Conclusion

In our study we were investigating the effect of material proportions on the maturity of concrete. The results highlight the impact on strength when using optimized graded concrete over gap graded mixtures. The maturity-strength curves were found to improve with increased dosage of water reducer, reducing w/cm, and adding intermediate aggregate size.

The concrete strength predicted by the maturity equations has closely matched the measured compressive strength.

The necessary input parameters were found to describe the maturity-strength relationship for each of the mixtures investigated.

REFERENCES

1. Kosmatka, Steven H., Beatrix Kerkhoff, and William C. Panarese. Design and Control of Concrete Mixtures. 14th ed. 2002.
2. Roberts, F.L., P.S. Kandhal, E.R. Brown, D.Y. Lee, and T.W. Kennedy. Hot Mix Asphalt Materials, Mixture Design, and Construction. National Asphalt Paving Association Education Foundation. Lanham, MD. 1996.
3. University of Missouri-Rolla. Aggregate Gradation Optimization. January 2005.
4. Koehler, E.P., and D.W. Fowler. Role of Aggregates in Self-Consolidating Concrete, ICAR Report 108-F, International Center for Aggregates Research, Austin, TX. 2007.
5. Lamond, J.F., and J.H. Pielert. "Significance of Tests and Properties of Concrete and Concrete-Making Materials," American Society for Testing and Materials, Philadelphia, PA. 2006. pp. 337–354.
6. Neville, A.M. Properties of Concrete, Prentice Hall. 2000. p. 844.
7. ASTM C 33/C 33M Standard Specification for Concrete Aggregates.
8. Ahn, N.S., and D.W. Fowler. "An Experimental Study on the Guidelines for Using Higher Contents of Aggregate Microfines in Portland Cement Concrete," International Center for Aggregates Research Report 102-1F. Austin, TX. 2001.
9. Talbot, A.N., and F.E. Richart. "The strength of concrete – Its relation to the cement aggregates and water - Engineering Experiment Station Bulletin No. 137," University of Illinois Bulletin, Vol. 21, No. 7. 1923. p. 116.
10. Good, J.F., and L.A. Lufsy. "Voids, Permeability, Film Thickness vs. Asphalt Hardening." Proceeding of the Association of Asphalt Pavement Technologists, Vol. 34. 1965.
11. Abrams, D.A. "The Basic Principles of Concrete Mixes." Mining and Scientific Press. 1918. pp. 23–24.
12. Abrams, D.A. "Design of Concrete Mixtures." Bulletin No. 1, Structural Materials Research Laboratory. 1918. pp. 1–22.
13. Young, R.B. "Some Theoretical Studies on Proportioning Concrete by Method of Surface Area of Aggregate." Proceedings, ASTM 19 (Part II). 1919. pp. 444–509.

14. Newman, A.J., and D.C. Teychenné. A classification of sands and its use in concrete mix design, Symposium on Mix Design and Quality Control of Concrete, Cement and Concrete Association, London. 1954. pp. 175–193.
15. Day, Ken W. Concrete Mix Design, Quality Control and Specification. 2006.
16. Shilstone, J.M. "Concrete Mixture Optimization." Concrete International 12(6). 1990. pp. 33–39.
17. Shilstone, J.M..Mixture Optimization for Fast-Track. 69th Annual Transportation Research Board Meeting, Washington, D.C. 1990.
18. Holland, J.A. "Mixture Optimization." Concrete International 12 (10) 1990.
19. Quiroga, P.N., and D.W. Fowler. "Guidelines for Proportioning Optimized Concrete Mixtures with High Microfines." International Center for Aggregates Research Report 104-2, Austin, TX. 2004.
20. ASTM C 29. Standard Test Method for Bulk Density ("Unit Weight") and Voids in Aggregate.
21. Vloem, D.L., and R.D. Gaynor. Effects of aggregate properties on strength of concrete. Journal of American Concrete Institute. 1963. pp. 429–455.
22. Fuller, W.B., and S.E. Thompson. The laws of proportioning concrete, Trans., ASCE 59. 1907. pp. 67–143.
23. Furnas, C.C. Grading the aggregates I-Mathematical relations for beds of broken solids of maximum density. Ind. Eng. Chem. Vol. 23. No. 9. 1931, pp. 1052–58.
24. ASTM C 39/C 39M – 11a: Standard Test Method for Compressive Strength of Cylindrical Concrete Specimens.
25. Glavind, M., and E.J. Pedersen. Packing Calculations Applied for Concrete Mix Design. Danish Technological Institute, Denmark. University of Dundee. May 1999.
26. ASTM C 143. Standard Test Method for Slump of Hydraulic-Cement Concrete.
27. ASTM C 231. Standard Test Method for Air Content of Freshly Mixed Concrete by the Pressure Method.
28. ASTM C 138. Standard Test Method for Density (Unit Weight), Yield, and Air Content (Gravimetric) of Concrete.
29. ASTM C 39. Standard Test Method for Compressive Strength of Cylindrical Concrete Specimens.
30. ASTM C 136. Standard Test Method for Sieve Analysis of Fine and Coarse Aggregates.
31. Saul, A.G.. Principles underlying the steam curing of concrete at atmospheric pressure, Mag. Concr. Res., Vol. 2. No. 6. 1951. p. 127.
32. ASTM C 1074 – 11. Standard Practice for Estimating Concrete Strength by the Maturity Method.
33. ASTM C 918/C 918M – 07. Test Method for Measuring Early-Age Compressive Strength and Projecting Later-Age Strength.

34. Wade, Samuel A., Anton K. Schindler, Robert W. Barnes, and Jeffery M. Nixon. Alabama Department of Transportation. Evaluation of the Maturity Method to Estimate Concrete Strength. May 2006.
35. Plowman, J.M. Maturity and the strength of concrete, Mag. Conc. Res, Vol. 8. No. 22. 1956. p.13.
36. Copland, L.E., D.L. Katro, and G. Verbeck. Chemistry of hydration of Portland cement, Part III: Energetics of the hydration of Portland cement. In Proc. Fourth Int. Symp. on Chemistry of Cement, NBS Monograph 43, Washington, D.C. 1962. p. 453.
37. Freiesleben, Hansen P., and E.J. Pederson. Maturity computer for controlled curing and hardening of concrete, Nord. Betong, 1. 1977. p. 19.
38. Carino, N.J., and H.S. Lew. The Maturity Method: from Theory to Application. Structures Congress and Exposition, American Society of Civil Engineers, May 2011.
39. Rastrup, E. Heat of hydration in concrete, Mag. Concr. Res., Vol. 6. No. 17. 1954. p. 79.
40. Wastland, G., Hardening of concrete as influenced by temperature, General Report of Sesssion BII, in Pro. RILEM Symposium on Winter Concreting, Copenghagen, Danish Institute for Building Research, Copenghagen. 1956.
41. Weaver, J., and B.M. Sadgrove. Striking times of formwork--tables of curing periods to achieve given strength, Construction Industry Research and Information Association, Rep. 36, London, October 1971.
42. Sadgrove, B.M. Prediction of strength development in concrete structures, Trans. Res. Rec., 558, 19, 1975.
43. Naik, T.R. Maturity functions for concrete cured during winter conditions. In Temperature Effects on Concrete, T.R. Naik, Ed., ASTM STP 858. 1985. p. 107.
44. Malhotra, V.M., and N.J.Carino. Nondestructive Testing of Concrete. CRC Press, 2003.
45. Nykanen, A. Hardening of concrete at different temperatures, especially below the freezing point, in Proc. RILEM Symp. on Winter Concreting, Session BII, Copenghagen, Danish Institute for Building Research, Copenghagen. 1956.
46. Discussion of Reference 3, Mag. Concr. Res., Vol. 8. No. 24. 1956. p. 169.
47. Lew, H.S., and T.W. Reichard. Prediction of strength of concrete from maturity. Accelerated Strength Testing, ACI SP-56, V.M. Malhotra, Ed., American Concrete Insitute, Farmington Hills, MI. 1978. p. 229.
48. Prediction of creep, shrinkage, and temperature effects in concrete structures, ACI 209R-92, Report of Committee 209. Manual of Concrete Practice, American Concrete Institute, Farmington Hills, MI. Reapproved 1997.
49. Chin, F.K. Relation between strength and maturity of concrete, J.Am.Conc. Inst., Vol. 68. No. 3. 1971. p. 196.
50. Carino, N.J. Discussion of Reference 32, J. Am. Conc. Inst., Vol. 81. No. 1. 1984. p. 98.
51. Carino, N.J. Temperature effects on strength – maturity relation of mortar, NBSIR8 81-2244, U.S. National Bureau of Standards. March 1981.

52. Freiesleben, Hansen P.,, and E.J. Pederson. Curing of concrete structures, CEB Inf. Bull. May 1985. p. 166.
53. ASTM C 31/C 31M – 10: Standard Practice for Making and Curing Concrete Test Specimens in the Field.

CHAPTER 8 CONCRETEWORKS CALIBRATION

Temperature data collected from the concrete pavement placed on FM 1938 in March and August of 2011 were used to calibrate the concrete pavement temperature prediction model in ConcreteWorks. Thermocouples were placed 8.5 inches, 4.25 inches, and 1.25 inches from the top of the concrete pavements at Section 2 [Station 115 to 132] and Section 4 [Station 160 to 205] to measure the concrete temperature development with time after placement. The air temperature was also measured and was used in the calibration.

Inputs for the ConcreteWorks analysis came from project concrete mixture proportions and pavement dimensions used on site, air temperature recorded on site, and measured relative humidity and wind speed in Ft. Worth from Weather Underground (http://www.wunderground.com/history/airport/KAFW/2011/3/29/DailyHistory.html). Table 22 shows the general inputs used in the pavement temperature modeling. Table 23 shows the concrete mixture proportions, materials, and construction methods used in the analysis. Table 24 shows the maximum and minimum temperatures, maximum and relative humidity, and maximum wind speeds used in the modeling. The maximum and minimum daily air temperature measured on site was used in the analysis. The maximum and minimum relative humidity and maximum wind speed from Ft. Worth were also used in the analysis.

Table 22. General Inputs Used in Pavement Temperature Modeling.

| Input	Section 2	Section 4
Placement Time	12 A.M. (midnight)	4:00 P.M.
Placement Date	Aug. 7	Mar. 16
Location	Ft. Worth	Ft. Worth
Pavement Thickness (inch)	9	9
Subbase 1 Thickness (inch)	1	1
Subbase 1 Type	Asphalt Concrete	Asphalt Concrete
Subbase 2 Thickness (inch)	14	14
Subbase 2 Type	Cement Stabilized	Cement Stabilized
Subgrade Type	Clay	Clay

Table 23. Concrete Mixture Proportions, Materials, and Construction Methods Used in Modeling.

Input	Section 2	Section 4
Water Content (lb/yd^3)	165.23	191.9
Cement Content (lb/yd^3)	300	362
Class F Fly Ash (lb/yd^3)	156	155
Coarse Aggregate Content (lb/yd^3)	2106	1965
Fine Aggregate Content (lb/yd^3)	1197	1194
Air Content (%)	5	5
Water Reducer Used	Mid-Range Water Reducer	Mid-Range Water Reducer
ASTM C 150 Cement Type	I/II	I/II
Coarse Aggregate Type	Limestone	Limestone
Fine Aggregate Type	Siliceous River Sand	Siliceous River Sand
Placement Temperature (°F)	80	75
Curing	Double Coat Curing Compound	Double Coat Curing Compound

Table 24. Environmental Inputs Used in Modeling.

	Section 2					Section 4				
	Temperature		Relative Humidity		Max. Wind Speed	Temperature		Relative Humidity		Max. Wind Speed
Day	Max.	Min.	Max.	Min.		Max.	Min.	Max.	Min.	
1	104	84	61	24	14	78	51	88	52	21
2	108	86	55	22	15	88	63	84	38	25
3	117	85	64	19	14	94	65	88	38	18
4	115	85	60	18	13	87	65	90	38	21
5	105	82	74	39	21	85	62	87	39	23
6	115	76	67	25	23	86	64	83	39	18
7	88	76	100	53	14	86	65	77	41	25
8	106	79	94	33	6	83	62	93	13	15
9	113	87	85	25	10	83	46	82	19	13
10	110	86	56	19	14	92	61	90	38	17
11	113	84	56	18	9	89	68	90	20	21
12	114	85	65	15	13	51	47	93	74	14
13	115	87	54	18	14	69	47	87	52	13
14	115	86	54	19	14	55	50	97	69	15
15	113	85	62	26	12	61	38	93	58	13

In order to calibrate the model, the predicted temperature results for Section 2 were first compared to the measured results. It was found that the predicted temperatures were too low. The solar absorptivity and concrete surface emissivity coefficients for cases with concrete curing compound were then adjusted. The solar absorptivity is a ratio of the amount of solar radiation heat that is absorbed by the surface to the total amount of solar radiation heat that impacts the surface. The concrete solar absorptivity for a double coat of curing compound was set to 0.52, whereas the surface emissivity was set to 0.65. Section 4 was then analyzed to validate the solar absorptivity and emissivity values selected. Figure 97a–c shows the temperature development for Section 2 top, middle, and bottom temperature sensors and corresponding modeled temperatures. Figure 98a–c shows the temperature development for Section 4 top, middle, and bottom temperature sensors and corresponding modeled temperatures.
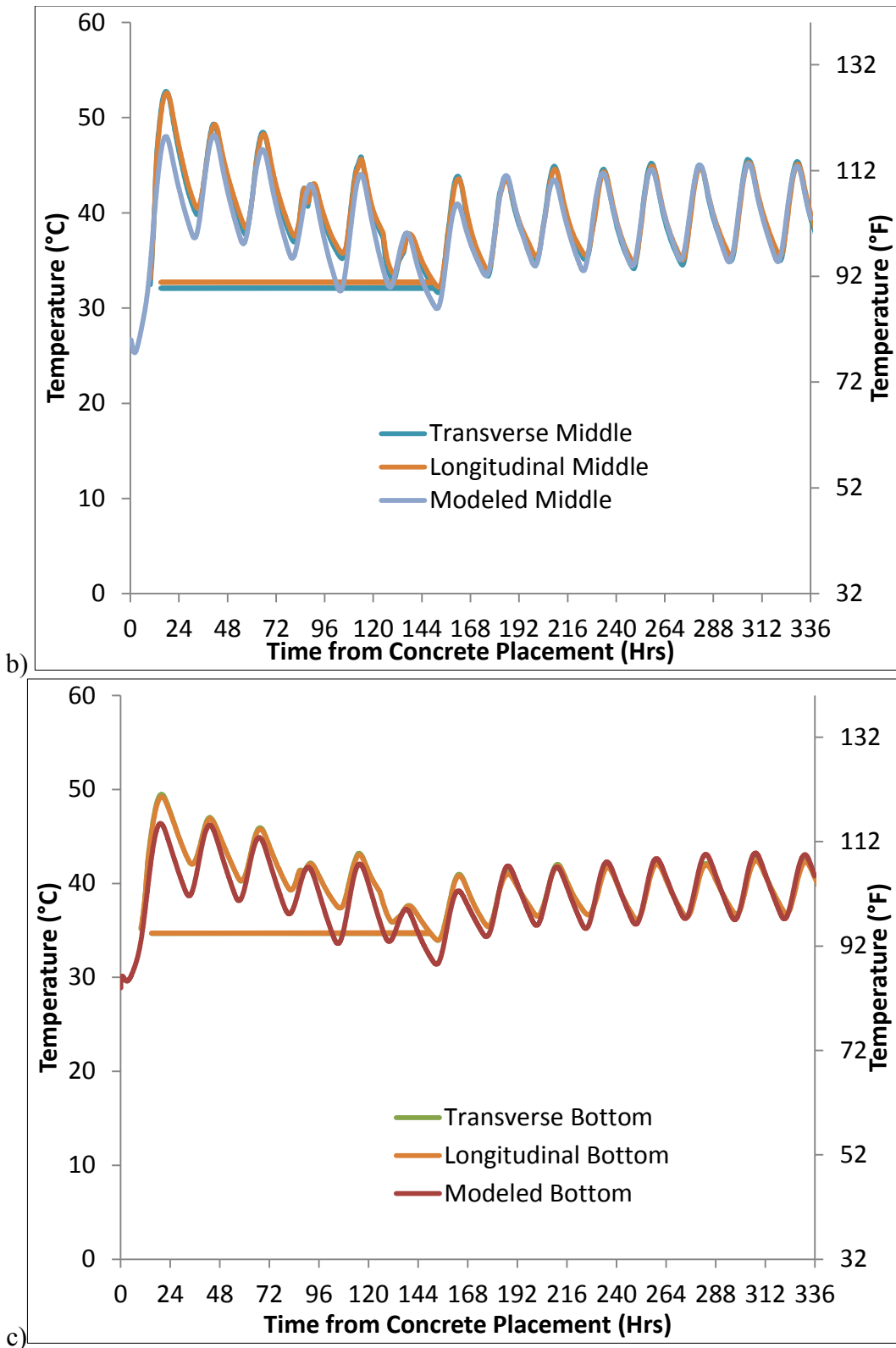

a)
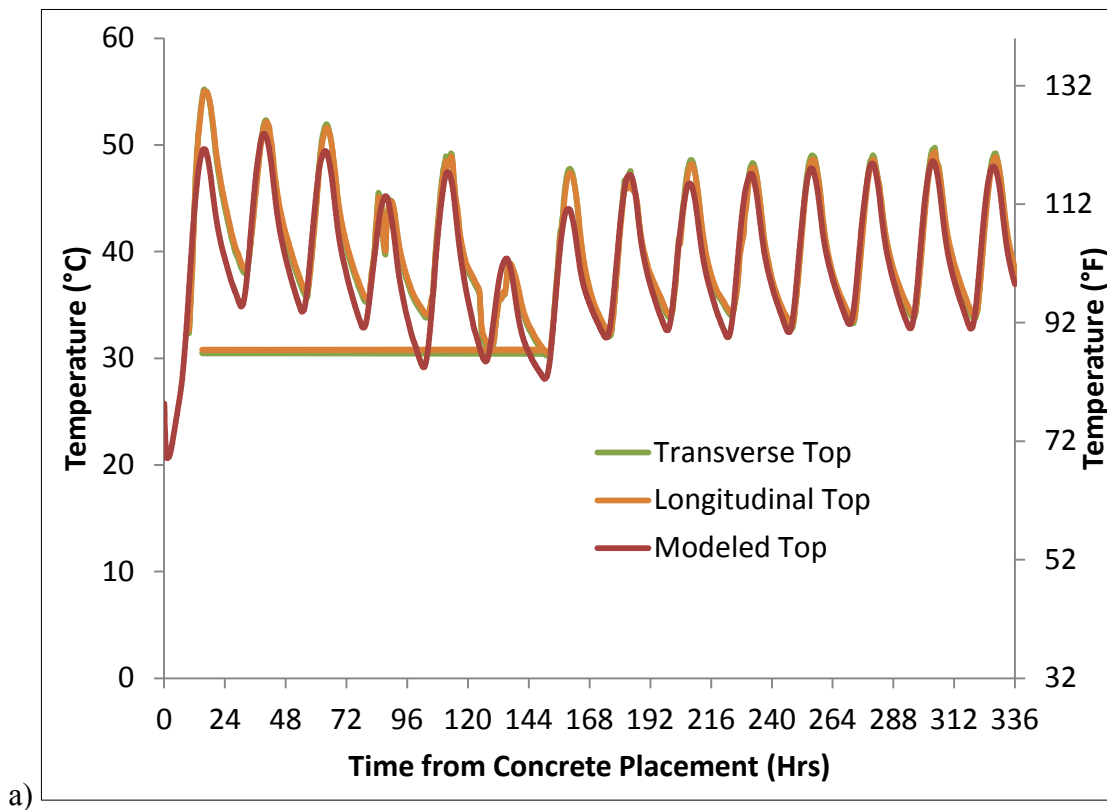
Figure 98. Temperature Development in Section 2 a) Top, b) Middle, and c) Bottom.

a)

b)

119

c)
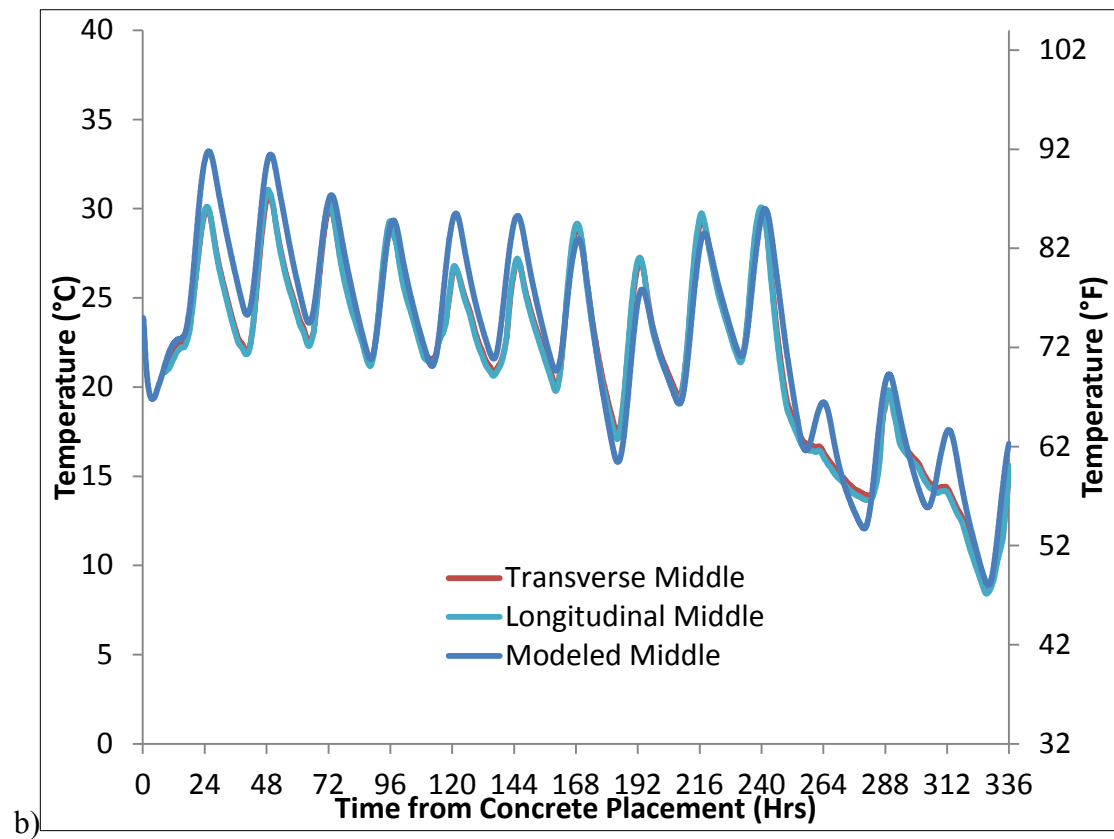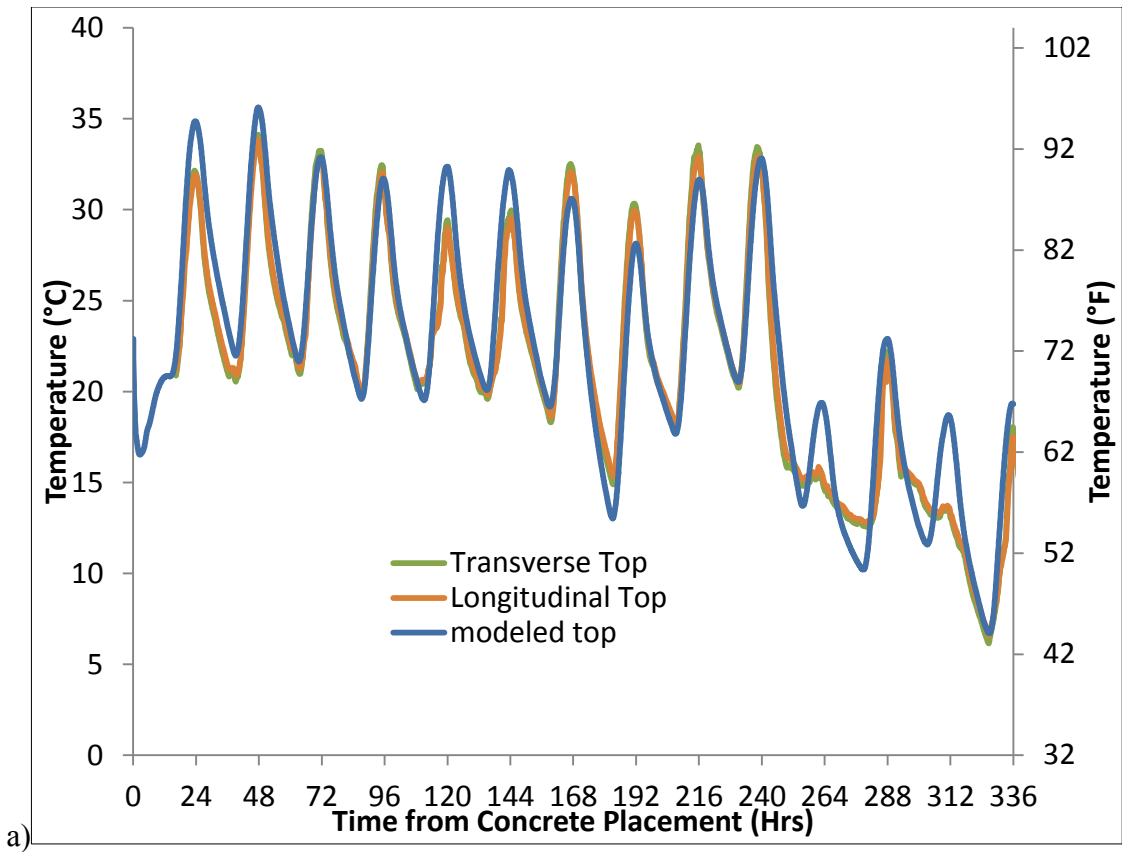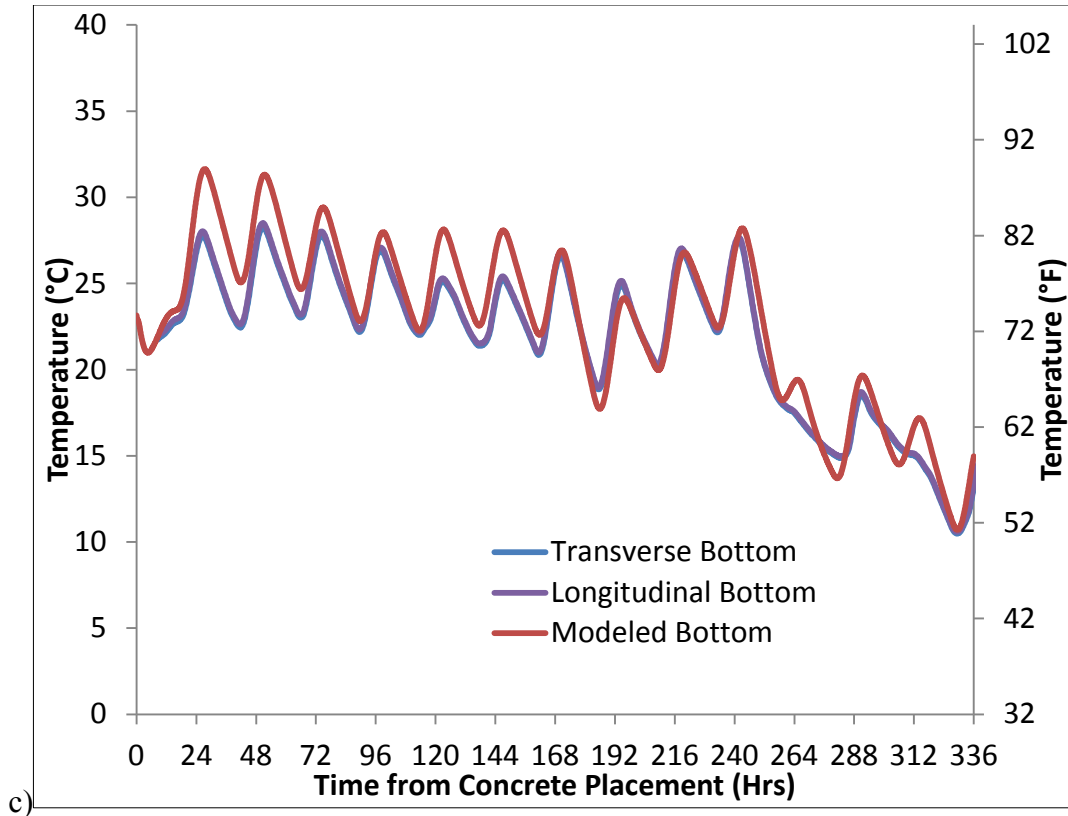
Figure 99. Temperature Development in Section 4 a) Top, b) Middle, and c) Bottom.

The modeled concrete pavement temperature fit the measured temperatures well. Table 25 shows the mean absolute error and R^2 value for each modeled section compared to the temperature measured on the transverse section.

Table 25. Error Estimates for Modeled Pavement Temperatures.

Error Estimates	Temperature Sensor Location in Pavement	Pavement Test Section	
		Section 2	Section 4
Mean Absolute Error (°C)	Top	1.88	1.58
	Middle	1.16	1.32
	Bottom	1.28	1.36
R^2	Top	0.89	0.92
	Middle	0.91	0.93
	Bottom	0.89	0.94

CONCRETEWORKS AGGREGATE OPTIMIZATION

An aggregate gradation optimization tool has been made for ConcreteWorks as shown in Figure 99. The tool allows the user to select to use the ACI 211 method for selecting coarse and fine aggregate weights or to optimize the aggregate gradation. For all concrete mixture proportioning options, the total aggregate volume is calculated as the volume in a cubic yard remaining after the air content is selected, and the maximum size aggregate used, the water content needed to provide a given slump for the maximum size aggregate, and the cement content needed to achieve a target strength are selected. For the aggregate optimization methods, once the aggregate volume is calculated, the software calculates the optimum combination of aggregate weights for each aggregate with a sieve gradation entered. For the Power 0.45 curve optimization, the sum of the absolute differences between the optimum Power 0.45 line and the combined gradation on each sieve is minimized. For the percent retained curve, the combined gradation was optimized to minimize the difference between the combined gradation and 13 percent retained on each sieve. For the coarseness factor chart, the combined gradation is fit to a coarseness factor of 60 and a workability factor of 35.
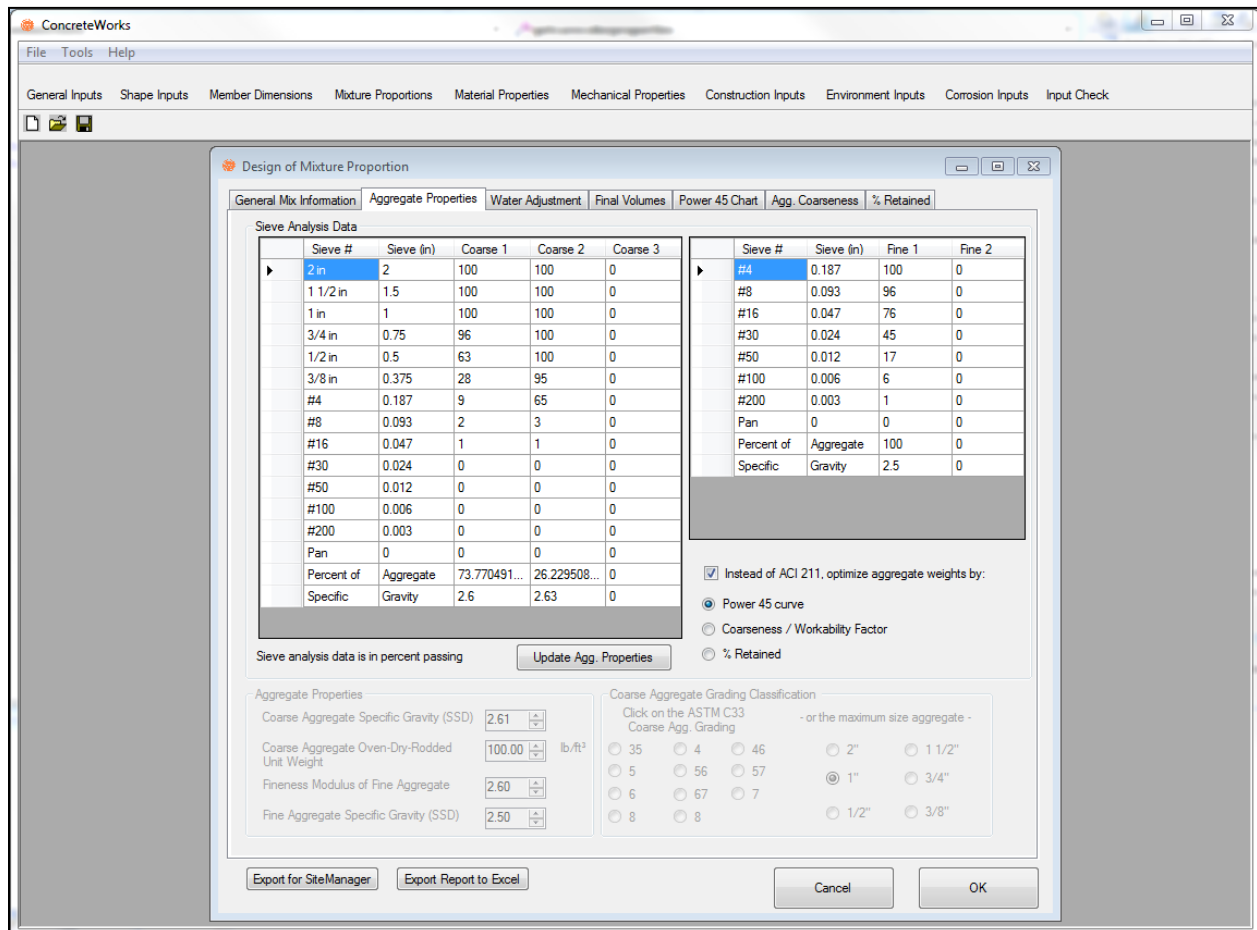

Figure 100. ConcreteWorks Options for Selecting Aggregate Optimization in Mixture Proportioning.

ConcreteWorks has been updated to export the concrete mixture proportions and inputs used in the mixture proportions design to Microsoft Excel® as shown in Figure 100.

Concrete Mixture Proportion Designed Using ConcreteWorks

Final Concrete Design Weights

Material	Value	Units
Cement	684	lb.
Water	351.6	lb.
Coarse Agg. #1 Content	1195.98668303106	lb.
Coarse Agg. #2 Content	425.23970952215	lb.
Coarse Agg. #3 Content	212.619854761077	lb.
Fine Agg. #1 Content	183.120077935480	lb.
Fine Agg. #2 Content	627.84026720737	lb.

General Mixture Inputs/ Assumptions

Input	Value	Units
Design Slump	5	in.
Design Air Content	6	%
Minimum fc'	3000	psi
Targetstrength Strength	3670	psi
w/cm	0.513881353847601	

Coarse Aggregate Sieve Information

Sieve #	Sieve (in)	Coarse 1	Coarse 2	Coarse 3
1 1/2 in	1.5	100	100	100
1 in	1	100	100	100
3/4 in	0.75	96	100	100
1/2 in	0.5	63	100	100
3/8 in	0.375	28	95	100
#4	0.187	9	65	100
#8	0.093	2	3	90
#16	0.047	1	1	40
#30	0.024	0	0	1
#50	0.012	0	0	0
#100	0.006	0	0	0
#200	0.003	0	0	0
Pan	0	0	0	0
Percent of	Aggregate	65.21739130434	23.1884057971014	11.5942028985507
Specific	Gravity	2.6	2.63	2.7

Fine Aggregate Sieve Information

Sieve #	Sieve (in)	Fine 1	Fine 2
#8	0.093	96	99
#16	0.047	76	85
#30	0.024	45	70
#50	0.012	17	60
#100	0.006	6	30
#200	0.003	1	1
Pan	0	0	0
Percent of	Aggregate	22.5806451612901	77.4193548387097
Specific	Gravity	2.5	2.6

Figure 101. Report Generated in Microsoft Excel® Concrete Mixture Proportions and Inputs from Concrete Mixture Design.

CHAPTER 9 CONCLUSIONS AND RECOMMENDATIONS

The following is a summary of the major conclusions and recommendations from the testing and evaluation conducted on the FM 1938 test sections.

The instrumented roller package was effective in locating areas of low stiffness in subgrade soils. However, the correlation was rather weak in one area with the California bearing ratio obtained from the DCP. It appears the package can be used for proof rolling, i.e., checking the stiffness of the subgrade before construction operations commence on the upper pavement layers. The researchers recommend further field testing with this equipment in other areas of the state.

The falling weight deflectometer and dynamic cone penetrometer data can be used to evaluate the stiffness of stabilized subbases before concrete paving commences. The researchers recommend that the FWD and DCP be considered for use in evaluating such subbases in construction projects.

No good correlations were observed between *k*-values from plate bearing tests on cement treated subgrade and on asphalt stabilized base, which implies that *k*-values from the PBT are sensitive to the stiffness of the material immediately below the loading plate.

In general, *k*-values on stabilized base from the AREA method are smaller than those obtained by the PBT, which indicates that the PBT is valid only on natural subgrade.

When nonwoven fabric is used as base material, the AREA method should not be used to estimate *k*-values.

No good correlations were observed between deflections on CRCP and *k*-values from the PBT on natural subgrade or cement treated subgrade. It appears that the deflections on CRCP are more influenced by the thickness and stiffness of the base layer. Decent correlations were observed between deflections on top of the base and on top of the CRCP.

Erosion test using the Hamburg wheel-tracking device was conducted to evaluate the cement stabilized subgrade and subbase samples from FM 1938 CRC pavement construction area. The erosion resistance of the cement treated subgrade materials was increased along with more cement in the sample while the erosion rate of subbase material was not changed significantly by cement content since subbase materials have very low percentage of erodible fines. Cored cement stabilized subgrade samples showed various range of erosion rate because of irregularity of cement stabilization in the field.

Concrete pavement behavior due to environmental loading (temperature and moisture variations) was evaluated with various gages. Base frictional characteristics of two base materials—asphalt and nonwoven geotextile—were evaluated with concrete prisms. The findings from this study can be summarized as follows. Drying shrinkage at the mid-depth of the slab was quite small. The friction of the nonwoven geotextile was smaller than that of the asphalt layer. The smaller friction in the nonwoven geotextile section resulted in larger transverse crack spacing. Finally, the subbase stiffness has substantial effects on slab curling due to temperature variations in the concrete slab.

Based on the testing conducted under this study, it appears that the use of geotextile between CRCP and the subbase is questionable. The magnitude and variability of the FWD deflections on this CRCP section with the geotextile were considerably higher than the other sections; this is not desirable for ensuring good pavement performance.

The 2-inch ACP over 8 inches of cement stabilized subbase appears to be a viable subbase combination. It appears that construction traffic did not damage this section before CRCP placement. The researchers recommend that TxDOT personnel monitor the performance of this section for at least three years before recommending it as a subbase option.

The proposed curing compound evaluation protocol not only considered the moisture loss throughout the maturing process of concrete, but also introduced the relative humidity, surface abrasion strength, and water content of cured concrete samples to assess the curing compound effectiveness. More importantly, the effectiveness index showed good correlation with the abrasion test and dielectric constant data even with limited experimental results. The new protocol shows some promise as a means of evaluating the curing compound effectiveness.

The CRCP section with transverse tines at ½-inch spacing had the lowest measured noise sound intensity level of the four different textures applied on the project. However, the researchers recommend that TxDOT personnel collect noise data on this project again after at least three months of traffic loading on the section with longitudinal tining.

The CRCP section with a carpet drag finish had the lowest skid resistance value. The CRCP section with the transverse tines at 1-inch spacing had the highest skid resistance value.

The use of optimized aggregate gradation in CRCP on this project resulted in improved strength over gap graded mixtures. The maturity strength curves were found to be improved with adding the intermediate aggregate size, using an increased dosage of water reducer, and reducing the water to cement ratio.

The ConcreteWorks program was effectively calibrated using the data collected from this project.